

**Mechanisms of vectored vaccination for  
durable effector T cell immunity and  
sustained germinal center reactions**

**Inauguraldissertation**

zur

Erlangung der Würde eines Doktors der Philosophie

vorgelegt der

Philosophisch-Naturwissenschaftlichen Fakultät

der Universität Basel

von

**Matias Ciancaglini**

2024

Originaldokument gespeichert auf dem Dokumentenserver  
der Universität Basel <https://edoc.unibas.ch>

Genehmigt von der Philosophisch-Naturwissenschaftlichen Fakultät  
auf Antrag von

Erstbetreuer: Prof. Dr. Daniel Pinschewer

Zweitbetreuer: Prof. Dr. Dirk Bumann

Externer Experte: Prof. Dr. Ulrich Kalinke

Basel, den 25.06.2024

Prof. Dr. Marcel Mayor  
Dekan

# Table of Contents

<b>ABBREVIATIONS</b> .....	<b>5</b>
<b>GENERAL INTRODUCTION</b> .....	<b>8</b>
INTRODUCTION TO VACCINOLOGY .....	8
MAIN CATEGORIES OF HUMAN VACCINES .....	8
GENETIC VACCINE PLATFORMS OF INTEREST.....	9
<i>Lymphocytic choriomeningitis virus (LCMV) vaccine vectors</i> .....	9
<i>Vesicular Stomatitis Virus (VSV) vaccine vectors</i> .....	10
<i>Adenovirus vaccine vectors</i> .....	11
<i>mRNA – lipid nanoparticle (LNP) vaccines</i> .....	11
FACTORS THAT INFLUENCE THE IMMUNOGENICITY OF GENETIC VACCINES .....	12
<i>Antigen expression levels</i> .....	12
<i>Innate immunity and inflammatory milieu</i> .....	12
<i>Cellular tropism</i> .....	13
<i>Anti-vector immunity</i> .....	13
ADAPTIVE IMMUNE RESPONSES TO VECTOR VACCINATION: CD8 T CELLS .....	13
ADAPTIVE IMMUNE RESPONSES TO VACCINATION: B CELLS AND THE GERMINAL CENTER REACTION .....	14
<b>AIMS OF THE THESIS</b> .....	<b>16</b>
<b>NON-CYTOLYTIC VIRAL VECTORS INDUCE DURABLE EFFECTOR-MEMORY CD8 T CELL IMMUNITY BY TRIGGERING POTENT TYPE I INTERFERON RESPONSES</b> .....	<b>17</b>
ABSTRACT .....	18
INTRODUCTION .....	19
RESULTS .....	20
<i>Non-cytolytic rLCMV vectors persist longer than cytolytic rVSV vectors and induce long-lived antigen-specific CD8 T cell responses</i> .....	20
<i>Non-cytolytic rVSVMq induces long-lived effector-differentiated CD8 T cell memory and provides better protection against Listeria challenge</i> .....	24
<i>The phenotype of rVSVMq-induced CD8 T cell responses resemble those induced by rLCMV</i> .....	27
<i>rVSVMq vectors express less antigen than rVSV but triggers more IFN-I</i> .....	30
<i>rVSVMq promotes IFNAR-dependent expansion of antigen-specific CD8 T cells</i> .....	34
<i>rVSVMq vaccination allows antigen-specific CD8 T cells to spatio-temporally integrate cognate antigen and IFN-I signals</i> .....	37
DISCUSSION.....	39
LIMITATIONS OF THE STUDY .....	41
METHODOLOGY .....	42
<i>Animal experiments</i> .....	42
<i>Vector generation and titration</i> .....	42
<i>Flow cytometry</i> .....	42
<i>Neutralization assays, luciferase activity, S1 ELISA and IFN-<math>\alpha</math> measurements</i> .....	43
<i>Listeria challenge</i> .....	44
<i>scRNA-sequencing and bioinformatic analyses</i> .....	44
<i>In vivo IFNAR blockade and NK cell depletion</i> .....	44
<i>Adoptive transfers</i> .....	45
<i>Immunohistochemistry</i> .....	45
ACKNOWLEDGEMENTS.....	45
FUNDING .....	46
SUPPLEMENTARY FIGURES .....	47
<b>HOMOLOGOUS MRNA PRIME-BOOST VACCINATION PROMOTES CLONAL CONTINUITY IN GERMINAL CENTERS AND BREADTH OF NEUTRALIZING ANTIBODY RESPONSES</b> .....	<b>51</b>
ABSTRACT .....	52
INTRODUCTION .....	53
RESULTS .....	54

<i>Primary antigen specific B cell responses to mRNA-1273 immunization are longer-lived than those to ChAdOx-1</i> .....	54
<i>mRNA-1273/mRNA-1273 and ChAdOx-1/mRNA-1273 vaccination regimens induce secondary GC B cell responses of similar magnitude</i> .....	57
<i>Homologous mRNA-1273 prime-boost vaccination results in superior clonal continuity of GC B cell responses</i> .....	60
<i>Antibody responses to homologous mRNA-1273 prime-boost exhibits broader variant coverage than those to heterologous ChAdOx-1/mRNA-1273</i> .....	66
DISCUSSION .....	69
LIMITATIONS OF THE STUDY .....	71
METHODOLOGY .....	72
<i>Animal experiments, immunizations and tamoxifen administration</i> .....	72
<i>Flow cytometry</i> .....	72
<i>Sample collection and processing</i> .....	73
<i>Fluorescent SARS-CoV-2 spike probe generation</i> .....	73
<i>SARS-CoV-2 pseudovirus neutralization assays</i> .....	73
<i>Spike protein and adenovirus vector ELISAs</i> .....	73
<i>Immunohistochemistry</i> .....	74
ACKNOWLEDGEMENTS.....	74
<b>NOVEL ADENOVIRUS VACCINE VECTORS LACKING THROMBOSIS-ASSOCIATED INTERACTIONS WITH PLATELET FACTOR 4</b> .....	<b>77</b>
ABSTRACT .....	78
INTRODUCTION .....	79
RESULTS .....	81
<i>Screenings of AAV and natural Ad collections identified vectors lacking PF4 binding</i> .....	81
<i>Ad5 binding to PF4 is dependent on its hexon HVR1 loop</i> .....	85
<i>Ad5 infection levels in multiple immortalized or primary cell types were strongly influenced by PF4</i> .....	89
<i>PF4 non-binding model COVID-19 vaccine vectors induced cellular immune responses in mice</i> .....	91
DISCUSSION.....	94
METHODS .....	98
<i>Aggregate Pull-Down</i> .....	100
<i>Erythrocyte Pull-Down</i> .....	101
<i>Cell culture</i> .....	101
<i>Surface Plasmon Resonance</i> .....	102
<i>Sequence and protein structure analyses</i> .....	102
<i>Structural modellings and Molecular dynamic simulation</i> .....	102
<i>Brownian dynamic (BD) simulations and contact analyses</i> .....	103
<i>Infectivity assays</i> .....	103
<i>Mice and animal experimentation</i> .....	104
<i>Neutralizing antibody assays</i> .....	105
<i>Binding antibody assay</i> .....	106
<i>Statistical analyses</i> .....	106
ACKNOWLEDGMENTS .....	107
FUNDING .....	107
AUTHOR CONTRIBUTIONS .....	107
COMPETING INTERESTS .....	107
DATA AND MATERIALS AVAILABILITY .....	107
SUPPLEMENTARY FIGURES .....	107
<b>GENERAL DISCUSSION</b> .....	<b>114</b>
<b>REFERENCES</b> .....	<b>120</b>
<b>CURRICULUM VITAE</b> .....	<b>141</b>
<b>ACKNOWLEDGEMENTS</b> .....	<b>143</b>

## Abbreviations

AAV	Adeno-associated virus
Ab	Antibody
Ad	Adenovirus
APC	Antigen presenting cell
AID	Activation-induced cytidine deaminase
AID <sup>rep</sup>	AID fate mapping reporter mice
APD	Aggregate Pull-Down
ASC	Antibody-secreting cell
Bcl-2	B cell lymphoma 2
BCR	B cell receptor
BM	Bone marrow
CFSE	Carboxyfluorescein succinimidyl ester
CFU	Colony forming units
ChAd	Chimpanzee adenovirus
CNS	Central nervous system
COVID-19	Coronavirus Disease 19
CSR	Class-switch recombination
CTLA-4	Cytotoxic T-lymphocyte-associated protein 4
CTL	Cytotoxic T lymphocyte
DC	Dendritic cell
DG	Alpha-dystroglycan
DNA	Deoxyribonucleic acid
EBOV	Ebola virus
EGFP	Enhanced green fluorescent protein
ELISA	Enzyme-linked Immunosorbent Assay
EYFP	Enhanced yellow fluorescent protein
FACS	Fluorescent-activated cell sorting
GC	Germinal center
GFP	Green fluorescent protein
GPC	Glycoprotein precursor
HCV	Hepatitis C virus
HIV	Human Immunodeficiency virus
HVR	Hyper-variable region
IFNAR	Type I interferon receptor
IFN-I	Type I interferon

IFN- $\alpha$	Interferon alpha
IFN- $\gamma$	Interferon gamma
Ig	Immunoglobulin
IL	Interleukin
iLN	Inguinal lymph node
i.m.	Intramuscular
i.p.	Intraperitoneal
IRF	Interferon-regulatory factor
ISG	Interferon-stimulated gene
i.v.	Intravenous
JAK	Janus kinase
kb	Kilobases
Kbp	Kilobase pairs
kD	Kilodalton
ko	Knockout
LCMV	Lymphocytic choriomeningitis virus
LCMVGP	Lymphocytic choriomeningitis virus glycoprotein
LN	Lymph node
LNP	Lipid nanoparticle
MAPK	Mitogen-activated protein kinase
MBC	Memory B cell
MFI	Mean fluorescent intensity
mg	Milligram
MHC	Major histocompatibility complex
ml	Millilitre
MOI	Multiplicity of infection
mRNA	Messenger ribonucleic acid
MVA	Modified vaccinia ankara
nAb	Neutralizing antibody
NF- $\kappa$ B	Nuclear factor-kappa B
NHP	Non-human primate
NK cell	Natural killer cell
NP	Nucleoprotein
OVA	Ovalbumin
PAMP	Pathogen-associated molecular pattern
PC	Plasma cell
pDC	Plasmacytoid dendritic cell
PEG	Polyethylene glycol
PCR	Polymerase chain reaction

PD-1	Programmed cell death protein 1
PFU	Plaque forming unit
PF4	Platelet factor 4
p.i.	Post infection
PKR	Protein kinase R
PRR	Pathogen recognition receptor
rAd	Recombinant adenovirus
rLCMV	Recombinant lymphocytic choriomeningitis virus
RIG-1	Retinoid acid inducible gene 1
RLR	Retinoid acid inducible gene 1 (RIG-1) like receptors
RNA	Ribonucleic acid
RT-PCR	Reverse transcriptase PCR
rVSV	Recombinant vesicular stomatitis virus
rVSVMq	Recombinant vesicular stomatitis virus matrix quadruple mutant
SARS-CoV-2	Severe Acute Respiratory Syndrome Coronavirus 2
SD	Standard Derivation
SEC	second
SEM	Standard Error of the Mean
SHM	Somatic hypermutation
SIV	Simmian immunodeficiency virus
snLuc	Secreted nanoluciferase
SPR	Surface plasmon resonance
STAT	Signal transducer and activator of transcription
S1	Spike protein subunit 1
TCR	T cell receptor
Tcm	Central memory T cell
Tem	Effector memory T cell
Tfh	T follicular helper
TGF- $\beta$	Transforming growth factor beta
TLR	Toll like receptor
TYK	Tyrosine kinase
VITT	Vector-induced thrombotic thrombocytopenia
VP	Vector particles
VSV	Vesicular Stomatitis Virus
VSVG	Vesicular Stomatitis Virus glycoprotein
VV	Vaccinia
WHO	World Health Organization
wk	week
wt	Wild-type

# General introduction

## Introduction to vaccinology

Vaccination stands as one of the most significant medical interventions in human history. Estimates from the World Health Organization (WHO) show that vaccines prevent 3.5 to 5 million human deaths per year<sup>1</sup>, and around 1.5 million children die yearly due to diseases that could have been prevented by vaccination<sup>2</sup>. The concept of vaccination dates back to the 18th century, when Edward Jenner demonstrated that inoculation with cowpox material conferred protection against smallpox<sup>3</sup>, an experiment that constituted the first successful documented vaccination. He demonstrated that exposing a person to a manageable infection could confer protection against a more severe one, a principle that stands for all modern vaccines. This concept was further applied by Louis Pasteur, who elaborated methods to attenuate or inactivate pathogens to a non-pathogenic state that could still induce a protective immune response, leading to the development of vaccines against rabies, anthrax and chicken cholera<sup>4</sup>. Since then, vaccines have led to the control<sup>5</sup>, and in some cases the eradication of deadly pathogens, such as the global smallpox eradication in 1980<sup>6</sup>. Nowadays, the relevance of vaccines continues to be essential, as illustrated by the recent Coronavirus Disease 2019 (COVID-19) pandemic<sup>7</sup>. The development of vaccines against Severe Acute Respiratory Syndrome Coronavirus 2 (SARS-CoV-2) marked an unprecedented milestone in medicine, with the generation of novel vaccines and their deployment within a year from the virus identification<sup>8,9</sup>. Despite their success, the vast majority of vaccines have been developed empirically, with little or no understanding of the mechanisms by which they induce protection. The failure to develop vaccines against global pandemics such as the human immunodeficiency virus (HIV) despite decades of effort, or the threat of emerging pathogens, highlight the need to understand the immunological mechanisms by which vaccines confer protective immunity.

## Main categories of human vaccines

Historically, vaccines typically used antigens coming directly from the inactivated pathogen or an attenuated form. Live-attenuated vaccines contain a version of the living microbe that has been modified so it cannot cause disease in the targeted host. Because a live-attenuated vaccine is the closest to a natural infection, they elicit robust cellular and antibody responses and can confer long-term immunity with only one or two doses<sup>10-12</sup>. However, the remote possibility exists that an attenuated microbe in the vaccine could revert to a virulent form and cause disease, as it has happened with the oral poliovirus and rotavirus vaccines<sup>13-16</sup>. Furthermore, people who are immunocompromised, due to medical procedures or infection with HIV, are more susceptible to live vaccines reactogenicity<sup>17-19</sup>. Inactivated vaccines are created by inactivating a pathogen<sup>20</sup>, typically using heat or chemicals such as formaldehyde or formalin<sup>21</sup>, which destroys the microbe's ability to replicate but keeps the antigens so that the immune system can still recognize it. Inactivated vaccines are more stable and, when correctly



inactivated, safer than live vaccines<sup>22</sup>. However, their immunogenicity tends to be lower, leading to shorter duration of protection<sup>23</sup>.

The advent of recombinant DNA technology revolutionized the field of vaccinology, enabling the development of new antigenic delivery systems. Among these, recombinant viral vectors represent promising vaccine platforms due to their ability to deliver and express foreign antigens, triggering both cellular and humoral immune responses without exogenous adjuvants<sup>24</sup>. Because of their viral nature, they contain pathogen associated molecular patterns (PAMPs), which include viral proteins and nucleic acids. These molecules activate pathogen recognition receptors (PRR) in the host cells, providing viral vectors intrinsic adjuvant properties<sup>25</sup>. Genetic engineering of viruses to carry heterologous antigens information can be performed by replacing an essential viral gene with the transgene of interest. The gain is two-fold: it provides more space in the viral genome, which can be a limiting factor for many platforms<sup>26,27</sup>, and makes the vector unable to propagate within the host<sup>28,29</sup>. The tight block in the propagation of these vectors provides them with a high safety profile, which is fundamental in the context of vaccination<sup>30</sup>. At the same time, the vector is still able to transduce and replicate its genetic information (containing the heterologous antigen) within the host cell, instructing the cells of the vaccinee to produce the antigen internally. In this sense, replication-deficient viral vectors act as a platform that seeks to combine the safety of an inactivated vaccine with the immunogenicity of a live vaccine.

## **Genetic vaccine platforms of interest**

### **Lymphocytic choriomeningitis virus (LCMV) vaccine vectors**

LCMV is a prototypic member of the Old-World Arenaviruses, and a natural pathogen of mice. The non-cytolytic nature of the virus allows its persistence in the host, being able to establish chronic infections<sup>31</sup>. The virion is enveloped with a bi-segmented and single-stranded RNA genome<sup>32</sup>. Since it has an ambisense coding strategy, each segment encodes two proteins in opposite orientations separated by an intergenic region. The two genomic segments, designated L (from large) and S (from small) have an approximate size of 7.2 and 3.4 Kb, respectively. The L segment contains the genetic information from the RNA-dependent RNA-polymerase (L) and the ring finger protein (Z). The S segment encodes for the nucleoprotein (NP), which is the most abundantly expressed protein and associates with the genomic RNA molecule<sup>33</sup>. Importantly, NP possess exonuclease activity<sup>34</sup> and is able to antagonize type I interferon (IFN-I) activity by degrading immunostimulatory viral dsRNA structures, presumably avoiding recognition by protein kinase R (PKR)<sup>35</sup>. The second protein encoded by the S segment is the envelope glycoprotein precursor (GPC), which is cleaved into GP1 and GP2 after translation<sup>36</sup>. They mediate attachment and fusion with the membranes of their target cells<sup>37</sup>, which is dependent on CD164 and alpha-dystroglycan receptor (DG)<sup>38,39</sup>. LCMV glycoproteins represent the only target for LCMV-neutralizing antibodies<sup>40</sup>. The “glycan shield” present on the outer globular domain of the viral glycoprotein makes neutralizing antibody responses to LCMV remarkably weak<sup>41</sup>. This is an important difference between LCMV and other viral vectors because the former can be re-administered in

homologous prime-boost vaccination regimens without losing efficacy via antibody-mediated vector neutralization<sup>42</sup>.

With the development of arenavirus reverse genetic engineering techniques<sup>43</sup>, recombinant LCMV vectors (rLCMV) became a promising vaccine platform against infectious diseases and cancer<sup>44-46</sup>. Even though LCMV is capable of infecting humans and cause neurological disease, such as meningitis<sup>47</sup>, abrogation of its replicative capacity by replacement of the viral glycoprotein gene results in safe vectors suitable for clinical use<sup>44</sup>. Furthermore, the natural ability of rLCMV to directly target antigen-presenting cells (APC) leads to the induction of broad and long-lived CD8 T cell responses<sup>42,48</sup>, as it has been shown in clinical trials<sup>44</sup>.

### **Vesicular Stomatitis Virus (VSV) vaccine vectors**

VSV is a non-segmented negative-sense RNA virus, which belongs to the *Rhabdoviridae*. The wild type VSV virion is enveloped, with a genome composed of 11 Kb, which encodes five major viral structural proteins: nucleocapsid protein (N), phosphoprotein (P), matrix protein (M), glycoprotein (G), and the RNA-dependent RNA-polymerase (L)<sup>49,50</sup>. Each viral protein is translated from its own subgenomic monocistronic mRNA. Untranslated and intergenic junctions between the genes contain transcription termination and polyadenylation signals, and the transcription re-initiation signals for the subsequent downstream gene<sup>51</sup>. Besides its role in VSV morphogenesis and budding<sup>52</sup>, the M protein is the main determinant of VSV high cytolytic effect<sup>53-55</sup>. This is due to the host shut-off activity of VSV, mediated by inhibition of both nuclear transcription and nucleocytoplasmic RNA transport by the M protein<sup>56,57</sup>. This way the virus benefits from the cellular protein synthesis machinery while suppressing the antiviral IFN-I response<sup>58,59</sup>, allowing rapid replication and high virus yields.

The procedure for generating replication-competent VSV entirely from cDNA has been established using reverse genetic engineering<sup>60,61</sup>. This has allowed the development of recombinant VSV vectors (rVSV) that express foreign proteins at high levels<sup>62</sup>. In addition, the lack of preexisting human immunity against VSV and its inability to transform host cells make VSV a widely used experimental platform for vaccine vectors<sup>63</sup>. One of the main factors for the wide use of VSV is its broad cell tropism, that can be beneficial for several applications<sup>64</sup>. Specifically, VSV ability to infect and activate APCs<sup>65</sup> makes it particularly attractive for vaccine design. However, due to its high replication rate, neurotropism and cytopathic effect, VSV has raised concerns for its use as a vaccine delivery platform<sup>66,67</sup>. A recombinant VSV Ebola vaccine (rVSV-EBOV) was the first viral vector that received approval as a prophylactic vaccine for use in humans, but significant vector-associated reactogenicity was associated to replication of rVSV-EBOV in synovial fluid and skin lesions<sup>68</sup>. Replacing VSV glycoprotein gene for a transgene of interest that abrogates VSV replication could circumvent these safety issues<sup>69</sup>. Notably, many non-replicating VSV vaccine vectors have shown similar immunogenicity than their replication-competent form<sup>28,70,71</sup>.

### **Adenovirus vaccine vectors**

Adenoviruses are non-enveloped and contain a double-stranded DNA genome of 26 to 46 Kbp long. With more than 200 non-human adenovirus types and more than 100 human serotypes, they have a large natural diversity<sup>72</sup>. Adenoviruses encode 23-46 different proteins, but can still accommodate large transgenes. Furthermore, deletion of essential viral genes like E1 and E3 allows a heterologous transgene capacity of 7.5 Kbp<sup>73</sup>, making them replication-deficient and with a favorable safety profile. Recombinant Adenovirus vectors (rAd) display a number of desirable characteristics which makes them particularly well-suited to prophylactic vaccine applications. Their genome is stable and easy to manipulate, they can be amplified and produced to high titers<sup>74</sup>, and have been proved safe and immunogenic in several clinical trials<sup>75-77</sup>. However, despite their robust immunogenicity, the high seroprevalence of many adenoviruses in human populations greatly limits their efficacy<sup>78,79</sup>. This stimulated the research of novel adenovirus species, including less prevalent human serotypes<sup>80</sup> and non-human primate (NHP) adenoviruses<sup>81</sup>.

rAds became the center of attention in vaccinology since the SARS-CoV-2 pandemic, which prompted the development and deployment of a wide range of adenovirus-based vector platforms<sup>82</sup>. Among these, with more than 2 billion administered doses, the ChAdOx-1 nCoV-19 (AZD1222) vaccine represented over one third of all global SARS-CoV-2 vaccine doses administered in 2021<sup>7</sup>. ChAdOx-1 is based on a chimpanzee adenovirus isolate, which has very low seroprevalence in humans and could potentially avoid pre-existing immunity<sup>83</sup>. However, vaccination with ChAdOx-1 can produce vector-induced thrombotic thrombocytopenia (VITT), a side effect in around 1 in 100,000 vaccinees that is fatal in 23 to 40% of reported cases<sup>84</sup>. VITT is thought to be a consequence of the interaction between human platelet factor 4 (PF4, or CXCL4), a blood component, and proteins present on the rAd capsid<sup>85</sup>. After it became known that ChAdOx-1 was associated with VITT, the vaccination strategy changed, and many individuals who had received a first dose of ChAdOx-1 were given a boost with mRNA vaccines<sup>86</sup>. Notably, this heterologous prime-boost strategy provided enhanced immunogenicity<sup>87,88</sup>.

### **mRNA – lipid nanoparticle (LNP) vaccines**

mRNA vaccines represent a new class of vaccine platform, which consist of in vitro-transcribed mRNA strands encoding an antigen of interest, packaged in LNPs that deliver the genetic information to the vaccinee's cells. mRNA vaccines are not typical vectored vaccines in the sense that do not use traditional delivery systems like recombinant viruses or bacteria. Still, the LNP component acts as a vehicle that ensures the structural integrity of the mRNA. Upon administration, the polyethylene glycol (PEG)-lipid stabilizing the mRNA-LNP system against aggregation during manufacturing rapidly dissociates from the LNP, an essential step to promote cellular interactions<sup>89</sup>. This allows the mRNA-LNP to be endocytosed and a fraction of the mRNA released through a process of endosomal escape into the cytoplasm, where the antigen of interest is produced and presented by transfected cells, including muscle cells and APCs<sup>90</sup>. Furthermore, the LNP component of LNP-mRNA vaccines has adjuvant activity, which is dependent on its ionizable lipid component for IL-6 induction<sup>91</sup>.

Although mRNA-LNP vaccines were already being investigated in clinical trials for many diseases, their potential was revealed by the COVID-19 pandemic, that allowed mRNA vaccine candidates to enter clinical trials and obtain accelerated regulatory approvals<sup>92</sup>. Compared with traditional vaccines, which are relatively slow to develop, mRNA-based vaccines have features that allow them to be rapidly designed and upscaled while still being highly potent and with low costs<sup>93</sup>.

## **Factors that influence the immunogenicity of genetic vaccines**

### **Antigen expression levels**

The magnitude and persistence of antigen expression during immunization are critical for a robust stimulation of the immune system<sup>94</sup>. In this context, vectored vaccines are capable of supplying substantial quantities of vaccine antigen over extended periods of time, but this varies greatly and depends on the type of vector, dose and route of immunization. Although the antigen produced by replication-deficient vectors in the recipient is less abundant compared to their replication-competent form, it still greatly influences the potency of the immune response<sup>95</sup>. For instance, antigen persistence by adenoviral vectors has been shown to play a critical role in expanding and maintaining memory T cell responses<sup>96</sup>.

### **Innate immunity and inflammatory milieu**

Besides antigen availability, innate immune activation and the resultant inflammatory milieu are key elements in shaping the adaptive immune response to vaccination. Once vaccine vectors are administered, recognition is initiated by the association of vector-derived PAMPs with PRRs from the host cell. Depending on their nature and genome replication strategy, different PRRs get involved. In the case of RNA-based vectors like rLCMV<sup>97</sup>, rVSV<sup>98</sup>, or mRNA<sup>99</sup> vaccines, both Toll-like receptors (TLR) and the retinoid acid inducible gene 1 (RIG-1) like receptors (RLRs) play a role. They recognize RNA structures and activate IRF3 and IRF7, resulting in a robust production of IFN-I, which in turn signals in an autocrine and paracrine manner to induce the expression of interferon-stimulated genes (ISG)<sup>100</sup>. Adenoviral vectors can also be sensed by different TLRs<sup>101</sup> as well as the cytosolic DNA sensor cGAS<sup>102</sup>. The IFN-I family includes several IFN- $\alpha$ , mainly produced by APCs, especially plasmacytoid dendritic cells (pDCs)<sup>103</sup>; and represents a crucial factor of the antiviral response. All IFN-I subtypes signal through the same receptor, comprised of the interferon alpha receptor (IFNAR)1 and IFNAR2 chains, expressed on most nucleated cells. Upon ligation, several signal transduction pathways involving tyrosine kinases Janus kinase 1 (JAK1) and tyrosine kinase 2 (TYK2), and the signal transducers and activators of transcription (STATs), which are widely expressed in most cell types, become activated<sup>104</sup>. Autocrine IFN-I signaling induce a set of ISGs that activate the antiviral state, which leads to the suppression of viral replication in infected host cells<sup>105</sup>. This can negatively impact vector immunogenicity due to the suppression of antigen production<sup>95</sup>, limiting the priming of adaptive immune cells. At the same time, IFN-I signaling in APCs induces their phenotypic maturation by promoting the expression of major histocompatibility complex (MHC)-I, MHC-II, co-stimulatory

molecules and lymphoid-homing receptors<sup>106</sup>. Importantly, IFN-I can act as a potent signal 3 cytokine by directly signaling to T cells, promoting their proliferation, survival and effector cell differentiation<sup>107</sup>.

### **Cellular tropism**

The vectors' ability to target and infect specific cell types greatly influences the immune response<sup>108,109</sup>. Dendritic cells (DCs) can be infected or at least transduced by a broad range of viral vectors<sup>110</sup>. After entry and replication in the cytosol, proteasomal degradation of vector's gene products generates peptide fragments that associate with the host MHC-I. Loaded DCs can then interact with CD8 T cells through the process of direct presentation to drive the potent activation, expansion and differentiation of T cells<sup>111</sup>. The functional activation of DCs due to vector transduction in combination with direct presentation to CD8 T cells determines the ability of DCs to prime potent CD8 T cell responses<sup>112</sup>. In the absence of direct DC targeting, the phagocytic uptake of vector particles or their derived antigens by DCs can be cross-presented on MHC-I to prime CD8 T cells<sup>113</sup>.

### **Anti-vector immunity**

A major limitation of vaccine vectors delivery systems is the development of an immune response, either in the form of antibodies or cytotoxic T cells (CTL), directed to the vector backbone itself. This response interferes by competition with the transgene-specific response<sup>114,115</sup> and/or by directly dampening the amount of antigen expressed<sup>116-118</sup>. This phenomenon can be the consequence of prior vaccination with the same vector, or prior infection with the same or a related virus to the one used in the vector platform. For instance, vaccine trials utilizing adenovirus 5 (Ad5)-based vectors have been influenced by pre-existing anti-adenovirus immunity. Individuals that presented Ad5-specific antibodies were poor responders to Ad5 vaccination, compared to Ad5 seronegative participants<sup>119</sup>. VSV vectors can also induce potent neutralizing antibody responses after a single immunization, which interferes with subsequent administrations<sup>40</sup>. Notably, pseudotyping VSV with LCMV glycoprotein allows repeated vector re-administration without losing efficacy<sup>120</sup>. This way the vector is modified by exchanging its own neutralization-sensitive surface protein for a glycoprotein that is a poor inducer of neutralizing antibodies. Another strategy to circumvent anti-vector immunity include the direct modification of vector components to evade host neutralizing antibodies<sup>116</sup>. Furthermore, the use of two different (or distantly related) vectors carrying the same antigen in sequential immunizations, or heterologous prime-boost immunizations, is an effective strategy because immunity developed against the priming vector does not interfere with the boosting vector<sup>121</sup>.

### **Adaptive immune responses to vector vaccination: CD8 T cells**

CD8 T cells play a role in clearing primary and suppressing persistent intracellular infections. They may control the spread of intracellular pathogens before antibody responses have a chance to undergo affinity maturation<sup>122</sup>. The ability of CD8 T cells to recognize a broader antigenic repertoire than neutralizing antibodies<sup>123</sup> makes them particularly important in cases of heterosubtypic infection. This

occurs in a variety of infections including influenza and SARS-CoV-2 viruses, where cross-reactive CD8 T cells can make the difference between progression from mild to severe disease<sup>124</sup>.

As mentioned above, viral vaccine vectors can target and transduce DCs, stimulating their maturation for potent CTL priming. Priming of T cells relies on three key signals: TCR engagement by peptide/MHC complexes, co-stimulation by CD28 and members of the TNF receptor family, as well as specific cytokine signaling. DCs can supply these signals, provided that are adequately activated<sup>125</sup>. If the DC simultaneously presents identifiable MHC-II- and MHC-I-restricted antigens, it can get “licensed” by CD4 T cells and transmit help signals from CD4 to CD8 T cells<sup>126</sup>. These first stages of the immune response will determine the magnitude, quality and persistence of memory CD8 T cells. After activation and clonal expansion, effector CD8 T cells help clear the antigen through robust cytokine production and cytotoxic destruction of infected cells<sup>127,128</sup>. Following resolution of the antigen, the effector T cell pool contracts and a small number of memory cells are maintained for long-term protection of the host. Memory CD8 T cells can be broadly classified into effector or central memory cells based on the expression of the lymphoid homing receptors CD62L and CCR7, with effector memory (Tem) being CD62L<sup>lo</sup>/CCR7<sup>lo</sup> and central memory (Tcm) cells being CD62L<sup>hi</sup>/CCR7<sup>hi</sup><sup>129</sup>. Tem cells are more cytolytic and express integrins and chemokine receptors necessary for localization to inflamed tissues. This way, Tem cells can recirculate through the bloodstream and access peripheral tissues. The transcription factors T-bet, Zeb2 and ID2 are associated with Tem differentiation<sup>130,131</sup>. Expression of CCR7 and CD62L on Tcm cells facilitates homing to secondary lymphoid organs, where memory T cells are better equipped to persist following infection and to produce IL-2 and proliferate in response to antigenic stimulation<sup>132</sup>. Transcription factors that dictate Tcm fate are Eomes, TCF1, BCL-6 and ID3<sup>133,134</sup>.

## **Adaptive immune responses to vaccination: B cells and the germinal center reaction**

Antibodies represent the main correlate of protection for most vaccines<sup>135,136</sup>. The germinal center (GC) response is critical for the generation of affinity-matured plasma cells and memory B cells capable of producing antibodies that confer long-term protective immunity. Upon activation, B cells migrate from the follicle border to the T cell zone and start to expand, following various differentiation routes<sup>137</sup>. B and T cells interact to form GCs, as part of the T cell-dependent antibody response. The GCs are specialized structures where B cells undergo somatic hypermutation (SHM) and class-switch recombination (CSR), and both reactions are mediated by the activation-induced cytidine deaminase (AID)<sup>138,139</sup>. By CSR, B cells switch their antibody class from IgM to IgA, IgG or IgE, with different effector functions. Through SHM, the B cell receptor (BCR) acquires mutations in the variable regions of the immunoglobulin genes, some of which will lead to decreased interactions with the cognate antigen, and some will enhance the affinity for the antigen. Competition between B cell clones for interaction with the limited antigen, and help from CD4 T cells, leads to a process known as affinity maturation<sup>140</sup>. Iterative rounds of affinity maturation eventually generate isotype-switched B cells with higher affinity that differentiate into plasma cells (PCs) or memory B cells (MBCs)<sup>141</sup>.

Besides to increasing affinity, GCs also allow the clonal diversification of B cells and ensure that antibody responses also become more diverse over time<sup>142</sup>. This process can generate so called broadly neutralizing antibodies, that can recognize different virus variants and are important in response to rapidly evolving viruses, such as HIV<sup>143</sup> or SARS-CoV-2<sup>144</sup>. The role of GC-driven diversification is well documented for HIV, where the unmutated ancestors of the broadly neutralizing antibodies have little or no measurable affinity for the virus and must acquire large numbers of mutations to develop breadth and potency<sup>145,146</sup>. This has led to the search of B cell lineage immunogens design, with the aim of targeting naïve BCRs and “guide” these B cells through sequential immunogens that select for antibody mutations that lead to higher antibody breadth<sup>147,148</sup>.

Coronaviruses have a lower mutation rate and reduced frequency of escape from antibody neutralization compared with other RNA viruses, due to their expression of a proofreading 3'-5' exoribonuclease<sup>149</sup>. Despite this, thousands of mutations have been identified in circulating SARS-CoV-2 viruses, including mutations in the spike protein that impact the susceptibility to antibody neutralization<sup>150</sup>. Convalescent serum is capable of neutralizing viruses expressing the wild-type spike protein, however, there is a significant decrease in neutralization sensitivity for several mutated spike proteins that are found in viral variants of concern<sup>151,152</sup>. SARS-CoV-2 vaccination-induced MBCs that bind virus variants contain higher levels of SHM compared to B cells that bind only the original SARS-CoV-2, which suggests an important role of the GC reaction in the acquisition of broadly reactive antibodies<sup>153</sup>.

## **Aims of the thesis**

First, we aimed to study how the cytolytic behavior of viral vectors affects the resulting CD8 T cell response, and the molecular determinants of viral vectors associated to this process.

Second, we aimed to determine the potential of different COVID-19 vaccine regimens in clinical use to elicit and maintain germinal center B cell responses.

Third, we were interested in identifying adenoviral vectors with an improved safety profile and test their immunogenic capacity.



# **Non-cytolytic viral vectors induce durable effector-memory CD8 T cell immunity by triggering potent type I interferon responses**

Matias Ciancaglini<sup>1</sup>, Robin Avanthay<sup>2</sup>, Anna-Friederike Marx<sup>1</sup>, Tiago Abreu-Mota<sup>1</sup>, Florian Geier<sup>3</sup>, Dominik Burri<sup>3</sup>, Ingrid Wagner<sup>4</sup>, Doron Merkler<sup>4</sup>, Gert Zimmer<sup>2</sup> and Daniel D. Pinschewer<sup>1\*</sup>.

<sup>1</sup> Department of Biomedicine, University of Basel, Petersplatz 10, 4051 Basel, Switzerland.

<sup>2</sup> Institute of Virology and Immunology, Sensemattstrasse 293, 3147 Mittelhäusern, Switzerland.

<sup>3</sup> Department of Biomedicine, Bioinformatics Core Facility, University Hospital Basel, 4031 Basel, Switzerland

<sup>4</sup> Department of Pathology and Immunology, University of Geneva, Geneva, Switzerland

\*Corresponding author: Daniel D. Pinschewer, M.D., Department of Biomedicine-Haus Petersplatz, Division of Experimental Virology, 4009 Basel, Switzerland. E-Mail: [daniel.pinschewer@unibas.ch](mailto:daniel.pinschewer@unibas.ch).  
Phone: +41 79 543 39 70

## **Abstract**

Advances in viral vector platforms have revolutionized the development of CD8 T cell-based vaccines, with replication-deficient vector systems offering an excellent safety profile. By comparing lymphocytic choriomeningitis virus-based single-cycle vectors (rLCMV) with replication-deficient vesicular stomatitis virus-based (rVSV) vaccines this study explores the molecular mechanisms accountable for the induction of long-lived effector-memory CD8 T cell immunity. Non-cytolytic rLCMV elicited more durable CD8 T cell responses with a higher proportion of effector-memory CD8 T cells than cytolytic rVSV. When molecularly engineered to be non-cytolytic, rVSV-induced CD8 T cell memory was more durable and effector-differentiated, reminiscent of rLCMV-induced responses, and afforded superior protection against *Listeria* challenge. Improved cellular responses of non-cytolytic rVSV were due to an elevated type I interferon (IFN-I) response and its direct sensing by vaccination-induced CD8 T cells. Vector-infected antigen-presenting cells in the splenic marginal zone produced IFN-I within hours after vaccination, simultaneously with their priming of antigen-specific CD8 T cells. These observations establish IFN-I responses as the molecular link connecting non-cytolytic replication of viral vaccine vectors to long-lived and protective effector-memory CD8 T cell immunity.

## Introduction

CD8 T cells form a key pillar of adaptive immunity and represent a major component of protection against viral infections and tumors<sup>154</sup>. The recent SARS-CoV-2 pandemic allowed the rapid development of novel vaccine platforms and shed light on the role of CD8 T cells during infection and vaccination. CD8 T cells represent a critical component of immunity against severe disease<sup>155</sup> and are indispensable to achieve control of viral replication<sup>156</sup>. Vaccination-induced CD8 T cells can protect against infection in the absence of neutralizing antibodies<sup>157,158,159</sup> and are more durable than antibody titers<sup>160</sup>. Similarly, CD8 T cells can prevent the transmission of respiratory viruses independently of virus-specific antibodies and CD4 T cells<sup>161</sup>. More importantly, while rapidly evolving viruses can easily escape antibody responses<sup>162</sup>, they remain susceptible to recognition by vaccination-induced CD8 T cells that are cross-reactive to a wide range of viral variants<sup>159,163,164</sup>.

The development of CD8 T cell-eliciting vaccines has been historically difficult, but obstacles have now been reduced by the generation of effective platforms, especially those based on viral vectors<sup>165,42</sup>. Although viral vaccines represent a promising technology for the induction of potent cellular immunity, concerns have been raised regarding the safety of replication-competent platforms<sup>66,166</sup>, especially in the context of prophylactic vaccination. Replication-deficient vectors represent a safer approach due to their inability to propagate within the host, and some can induce levels of immunity comparable to their replication-competent counterpart<sup>70,28,69</sup>. Still, it is unclear which molecular determinants of viral vectors account for long-lasting CD8 immunity. The cytolytic effect of certain platforms has been proposed to represent a major driving of immunogenicity<sup>167</sup>, and it has been shown that cellular responses can differ between pairs of vectors with different cytolytic activity<sup>168</sup>. Furthermore, while antigen dose is commonly thought of as an important determinant of the potency of CD8 T cell responses<sup>96</sup>, the impact of type I interferon (IFN-I) induction on vector immunogenicity is controversially debated<sup>95,169-171</sup>. The relationship between vector cytolytic behavior and these critical factors of immunity remains elusive and a better understanding of the underlying principles will help advancing vaccine design.

In this study, we assessed the mechanisms that underlie CD8 T cell stimulation and longevity by replication-deficient non-cytolytic rLCMV and cytolytic rVSV vectors. While rLCMV-induced responses were long lived and effector-differentiated, those to rVSV contracted more rapidly and had a memory phenotype. Abrogation of rVSV cytolytic activity by means of matrix protein mutations (rVSVMq) resulted in improved CD8 T cell induction and longevity. Vaccination with rVSVMq induced substantially higher levels of systemic IFN-I, and adoptive transfer experiments revealed the dependency of rVSVMq-induced responses on direct IFN- $\alpha$  receptor (IFNAR) signaling by antigen-specific CD8 T cells. Our findings identify the non-cytolytic feature of replication-deficient viral vectors as a key determinant of substantial systemic IFN-I induction, which in return drives sustained CD8 T cell responses.

## Results

### **Non-cytolytic rLCMV vectors persist longer than cytolytic rVSV vectors and induce long-lived antigen-specific CD8 T cell responses**

To study and compare the ability of rVSV and rLCMV vectors to induce CD8 T cell immunity, we employed replication-deficient vectors where the glycoprotein gene was replaced by the prototypic model antigen ovalbumin (OVA). In order to determine the effect of the viral surface protein on the induction of CD8 T cell immunity, we generated rVSV-OVA and rLCMV-OVA carrying their respective own glycoprotein but also rLCMV vectors pseudotyped with VSV glycoprotein (rLCMV/VSVG-OVA) as well as rVSV vectors pseudotyped with LCMV glycoprotein (rVSV/LCMVGP-OVA). The four vectors were administered intravenously (i.v.) and CD8 T cell frequencies in blood were measured over time using MHC class I tetramers (Figure 1A and 1B). At Day 7 after immunization, all vectors elicited similar frequencies of OVA-specific CD8 T cells in blood (Figure 1C). The responses elicited by rLCMV-OVA and rLCMV/VSVG-OVA remained stable up to day 20, whereas rVSV-OVA- and rVSV/LCMVGP-OVA-induced CD8 T cells contracted 5- and 4-fold, respectively. These data suggest that rLCMV-induced CD8 T cell responses are more durable than those to rVSV, irrespective of the glycoprotein the vectors carry. Furthermore, the phenotype of responding CD8 T cells varied greatly between rLCMV- and rVSV-based vectors. By day 20 after immunization the response to the former consisted predominantly in effector-memory CD8 T cells (KLRG1<sup>+</sup> CD127<sup>-</sup>) while the response to the latter was dominated by more resting memory CD8 T cells (KLRG1<sup>-</sup> CD127<sup>+</sup>) (Figure 1D).

One main difference between VSV and LCMV consists in their cytolytic and non-cytolytic life cycles, respectively. Unlike rLCMV, which replicates without any noticeable cytopathic effect, rVSV causes infected cells to round up and detaching within 6 hours after inoculation (Figure 1E). Taking into account that these replication-deficient vectors cannot propagate from cell to cell, antigen expression is limited to the first round of infected cells and the cytolytic activity of the vector can represent a limiting factor for the amount of antigen expressed *in vivo*, thought to be a major determinant of vector immunogenicity<sup>94,95</sup>. In order to study the vectors' persistence *in vivo* we generated vectors expressing secreted nanoluciferase (snLuc), which can be sampled from serum to serve as a measure of the total amount of antigen expressed in the animal's body. Intravenous administration of recombinant snLuc revealed further that the protein's *in vivo* half-life was in the order of 1 hour, validating serum snLuc activity as a surrogate of active protein synthesis by vector-infected cells (Supplementary Figure 1). Four vectors analogous to those expressing OVA were generated and were administered to mice i.v. (Figure 1F). Similar levels of snLuc activity was detected at 6 hours after administration, irrespective of the vector used. By 24 hours after administration, however, snLuc activity in animals receiving rVSV

vectors had markedly declined, while snLuc expression by rLCMV vectors was still on the rise. By day 5, rVSV-expressed snLuc had dropped below detection limits while rLCMV-driven antigen expression was detectable until around day 10. These results indicated that rLCMV can persist *in vivo* expressing antigen for longer periods of time than rVSV. These observations raised the possibility that increased antigen availability for longer periods of time could provide a better stimulation to CD8 T cells, culminating in the more durable and effector-differentiated CD8 T cell response observed.

To test the ability of the various vector formats to boost OVA-specific CD8 T cell response upon re-administration, we performed a second immunization at day 21, in a homologous prime-boost regimen (Figure 1G). By day 28, 7 days after boost, only vaccination with vectors pseudotyped with LCMV glycoprotein induced a significant increase in circulating OVA-specific CD8 T cells. The frequencies of CD8 T cells to rLCMV-OVA and rVSV/LCMVGP-OVA were boosted 4.8 and 6.9-fold, respectively. While also VSVG-pseudotyped vectors showed a trend towards higher CD8 T cell frequencies after booster vaccination, these differences failed to reach statistical significance. Responses to the four vectors remained stable during an observation period of 21 days after boost. These results show that even though the viral glycoproteins did not measurably influence the primary responses, they had a major impact on the secondary response upon homologous boosting, with vectors carrying LCMV-GP allowing for a more efficient boost of antigen-specific CD8 T cell response than VSVG-pseudotyped ones.

Pre-existing anti-vector immunity and notably vector-neutralizing antibodies can interfere with homologous prime-boost immunization regimens<sup>117</sup>. LCMV and VSV glycoproteins differ substantially in their ability to elicit neutralizing antibodies<sup>40</sup>. To determine vector-neutralizing antibody induction by the different vectors, serum samples from immunized mice were assessed for their neutralization activity (Figure 1H). The two vectors that carried LCMV glycoproteins, i.e. rLCMV-OVA and rVSV/LCMVGP-OVA, did not exhibit any detectable LCMV-neutralizing antibody titer, neither prior to nor after homologous boost. On the contrary, VSV neutralizing antibodies were induced after single immunization with VSV glycoprotein-pseudotyped rVSV-OVA and rLCMV/VSVG-OVA, and these neutralizing titers increased further after homologous boost. These data suggest that the differential ability of the vectors to boost CD8 T cell responses is largely due to the differential induction of vector-neutralizing antibodies after primary immunization.

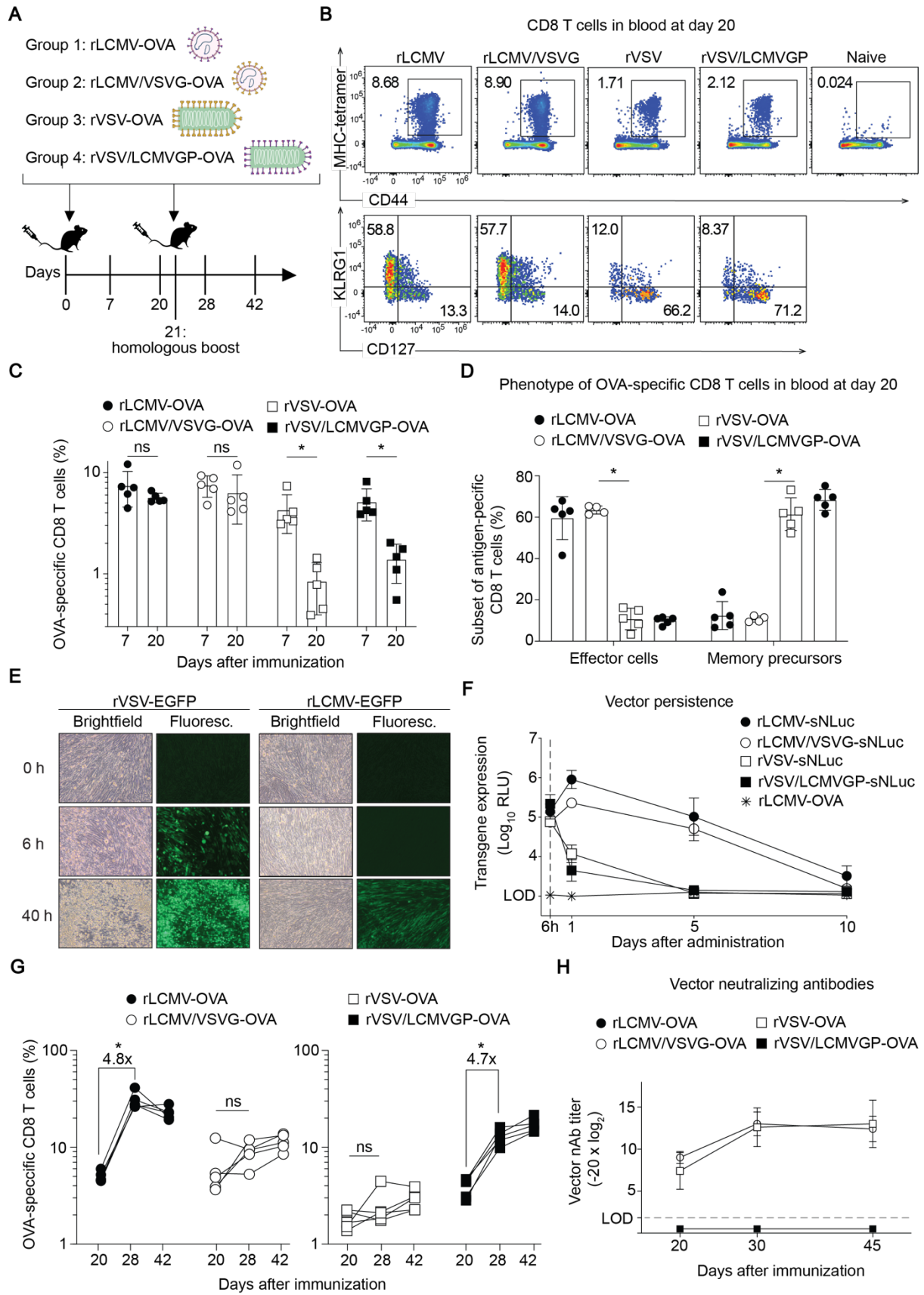


Figure 1. (A) Experimental design. Mice were immunized intravenously with 1E+06 PFU of rLCMV, rVSV or their reciprocal pseudotypes, expressing the ovalbumin protein, and blood samples were collected for MHC-I tetramer staining or neutralization assays. (B) Representative FACS plots of MHC-tetramer binding CD8 T cells and their phenotype based on KLRG1 and CD127 expression in blood at day 20 after immunization. (C) Frequencies of MHC-tetramer binding CD8 T cells in blood at days 7 and 20 after immunization with rLCMV- or rVSV-derived vectors. (D) Frequencies of MHC-tetramer binding CD8 T cells with an effector (KLRG1<sup>+</sup>/CD127<sup>-</sup>) or memory (KLRG1<sup>-</sup>/CD127<sup>+</sup>) phenotype in blood at day 20 after immunization. (E) Cytopathic effect of EGFP-expressing rLCMV and rVSV after infection of BHK21 cells. (F) Luciferase activity in serum of wild type mice immunized with snLuc-expressing vectors carrying VSVG or LCMVGP. Samples from mice immunized with rLCMV-OVA were used as technical background. (G) Frequencies of MHC-tetramer binding CD8 T cells in blood after primary (day 20) and secondary homologous (days 28 and 42) immunization with rLCMV- or rVSV-derived vectors. (H) Vector-neutralizing antibodies present in serum of vaccinated mice with rLCMV- or rVSV-derived vectors over time. Statistical analysis was performed with two-way ANOVA with Bonferroni's posttest for multiple comparisons (C, D and G); ns: not significant; \* P < 0.01.

## **Non-cytolytic rVSVMq induces long-lived effector-differentiated CD8 T cell memory and provides better protection against *Listeria* challenge**

We hypothesized that abrogating rVSV cytolytic activity might lead to prolonged antigen expression and by consequence improve the CD8 T cell response. For this, we employed an attenuated VSV matrix protein quadruple mutant vector (rVSVMq), which lacks host shut-off activity and does not cause cytopathic effect in cell culture<sup>54</sup>. As reported previously, rVSVMq cytolytic activity was abrogated, whereas rVSV induced pronounced rounding and detachment of Vero E6 cells from the flask surface over time (Figure 2A). In order to measure the CD8 T cell response, rLCMV, rVSVMq and rVSV vectors expressing the subunit 1 of SARS-CoV-2 spike protein (S1) were administered to mice and MHC-I tetramer-binding CD8 T cells in blood were analyzed over time (Figure 2B and 2C). As observed with the OVA-expressing vectors, responses to rLCMV-S1 were more durable than those to rVSV-S1, which again showed a strong contraction by day 14 after administration (Figure 2D). Immunization with rVSVMq-S1, however, induced frequencies and kinetics of S1-specific CD8 T cell that were similar to rLCMV-S1. Unlike rVSV-S1 induced CD8 T cell frequencies, which decreased by two weeks after immunization, the rVSVMq response expanded by day 14 and was maintained at high frequencies until day 21. Similar observations were made in an independent experiment comparing analogous vectors expressing OVA (see supplementary Figure 2A and B). Furthermore, we observed similar dynamics in the total numbers of S1-specific CD8 T cells from spleens of mice immunized with the three vectors (see supplementary Figure 2C). Another major difference between rLCMV- and rVSV-induced CD8 responses was the phenotype of the cells (see Figure 1D). As seen above rLCMV-S1 induced CD8 responses that were dominated by effector cells, as indicated by higher abundance of effector subsets KLRG1<sup>+</sup> CD127<sup>-</sup> and CX3CR1<sup>+</sup> CD27<sup>-</sup>, while the contracted rVSV-S1 response was biased towards the KLRG1<sup>-</sup> CD127<sup>+</sup> and CX3CR1<sup>-</sup> CD27<sup>+</sup> memory subsets (Figure 2E and 2F). The rVSVMq-S1 vector also induced higher frequencies of both effector subsets. Although not at the same level as rLCMV, the KLRG1<sup>+</sup> CD127<sup>-</sup> and CX3CR1<sup>+</sup> CD27<sup>-</sup> populations were 5- and 4-fold higher than those induced by rVSV-S1. Similarly, frequencies of memory subsets elicited by rVSVMq-S1 were intermediate between rLCMV and rVSV, with KLRG1<sup>-</sup> CD127<sup>+</sup> and CX3CR1<sup>-</sup> CD27<sup>+</sup> representing 25% and 10% of the total CD8 response, respectively. Antibody responses elicited by rVSV-S1 and rVSVMq-S1 did not differ substantially between these vectors, but rVSV-S1 show a trend towards higher titers of S1-binding antibodies (see supplementary Figure 3)

Finally, we assessed the protective efficacy of the different vaccine vectors against infection with the intracellular pathogen *Listeria monocytogenes*. For this, mice were immunized with the OVA-expressing vectors and challenged 2 weeks later with recombinant bacteria expressing OVA (rLM-OVA). Spleens were collected 3 days after infection to determine bacterial loads (Figure 2G). When compared to naïve animals all three vectors conferred some level of protection and mice immunized with rLCMV were almost free of rLM-OVA. Importantly, rVSV-OVA was only modestly protective while rVSVMq-induced immunity suppressed bacterial loads to 100-fold lower levels than rVSV vaccination. Taken together these data show that the non-cytolytic rVSVMq induces more durable and effector-



differentiated CD8 T cell memory than rVSV, resulting in substantially better protection against Listeria challenge.

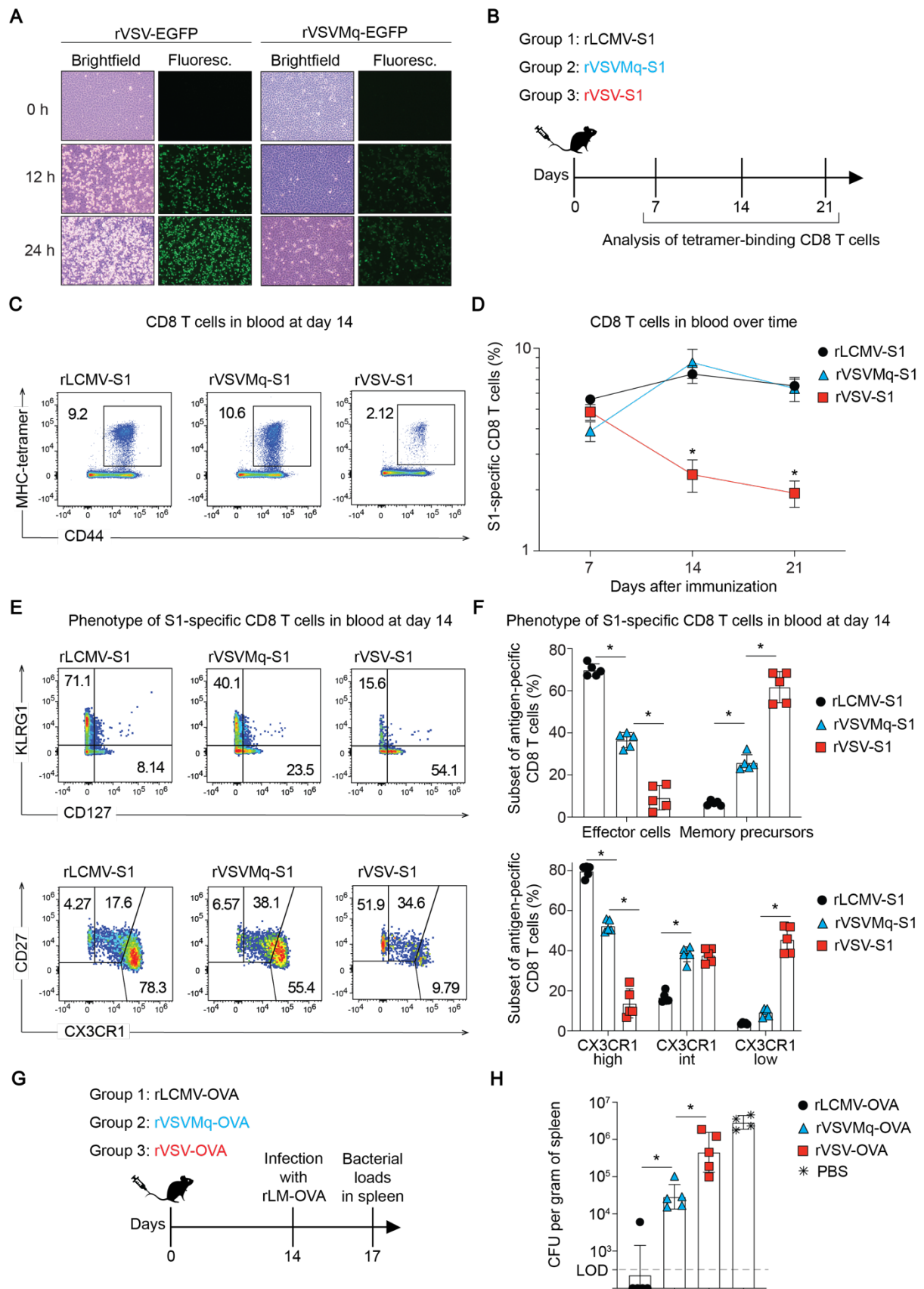


Figure 2. (A) Cytopathic effect of rVSV-EGFP and rVSVMq-EGFP vectors on Vero E6 cells after 0, 12 or 24 hours of incubation. (B) Experimental design. Mice were immunized intravenously with  $1E+05$  PFU of rLCMV, or  $1E+06$  PFU of rVSVMq or rVSV expressing the S1 domain of the SARS-CoV-2 spike protein (Wuhan Hu-1 strain), and blood was collected for MHC-I tetramer staining. (C) Representative FACS plots of MHC-tetramer binding CD8 T cells in blood at day 14 after immunization with rLCMV-S1, rVSVMq-S1 or rVSV-S1. (D) Frequencies of MHC-tetramer binding CD8 T cells in blood over time after immunization with rLCMV-S1, rVSVMq-S1 or rVSV-S1. (E) Gating strategy to identify CD8 T cell effector and memory populations based on KLRG1 versus CD127 and CD27 versus CX3CR1 expression, within S1-specific CD8 T cells at day 14 for the different vectors. (F) Frequencies of effector (KLRG1<sup>+</sup> CD127<sup>-</sup>) and memory precursor (KLRG1<sup>-</sup> CD127<sup>+</sup>) subsets, and CX3CR1-expressing subsets within S1-specific CD8 T cells induced by the different vectors at day 14 after immunization. (G) Experimental design for protection efficacy analysis. (H) Bacterial loads in spleens collected after 3 days of infection with OVA-expressing *Listeria monocytogenes* in mice immunized with the different vectors. Statistical analyses were performed with two-way ANOVA with Bonferroni's posttest for multiple comparisons (D and F) or unpaired two-tailed Student's t tests (H); ns: not significant; \*  $P < 0.01$ .

## The phenotype of rVSVMq-induced CD8 T cell responses resemble those induced by rLCMV

The dynamics of expansion and contraction of rVSVMq-induced CD8 T cells followed a pattern that resembled the one observed in rLCMV-immunized mice rather than responses to rVSV. Furthermore, flow cytometric analysis of surface markers on antigen specific CD8 T cells revealed substantial dissimilarity between the vectors, with rVSVMq inducing higher proportions of effector CD8 T cells than rVSV. In order to characterize the transcriptional profile of these cells, we vaccinated animals with either one of the three vectors and on day 7 and 14 sorted tetramer-binding splenocytes for single cell RNA sequencing (Figure 3A). Projection of the sequencing data onto a t-distributed stochastic neighbor embedding (t-SNE) dimensional reduction space showed the existence of 6 distinct clusters of cells with three more abundant clusters consisting of undifferentiated cells (cluster 1), effector cells (cluster 3) and memory cells (cluster 4), and three smaller clusters containing central memory cells, proliferating effector cells and cells with a pronounced interferon-stimulated gene signature (Figure 3B). An examination of genes differentially expressed between clusters revealed that cluster 3 contained increased expression of genes associated with cytotoxic activity (*Gzma*) and expression of the effector-associated fractalkine receptor, *Cx3cr1*, and *Klrg1* (Figure 3C). Additionally, expression of the migratory sphingosine-1-phosphate receptor 5, *S1pr5*<sup>172</sup>, and the terminal effector differentiation associated gene *Zeb2*<sup>173</sup> were elevated in this cluster. Cluster number 4 contained cells expressing the memory-associated transcription factor *Tcf-7*, the anti-apoptotic regulator *Bcl2* as well as the survival receptor *Ilr*. Cluster number 5 showed a similar memory signature as cluster 4, but had an increased expression of genes encoding lymphoid homing receptors such as L-selectin (*Sell*) and CCR7, indicating a more pronounced central memory phenotype. Cluster 2 shared with cluster number 3 the expression of effector genes such as *Gzma*, but had higher expression of the proliferative marker *Mki-67* (Figure 3D). Further analysis of cell cycle-associated gene expression confirmed that cluster 2 was the only one that contained cells undergoing cell division, indicating that these are proliferating effector cells. Cluster number 6 exhibited a pronounced IFN-stimulated gene signature, with higher expression of *Irf7* and several interferon stimulated genes (see supplementary Figure 4).

Analysis of the differential abundance for the three major clusters 1, 3 and 4 in the different vaccination conditions revealed differential dynamics of CD8 T cell differentiation from day 7 to 14 (Figure 3E and 3F). At day 7 all three vectors induced predominantly undifferentiated cluster 1 cells. Both rVSV-based vectors had a similar representation in the three clusters, but rLCMV already showed an enriched effector (cluster 3) and reduced memory (cluster 4) fractions. By day 14 T cell responses in all groups showed a decreased abundance in cluster 1. Interestingly, however, rVSV and rVSVMq-induced CD8 T cells took different differentiation pathways. While rVSV vaccination resulted in a clear shift towards the memory cluster 4, rVSVMq induced an enrichment in the effector cluster 3. Similar to rVSVMq, rLCMV stimulated cells were also enriched in the effector-differentiated cluster 3. These data corroborated our flow cytometric analysis and documented on a transcriptional level that rVSVMq-induced CD8 T cells were more similar to rLCMV-induced responses than those induced by rVSV, with

an associated differentiation trajectory over time that aligns somewhat with the one of rLCMV-induced CD8 T cells.

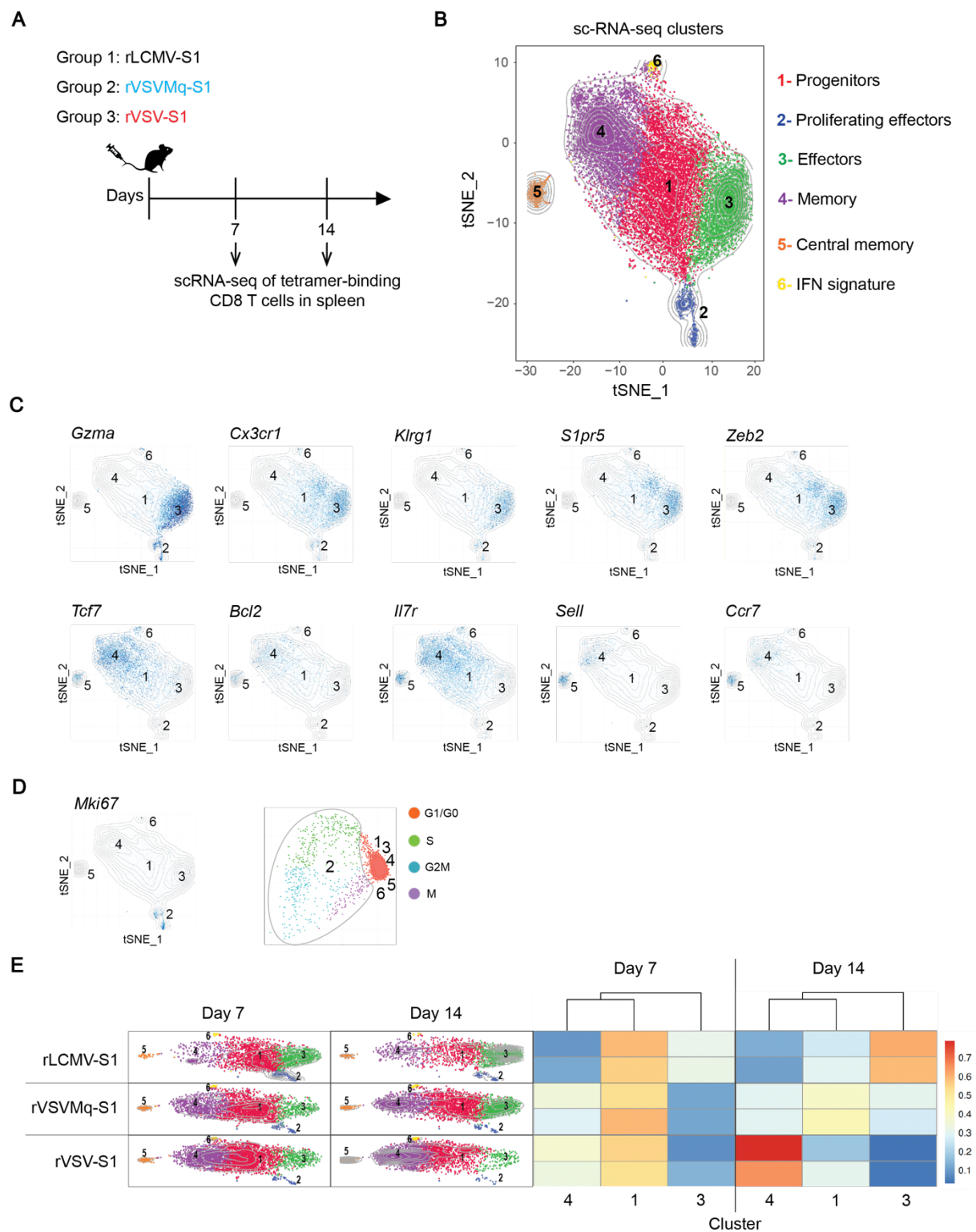


Figure 3. (A) Experimental design. Mice were immunized intravenously with 1E+06 PFU of rLCMV, rVSMQ or rVSV expressing the S1 domain of the SARS-CoV-2 spike protein (Wuhan Hu-1 strain) and spleens were collected at days 7 and 14 for analysis. (B) Clustering of splenic antigen-specific CD8 T cells from 2 mice per condition visualized using t-distributed stochastic neighbour (t-SNE) embedding. Each cell is represented by a point and colored by cluster. (C) Gene expression levels of *Gzma*, *Cx3cr1*, *Klrg1*, *S1pr5* and *Zeb2*, *Tcf7*, *Bcl2*, *Il7r*, *Sell* or *Ccr7*; visualized by color intensity in the t-SNE plot. (D) Gene expression of *Mki67* and tricycle-embedding inference of cell cycle positions within the different clusters. (E) t-SNE plots of individual conditions and heatmap comparing the differential abundance of clusters 1, 3 and 4 for each individual sample at days 7 and 14.

## **rVSVMq vectors express less antigen than rVSV but triggers more IFN-I**

The lack of a cytopathic effect of rLCMV and rVSVMq in cell culture and, when compared to rVSV, more pronounced effector-differentiated CD8 T cell responses were compatible with our initial hypothesis that the former vectors may benefit from longer antigen expression in vaccinated hosts. To formally test this hypothesis, we turned again to snLuc-expressing vectors (Figure 4A). By 6 hours of administration, both rLCMV-snLuc and rVSV-snLuc expressed similar snLuc levels whereas those of rVSVMq-snLuc-vaccinated mice was about 10 times lower. rLCMV-vectored snLuc levels remained constantly until 3 days whereas rVSV-vectored snLuc declined, as expected (compare Fig. 1F). Intriguingly and counter to our expectations, rVSVMq resulted in a decline of snLuc expression parallel to the one of rVSV, reaching background levels on day 3. rVSV-vectored snLuc became undetectable by day 5 whereas sera from animals given rLCMV-snLuc exhibited luciferase activity over background up to day 7 (Figure 4B). The unexpectedly low and transient levels of snLuc expressed by rVSVMq suggested that there may be vector-extrinsic mechanisms that influenced its persistence in the host cell. For instance, interferon responses as well as adaptive immunity can have a major impact on antigen expression levels of viral vectors<sup>117,170,174</sup>. To test the intrinsic ability of the vector to persist *in vivo*, we employed mice that lack type I and II interferon receptors as well as T and B lymphocytes. Both non-cytolytic vectors, rLCMV-snLuc and rVSVMq-snLuc, were able to maintain high levels of snLuc expression in these immunodeficient mice for more than 30 days (Figure 4C), indicating that these single-round vectors persisted in the cells they had infected. In contrast, antigen levels expressed from the cytopathic rVSV-snLuc showed a steady decline, reaching background levels by around day 15. Given that rVSV and rVSVMq carried the same glycoprotein and hence targeted the same cell types indicated that the antigen decay observed by rVSV, but not by rVSVMq, was related to an intrinsic property of the vector rather to the type of cell transduced. Moreover, in animals lacking IFN sensing as well as B and T cells, a non-cytolytic vector life cycle allowed its persistence at constant levels for prolonged periods of time, whereas cytopathic activity caused progressive loss of antigen expression, which was presumably reflective of host cell death.

One of the main consequences of the VSV M proteins host cell shut-off activity is the suppression of the IFN-I response<sup>53,58,59</sup>, and the mutations in the rVSVMq M protein variant disable this function<sup>175</sup>. To assess how differential sensitivity of VSV and VSVMq vectors to IFN-I impacted antigen expression in mice, we analyzed vectored snLuc expression in interferon type I receptor-deficient (IFNAR<sup>-/-</sup>) mice (Figures 4D and 4E). Both vectors showed higher antigen expression in IFNAR<sup>-/-</sup> than in WT mice, but this difference was much more pronounced for rVSVMq-snLuc than for rVSV-snLuc, indicating that the former vector's heightened sensitivity to IFN-I inhibition resulted in substantially reduced antigen expression. Already at 6 hours after administration, rVSVMq-snLuc expressed 100-times less antigen in WT mice than in IFNAR KO mice. By consequence, serum snLuc activity in rVSVMq-vaccinated IFNAR<sup>-/-</sup> mice remained detectable for 2 days after its disappearance from WT mice. By contrast, rVSV-vaccinated WT and IFNAR<sup>-/-</sup> mice showed very similar levels of serum snLuc on 1 day of administration, with only minor differences also on day 3, 5 and 7. These results

corroborate that the matrix protein mutations in rVSVMq result in higher sensitivity of the vector to IFN-I signaling, and highlighted the inability of this mutant vector to evade the resulting innate antiviral response. These data led us to hypothesize that rVSVMq infection of the host cell may result in enhanced IFN-I induction. To test this we measured IFN- $\alpha$  concentrations in the serum immunized animals (Figure 4F). Both non-cytolytic rLCMV and rVSVMq vectors induced similar peak levels of IFN- $\alpha$ , although the response to rVSVMq peaked at 6 hours whereas the one induced by rLCMV reached its maximum at 24 hours. Intriguingly and in contrast to published findings with replicating VSV we failed to detect systemic IFN- $\alpha$  at any timepoints after rVSV administration. Altogether, these results show that the non-cytolytic vectors rLCMV and rVSVMq induce substantially higher levels of systemic IFN-I than cytolitic rVSV, and that the inability of rVSVMq to suppress IFN-I responses resulted in curtailed and shortened antigen expression in vivo.

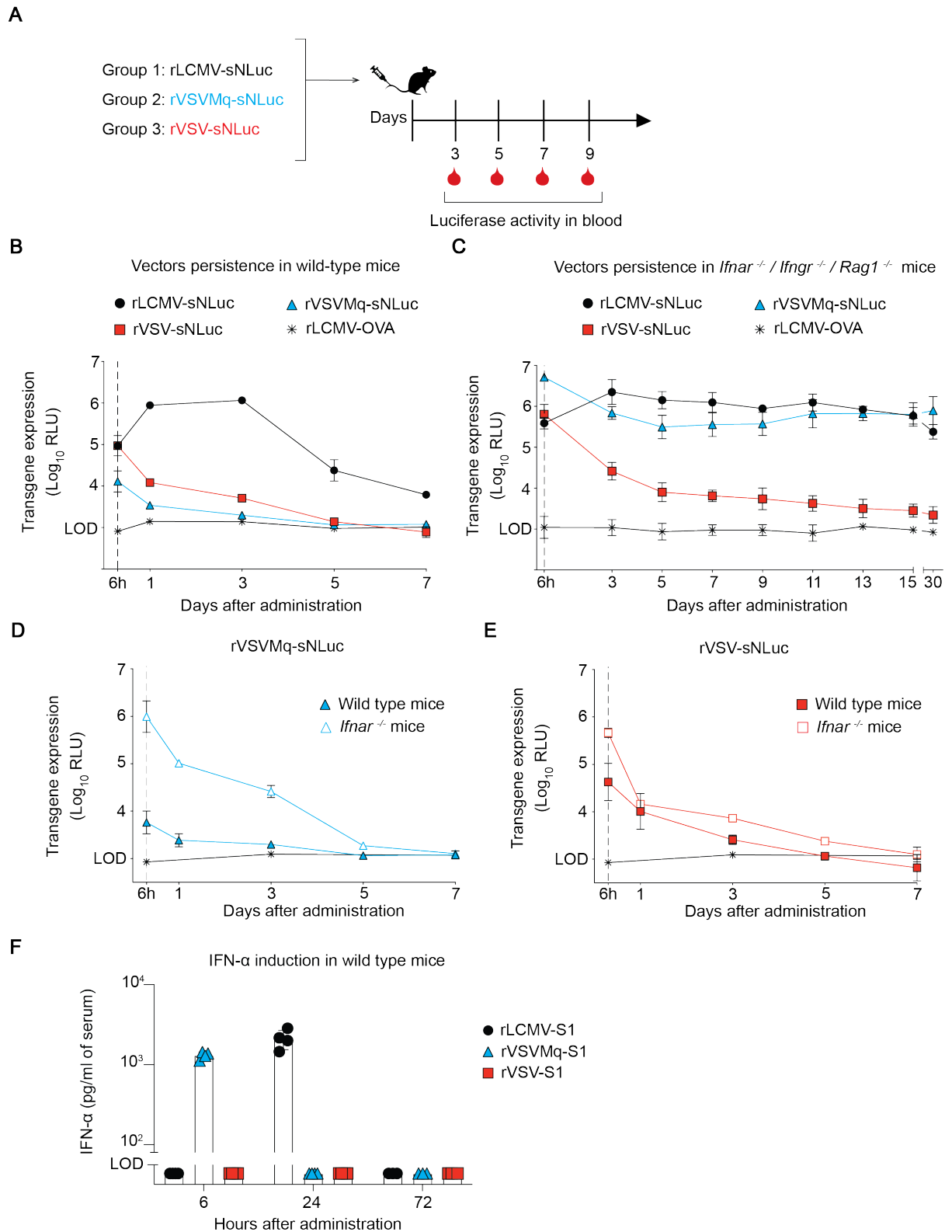


Figure 4. (A) Experimental design. Mice were immunized intravenously with  $1\text{E}+06$  PFU of rLCMV, rVSVMq or rVSV expressing a secreted nanoluciferase and blood samples were collected over time to determine luciferase activity. (B) Luciferase activity in serum of wild type mice immunized with sNLuc-expressing vectors. Samples from mice immunized with rLCMV-OVA were used as technical background. (C) Luciferase activity in serum of *Ifnar*<sup>-/-</sup> / *Ifngr*<sup>-/-</sup> / *Rag1*<sup>-/-</sup> mice immunized with sNLuc-



expressing vectors. (D) Luciferase activity in serum of wild type and *Ifnar*<sup>-/-</sup> mice immunized with sNLuc-expressing rVSVMq. (E) Luciferase activity in serum of wild type and *Ifnar*<sup>-/-</sup> mice immunized with sNLuc-expressing rVSV. (F) IFN- $\alpha$  levels in serum of mice immunized with rLCMV-S1, rVSVMq-S1 or rVSV-S1.

## **rVSVMq promotes IFNAR-dependent expansion of antigen-specific CD8 T cells**

Virus-induced expansion of CD8 T cells can be promoted by IFN-I, the extent of which depends on the infecting pathogen. The observation that rVSVMq expressed less antigen than rVSV but triggered substantially higher IFN- $\alpha$  responses and promoted more durable and effector-differentiated CD8 T cell memory led us to test how these observations were interconnected. To study to which extent IFN-I induction plays a role in the expansion and differentiation of CD8 T cell responses to rVSV and rVSVMq, respectively, we administered to mice an IFNAR-blocking antibody or isotype control, followed by rVSV or rVSVMq expressing S1. On day 7 and day 14 after immunization with rVSV-S1, IFNAR blockade had no clear impact on S1 tetramer-binding CD8 T cells in blood of mice (Figure 5A) (Figure 5B). In remarkable contrast, responses to rVSVMq-S1 were substantially suppressed at both timepoints when IFNAR was blocked (Figure 5C). Furthermore, IFNAR blockade impaired the differentiation of rVSVMq-S1-induced CX3CR1<sup>+</sup> CD27<sup>-</sup> effector CD8 T cells but had little impact on the phenotype of rVSV-induced responses (Figure 5D). These data shows that the magnitude and effector differentiation of CD8 T cells responding to rVSVMq-S1 were much influenced by IFNAR signaling while those elicited by rVSV were largely unaffected IFNAR blockade.

To determine whether IFN-I-driven CD8 T cell expansion and differentiation by rVSVMq depends on CD8 T cell-intrinsic IFNAR signaling we adoptively transferred OVA-specific OT-I CD8 T cells either deficient or sufficient in IFNAR and performed immunizations with rVSV-OVA or rVSVMq-OVA (Figure 5E). In order to avoid NK cell-mediated killing of IFNAR-deficient T cells<sup>176</sup>, anti-NK1.1 antibody was administered one day before and after immunization. When animals were immunized with rVSVMq-OVA frequencies of OT-I-IFNAR<sup>-/-</sup> cells in peripheral blood were 4.5- to 5.8-fold lower than those reached by IFNAR-sufficient OT-I WT cells (Figure 5F). On the contrary, OT-I-IFNAR<sup>-/-</sup> CD8 T cells expanded comparably to IFNAR-sufficient OT-I cells when activated by rVSV-OVA. Responses in the spleen followed the same pattern as those observed in blood. A 9-fold lower expansion of OT-I IFNAR<sup>-/-</sup> cells as compared to IFNAR-sufficient OT-I cells when responding rVSVMq-OVA immunization was even somewhat more pronounced (Figure 5G). In context of rVSV-OVA immunization a trend in the same direction was noted by was not statistically significant. Effector-memory as well as central memory compartments of CD8 T cells responding to rVSVMq immunization depended on CD8 T cell-intrinsic IFNAR signaling. Accordingly, OT-I-IFNAR<sup>-/-</sup> CD8 T cells yielded lower numbers of both CX3CR1<sup>+</sup> CD27<sup>-</sup> and CX3CR1<sup>-</sup> CD27<sup>+</sup> progeny than IFNAR-sufficient OT-I cells (Figures 5H and 5I). These data showed that the more potent CD8 T cell expansion and effector differentiation in response to rVSVMq immunization depended to a significant extent on direct IFN-I signaling to antigen-specific CD8 T cells.

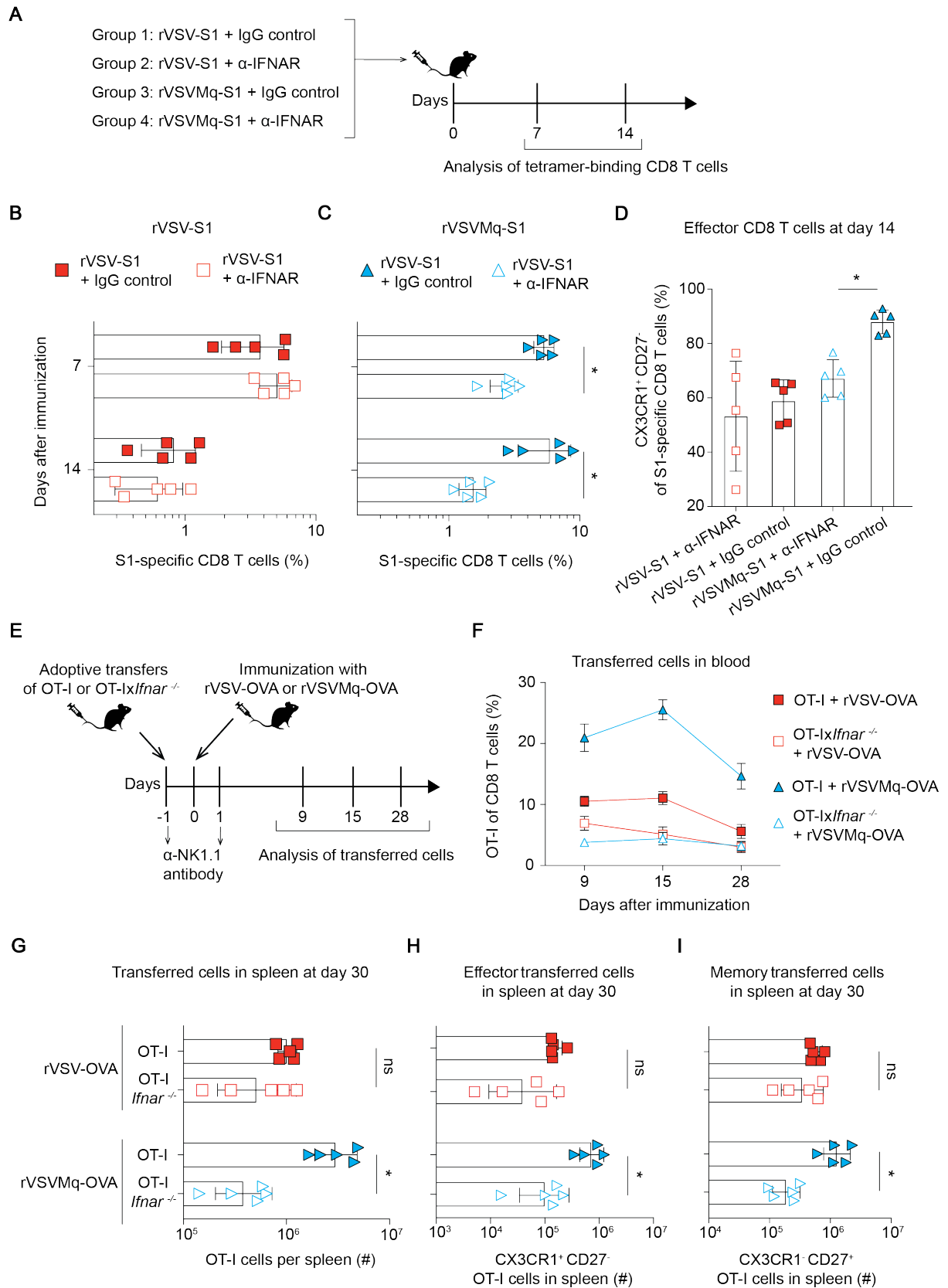


Figure 5. (A) Experimental design. rVSV-S1 or rVSVMq-S1 were administered intravenously at  $1E+06$  PFU in combination with anti-IFNAR antibody or IgG control. (B) Frequencies of S1-specific CD8 T cells in blood after immunization with rVSV-S1 and IgG control or anti-IFNAR antibody. (C) Frequencies of S1-specific CD8 T cells in blood after immunization with rVSVMq-S1 and IgG control or  $\alpha$ -IFNAR antibody. (D) CX3CR1<sup>+</sup> effector CD8 T cell frequencies in blood after immunization with rVSV-S1 or rVSVMq-S1 plus IgG control or  $\alpha$ -IFNAR antibody. (E) Experimental set up of OT-I transfers. Mice received 2000 OT-I or OT-Ix*Ifnar*<sup>-/-</sup> cells intravenously at day -1 and immunized at day 0 with rVSV-OVA or rVSVMq-OVA. NK cell-depleting antibody was administered at days -1 and 1. (F) Frequencies of transferred cells in blood of mice immunized with rVSV-OVA or rVSVMq-OVA over time. (G) Total numbers of transferred cells in spleens of mice immunized with rVSV-OVA or rVSVMq-OVA at day 30. (H) Total numbers of transferred cells with an effector phenotype (CX3CR1<sup>+</sup>/CD27<sup>-</sup>) in spleens of mice immunized with rVSV-OVA or rVSVMq-OVA at day 30. (I) Total numbers of transferred cells with a memory phenotype (CX3CR1<sup>-</sup>/CD27<sup>+</sup>) in spleens of mice immunized with rVSV-OVA or rVSVMq-OVA at day 30. Statistical analyses were performed with two-way ANOVA with Bonferroni's posttest for multiple comparisons (B, C, D, G, H and I); ns: not significant; \*  $P < 0.01$ .

## **rVSVMq vaccination allows antigen-specific CD8 T cells to spatio-temporally integrate cognate antigen and IFN-I signals**

The above experiments indicated that IFN-I induction by rVSVMq was directly sensed by responding CD8 T cells, promoting their expansion and differentiation into effector cells. To determine the spatial relationships between vector-transduced cells, IFN-I producing cells, and antigen specific CD8 T cells, we adoptively transferred OT-I cells into wild-type mice, followed by rVSVMq-OVA-EGFP immunization two days later. Spleens were harvested at various timepoints around the 6 hours peak of IFN- $\alpha$  production (Figure 6A, compare Figure 4F). Immunohistochemical analyses of tissue sections revealed that most of the GFP expressing cells were located in the marginal zone of the spleen (Figure 6B). Furthermore, a majority of these vector-transduced cells produced IFN- $\alpha$ , and the abundance of these cells paralleled the kinetics of IFN- $\alpha$  peaking in blood at 6 hours after rVSVMq administration (Figure 6B and 6C). As judged by histology, IFN- $\alpha$  production was very transient with only few remaining IFN- $\alpha$  positive cells in the spleen by 12 hours after immunization (Figure 6D). Importantly, a substantial proportion of transferred OT-I cells were localized in the marginal zone in immediate proximity to IFN- $\alpha$ -expressing, vector-transduced (GFP+) cells, suggesting cognate interactions as early as 6 hours after immunization. OT-I cells started to form clusters around GFP-positive cells, indicating their recruitment into the immune response. By 18 to 24 hours after immunization, IFN- $\alpha$  producing cells became undetectable, but the transferred cells continued to cluster and co-localize with vector-transduced cells (Figures 6E and 6F). Taken together, these observations suggested that antigen-specific CD8 T cells engage with VSVMq-transduced antigen presenting cells (APCs) in the marginal zone as early as 6 hours after immunization and continue to form conglomerates with vector-transduced cells up to at least 24 hours post-immunization. Importantly also, early interactions of CD8 T cells at 6 hours after vaccination comprise APCs that not only express (and likely present on MHC class I) cognate antigen but that produce also high amounts of IFN-I, allowing CD8 T cells to integrate signals of antigen-specific priming with IFNAR signaling.

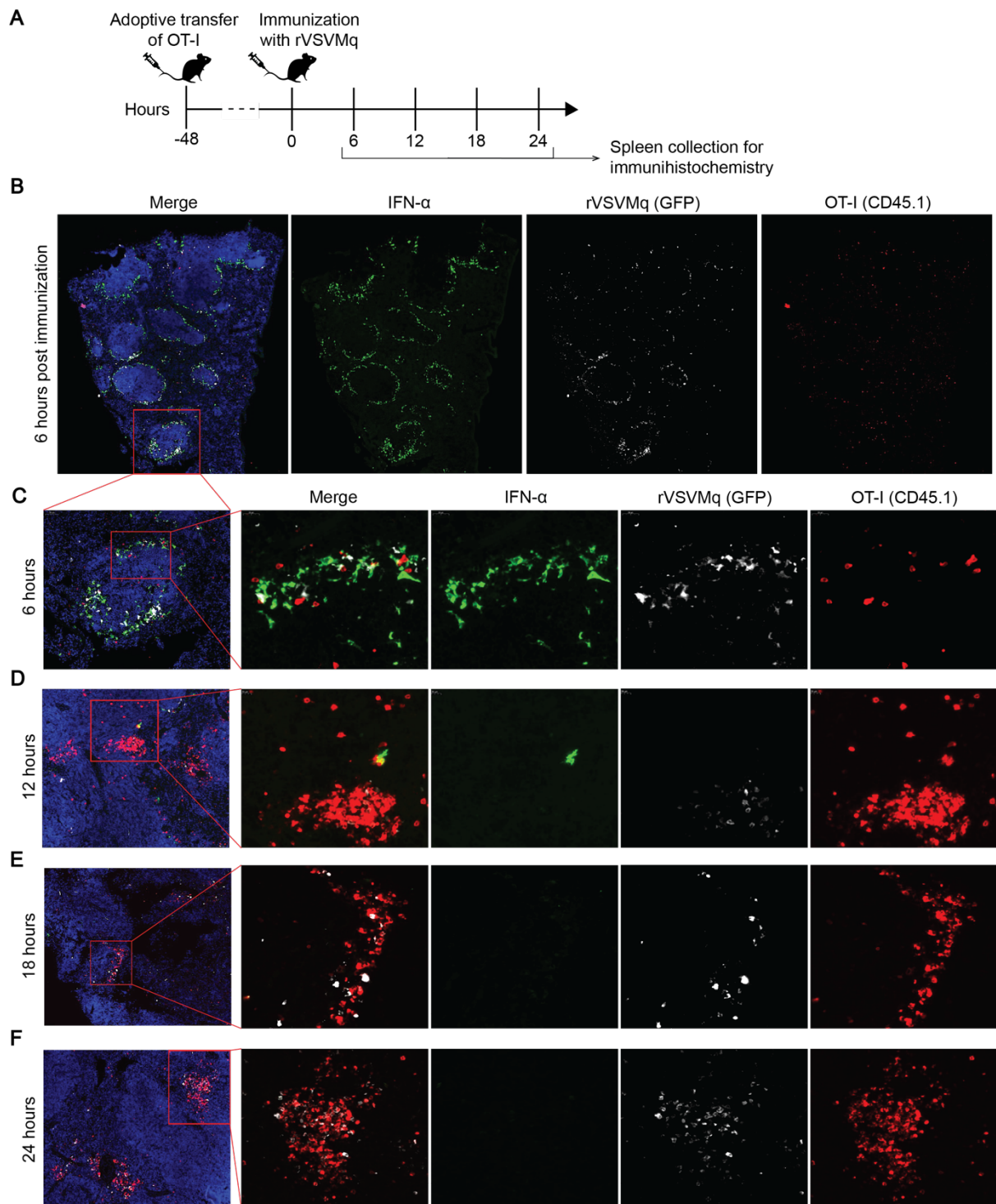


Figure 6. (A) Experimental design. Mice received  $2E+06$  OT-I cells and were immunized intravenously with rVSVMq-EGFP-OVA two days later. Spleens were collected at 6, 12, 18 and 24 hours after immunization for immunohistochemistry. (B-F) Spleen sections were stained for IFN- $\alpha$ , GFP and CD45.1.

## Discussion

Vaccines that induce robust and durable CD8 T cells represent important prophylactic and therapeutic approaches against a range of infections and tumors. Due to their safety profile, replication-deficient viral vectors represent a useful platform for clinical translation. In this study, we show that the non-cytolytic behavior of replication-deficient vectors is key for the induction of protective and durable CD8 T cell responses. The characterization of these responses by single-cell transcriptional analysis demonstrated that antigen-specific CD8 T cells induced by rVSVMq exhibited a differentiation trajectory towards an effector phenotype, resembling more closely the responses to rLCMV rather than to the parental rVSV. Adoptive transfer experiments demonstrated that substantial IFN-I induction was a requirement for the increased CD8 T cell expansion after immunization with rVSVMq, but not for those responses to rVSV. Furthermore, we could observe the co-localization of vector-transduced IFN-producing cells and antigen-specific CD8 T cells at the peak of the IFN-I response. The concomitant induction of IFN- $\alpha$  and CD8 T cell engagement revealed by our immunohistochemical analysis suggest that IFN-I signaling is acting in-sequence with T cell receptor (TCR) triggering, which has been previously shown to promote proliferation, survival and effector cell differentiation<sup>177</sup>.

In addition to our main findings, we observed that vector glycoprotein swap did not have a substantial effect during primary responses. Although the vector surface protein is a major determinant factor of vector tropism and subsequent primary immune response<sup>178</sup>, we did not observe major differences with respect to antigen expression levels and CD8 T cell responses with paired vectors carrying LCMVGP or VSVG. Even though these glycoproteins interact with different cell surface receptors<sup>38,64</sup>, vectors carrying LCMVGP or VSVG infect dendritic cells with the same efficiency<sup>65</sup>, which could explain why pseudotyping did not have a major influence on CD8 T cell induction. On the other hand, vector glycoprotein had a strong impact upon homologous boosting, with vectors pseudotyped with LCMVGP being more efficient at inducing secondary responses than those with VSVG. We observed that these differences were associated to strong induction of vector-neutralizing antibodies detected after immunization with VSVG-pseudotyped vectors compared to LCMVGP, which has also been observed in previous studies on replicating vectors<sup>40,120</sup>.

We observed that the magnitude of the CD8 T cell response to rVSV and rVSVMq was similar at 7 days after immunization, but immunization with the cytolytic rVSV caused a much drastic contraction. Previous studies have assessed the effect of cytolytic vector activity on immunogenicity, using paired rabies vectors expressing VSV M<sub>wt</sub> or VSV M<sub>33,51</sub> double mutant. The higher cytopathic vector accelerated the expansion of CD8 T cells, but this response did not differ from its non-cytopathic pair by day 30 after immunization<sup>168</sup>. A major difference that can account for the discrepancies between these and our results may be related to the use of vectors with reduced cytolytic activity, but not completely abrogated, as is the case of VSV M<sub>33,51</sub> double mutant<sup>54</sup>. We showed that the quadruple matrix mutations in rVSVMq allowed its persistence in immunodeficient mice for more than 30 days, with very similar kinetics to rLCMV, strongly suggesting the absence of vector cytolytic effect in vivo.

Our study supports prior observations by Hoffmann, et al., that found long term survival of rVSVMq-infected cells in vitro<sup>54</sup>.

A key finding of this study is that systemic IFN-I production is a general requirement for non-cytolytic viral vector-induced CD8 T cell immunity. Prior studies have shown that type I IFN induced upon viral infections can signal CD8 T cells directly during the expansion phase to promote their survival in memory populations<sup>107,179,180</sup>, but the role of vaccination-induced IFN-I is less clear. It has been shown that IFN-I blockade can enhance the immunogenicity of different types of viral vaccines by promoting antigen expression<sup>170</sup>. Moreover, IFN-I signaling triggered upon adenoviral vector vaccination limits the expansion of CD8 T cells<sup>95</sup>. In contrast, vaccination with the attenuated modified vaccinia virus Ankara (MVA) induces IFN-I responses that promote CD8 T cell expansion and humoral immunity<sup>169,171</sup>. In the specific case of VSV, CD8 T cell responses induced after infection have been shown to be entirely independent of IFN-I<sup>181</sup>. Our results support this finding, since co-administration of rVSV with IFNAR-blocking antibody or the absence of IFNAR on CD8 T cells did not affect the response. On the contrary, the same experiments showed that high CD8 T cell expansion to rVSVMq vaccination was dependent on IFNAR-signaling. Furthermore, IFN-I induction was substantially higher after administration of rVSVMq compared to rVSV. These results align with previous studies that observed very different inflammatory environments induced by rVSV *M<sub>wt</sub>* and rVSV M variants, where the later was shown to promote better maturation and cytokine production upon infection of dendritic cells<sup>65</sup>.

In summary, this study highlights the potential of non-cytolytic, replication-deficient viral vectors in generating potent and long-lasting CD8 T cell immunity, underscored by the necessity of systemic IFN-I production. These insights refine our understanding of the immunological mechanisms behind successful vaccination strategies and emphasize the potential of such viral vectors in developing safe and effective vaccines against diverse infections and tumors. This work paves the way for refined vaccine design harnessing the full potential of viral vectors in immunotherapy.



## **Limitations of the study**

The data generated in the present study come from mouse models and may not fully replicate human immunology and predict the clinical applicability of these results. Furthermore, the immunization route was exclusively intravenous, which may imperfectly mirror intramuscular administration as the most commonly exploited route of vaccine vector delivery in clinical settings. However, i.v. immunization exhibit lower variability than i.m. in mice and therefore represents a more robust route for the purpose of mechanistic studies. Additionally, the extrapolation of these findings to other vector platforms requires further validation, as it has been shown that IFN-I stimulation of CD8 T cells can depend on the pathogen evaluated<sup>181</sup>. These limitations highlight the need for broadening the scope of future research to include diverse viral vectors and immunological contexts, thereby enhancing the generalization and clinical applicability of the findings.

## Methodology

### Animal experiments

C57BL/6 wt mice were purchased from Charles River laboratories and were kept under specific-pathogen-free conditions for colony maintenance and experiments. *IFN $\alpha$ / $\beta$ R<sup>-/-</sup>*, *IFN $\gamma$ R<sup>-/-</sup>*, *RAG1<sup>-/-</sup>* triple-deficient mice<sup>182</sup>, *IFN $\alpha$ / $\beta$ R<sup>-/-</sup>* mice<sup>183</sup> and OT-I mice<sup>184</sup> in a C57BL/6 background have been described previously. Experimental groups were sex- and age-matched. Mice were bred at the ETH Phenomics Center Zurich (EPIC), whereas experiments were performed at the University of Basel in accordance with the Swiss law for animal protection and with permission by the Cantonal Veterinary Office of Basel City. Vector immunizations were performed at a dose of 1E+06 PFU/mouse unless specified differently and administered in a volume of 200  $\mu$ l into the tail vein.

### Vector generation and titration

The reverse genetic engineering of rLCMV-OVA vectors using a polymerase I-/ polymerase II-based plasmid system has been described<sup>43</sup>. For the generation of rLCMV-S1 and rLCMV-sNLuc, the viral glycoprotein gene was replaced with cDNA of the subunit 1 of SARS-CoV-2 spike protein (strain Wuhan-Hu-1, comprising the immunodominant epitope VNFNFNGL), or the secreted nanoluciferase (Promega) into the respective vectors using similar cloning strategies previously described<sup>43</sup>. The rLCMV vectors were grown in BHK23 cells and titrated by immunofocus assay<sup>40</sup> on 293T-GP cells. For generation of rVSV and rVSVMq vectors, VSVG-deleted genomic plasmids pVSV $\Delta$ G and pVSVMq $\Delta$ G were produced by replacing VSV glycoprotein with ovalbumin, the subunit 1 of SARS-CoV-2 spike protein or the secreted nanoluciferase genes, with the EGFP gene with molecular cloning, growth in BHK-G43 cells and titrated as previously described<sup>54</sup>.

In order to produce pseudotyped vectors, rLCMV vectors were grown in BHK-G43 cells<sup>54</sup> to produce rLCMV/VSVG. In brief, expression of VSVG in BHK-G43 cells was induced by adding 1E-9 M of Mifepristone to the culture medium and incubated for 6 hours. After incubation, cells were infected with rLCMV at MOI: 0.01 for 3 hours. Cell were washed with PBS, and incubated with new media at 37°C. Vectors were harvested after 72 hours and stored at -80°C. rVSV vectors were grown in BHK23 cells<sup>43</sup> to produce rVSV/LCMVGP, at an MOI: 0.1.

### Flow cytometry

Blood samples were stained immediately after collection with antibodies against CD45R/B220 (RA3-6B2), CD8 (53-6.7), CD44 (IM7), CD62L (MEL-14), CD127 (A7R34), Klrp1 (2F1), CX3CR1 (SA011F11), CD27 (LG3A10) and CD43 (1B11) purchased from BioLegend and subsequently treated with FACS lysing solution (BD Biosciences, Cat. #349202) to remove erythrocytes and fix the cells. For detection of S1-specific CD8 T cells, H2-Kb tetramers were conjugated to PE and loaded with the SARS-CoV-2 spike epitope (VNFNFNGL). For detection of ovalbumin-specific CD8 T cells, H2-Db tetramers were conjugated to PE and loaded with the SIINFELK epitope. Peptide-MHC tetramers were

prepared by the University of Lausanne Tetramer core facility. The tetramers were added to the antibody mix for staining. Spleens were mechanically disrupted and counted with a Immunospot S6 device (C.T.L.). For surface staining, splenocytes were incubated with the same cocktail of antibodies and tetramer as used for blood with the addition of anti-erythroid cells antibody (TER-119). Dead cells were stained with Zombie-NIR Fixable Viability Kit (BioLegend, Cat: #423105). Samples were fixed by incubation with 2% paraformaldehyde for 15 minutes at room temperature. All samples were measured on a 5-laser Aurora spectral flow cytometer (Cytex Biosciences, Fremont, CA, USA) and analyzed with FlowJo Software (BD Biosciences).

### **Neutralization assays, luciferase activity, S1 ELISA and IFN- $\alpha$ measurements**

Microtainer tubes (Becton-Dickinson) were used for serum collection. Immunofocus reduction assays were used for the detection of LCMV neutralizing antibodies<sup>185</sup>. VSV neutralizing antibodies were measured by plaque reduction assays<sup>186</sup>.

Luciferase luminescence in serum samples was measured using the Nano-Glo® Luciferase Assay kit (Promega, Madison, USA), a Sapphire Tecan infinite plex plate reader and white 96-well luciferase plates (Thermo Fisher Scientific Nunc A/S). For determination of snLuc in vivo half-life, snLuc coding sequence was cloned into pCAGGS mammalian expression plasmid and HEK-293T cells were transfected with Lipofectamine 2000 (ThermoFisher). After 24 hours, cell supernatant was harvested to determine luciferase activity. Supernatant was administered i.v. into the tail vein of C57BL/6 mice and blood samples were collected at different timepoints. Luciferase activity was measured from the serum. The half-life of snLuc was determined by non-linear regression and one phase decay parameters using GraphPad Prism version 10.2.1.

For detection of S1-specific antibodies, high-binding 96-well flat bottom plates (Sarstedt AG & Co.KG) were coated with 50 ng of spike protein per well in 50  $\mu$ L coating buffer over night at 4 °C. Plates were washed twice with PBS-T (0.05% Tween-20/PBS), then blocked with 200  $\mu$ L 5% BSA/PBS-T at room temperature for 45 min. 2-fold serial dilutions of serum samples in blocking solution were performed after washing five times with PBS-T. Plates were incubated at 37 °C for 1 h and washed five times with PBS-T. Peroxidase-conjugated polyclonal anti-mouse antibody (1:2000 in blocking solution; Jackson, 115-035-062) was added and the plates were incubated at 37 °C for 60 min. After washing five times with PBS-T, HRP activity was detected using ABTS as a chromogen (Pierce) and the absorbance was measured at 405 nm using the Sapphire plate reader (Tecan). Arbitrary units are computed as  $\ln(1000 \times A_{491nm})$ ; the limit of detection corresponds to the maximum value reached by negative controls.

Concentrations of IFN- $\alpha$  in serum were determined using the VeriKine Mouse Interferon Alpha ELISA Kit (PBL Assay Science).

## **Listeria challenge**

The recombinant *Listeria monocytogenes* expressing ovalbumin has been described<sup>187</sup>. The bacteria were grown in blood-heart infusion media (Sigma-Aldrich) at 37°C, harvested during the exponential growth phase and washed with phosphate-buffered saline. A dose of 1E+03 colony forming units (CFU) was administered intravenously to mice for infections.

## **scRNA-sequencing and bioinformatic analyses**

Tetramer binding CD8 T cells were enriched with magnetic-activated cell sorting (CD8+ T cells Isolation Kit, mouse, STEMCELL), but the antibody mix was replaced for a mix containing the following biotin-conjugated antibodies against B220 (RA3-6B2), CD19 (6D5), Ly-76 (TER-119), CD4 (H129.19) and CD138 (281-2). Tetramer-binding CD8 T cells were FACS sorted (FACS Aria II, BD). Samples went immediately for cell capture and library preparation using the 10x Genomics Chromium Controller and Chromium Single Cell 5' Reagent kits version 3 according to the manufacture's instruction. Paired-end sequencing was performed with the NovaSeq 6000 (Illumina) using an S1 Reagent Kit version 1 (100 cycles) at the Genomics Facility Basel (28 nucleotides for the cell barcode and unique molecular identifier, 8 for the sample index, and 91 for the transcript read).

Sequencing data was processed via Cellranger software from 10X Genomics, version 3.1.0, utilizing a transcriptome reference mm10-3.0.0. Raw molecule information from Cellranger was subjected to a lenient filtering process. The step involved discarding cells exhibiting fewer than 100 unique molecular identifier (UMI) counts and those with over 60000 UMI counts to eliminate potential doublets. The UMI matrix derived from this process was further refined to retain only cells with a log library size greater than 3.3, log number of features above 3.0, a percentage of mitochondrial reads of 5% or less, and percentage of ribosomal protein reads of 20% or more. The normalization of this data was performed using the deconvolution method available in the scran package from R. Scran was also utilized to model technical noise present in gene expression data and to identify biologically significant highly variable genes by distinguishing technical variance from biological variance, employing a false discovery rate (FDR) of less than 0.05 and a threshold for biological variance greater than 0.1. A t-distributed stochastic neighbor embedding (t-SNE) was generated with a perplexity setting of 75. Hierarchical clustering of cells was performed using Ward's method on the PCA-derived distance matrix. The clustering outcomes were optimized to match the highest average silhouette width through the use of a default dendrogram cut height, determined by the dynamicTreeCut package in R. To identify genes defining each cluster, comparisons between cells within a cluster and those across all other clusters were made using the limma package from R.

## **In vivo IFNAR blockade and NK cell depletion**

For IFNAR blocking mice were given 1 mg of anti-IFNAR monoclonal antibody (MAR-1-5A3, BioXcell) in the same injection mix containing viral vectors. Control groups were administered 1 mg of isotype control antibody (MOPC-21, BioXcell) in the same mix with viral vectors. For transfer experiments

involving OT-Ix/*Ifnar*<sup>-/-</sup> cells, NK cells were depleted by administration of 300 mg of anti-NK.1.1 (PK136, BioXcell) monoclonal antibody to mice on day -1 and on day 1 of vector immunization, as described in<sup>176</sup>.

### **Adoptive transfers**

For OT-I cells transfer, single cell suspensions were prepared from spleens of naive OT-I or OT-Ix/*Ifnar*<sup>-/-</sup> C57BL/6J donor mice. Purification of CD8 T cells was performed with magnetic-activated cell sorting (naïve CD8 T+ T cells Isolation Kit, mouse, Miltenyi Biotec). The purity (>95%) was checked before transfer by FACS. Cells were administered i.v. into the tail vein of C57BL/6J recipients at 2000 cells/mouse for Figure 5 experiments or 2E+06 cells/mouse for Figure 6 experiments. Transferred OT-I populations were differentiated from the recipient's cells by means of the oncogenic marker CD45.1.

### **Immunohistochemistry**

For immunofluorescence analysis of spleen sections, OT-I cells were MACS-purified (Miltenyi Biotec naive CD8+ T cell isolation kit, mouse) from the spleens of naive donor mice and 2E+06 cells were injected i.v. into the tail vein of wild-type recipient mice followed by vector immunization 2 days later. Animals were sacrificed at the indicated time points and spleens fixed in 1% PFA in PBS, infiltrated with 30% sucrose and then embedded and frozen in OCT compound (Tissue-Tek, Sakura Finetek Europe). Tissue cuts were stained for IFN- $\alpha$ , GFP and CD45.1 as described previously<sup>188</sup>. In brief, cryostat sections were collected on Superfrost Plus Slides (Fisher Scientific), air dried and preincubated with blocking solution (bovine serum albumin with mouse and chicken serum (Sigma) in 0.1% Triton/PBS). Then they were incubated overnight at 4C with primary antibodies in 0.1% Triton/PBS. After washing with 0.1% Triton/PBS, the secondary detection reagents were added for 2 hours at room temperature in 0.1% Triton/PBS. After additional wash, the slides were mounted in 1,4-Diazabicyclo-2-octan (DABCO). Sections were visualized following whole image capture using a Hamamatsu NanoZoomer S60 and an 40x objective, utilizing a 8-bit color CMOS camera (Hamamatsu Photonics). Images were processed using NDP-viewer 2 software (Hamamatsu Photonics).

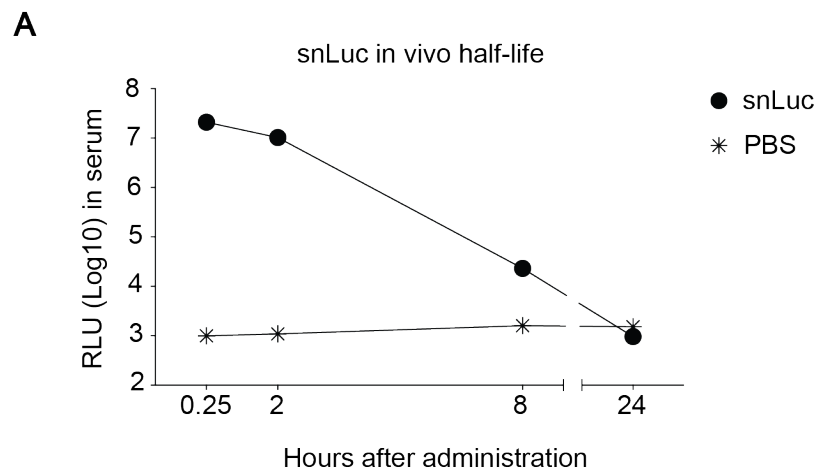
### **Acknowledgements**

We wish to thank Karsten Stauffer for his exceptional support in animal handling and care, Min Lu and Karen Cornille for excellent technical support. We also thank Christian Beisel and Mirjam Feldkamp from the Genomics Facility Basel of the University of Basel and D-BSSE of ETH Zurich for single-cell RNA-seq library preparation and next generation RNA sequencing; Ilena Vicenti and Cynthia Saadi for their assistance with immunohistochemistry. We acknowledge the DBM flow cytometry core facility and Morgane Hilpert for their help with cell sorting. Lastly, we are grateful to the entire Experimental Virology group for their helpful discussions.

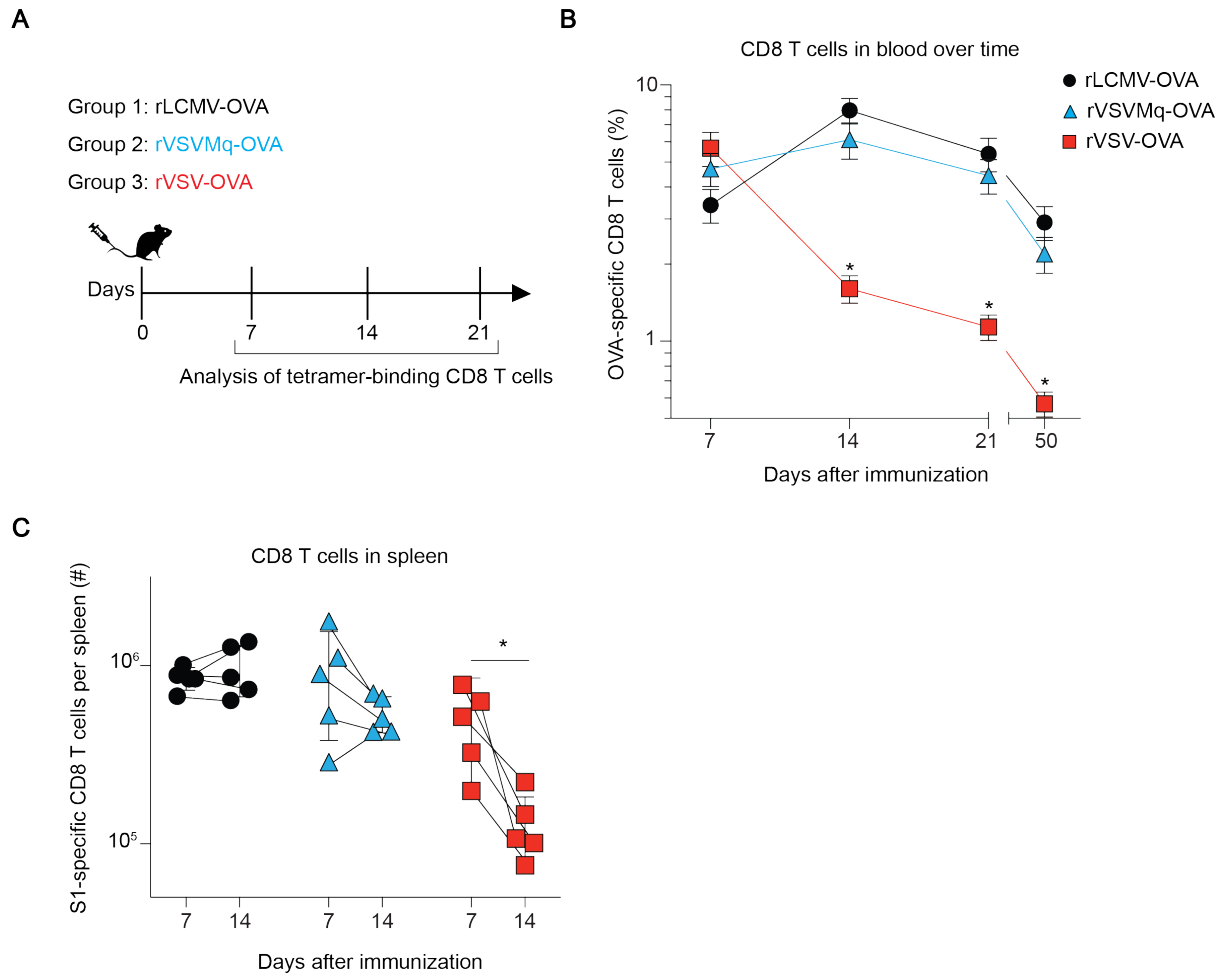
## **Funding**

This project has received funding from the European Union's Horizon 2020 research and innovation programme under the Marie Skłodowska-Curie grant agreement No 812915.

## Supplementary figures



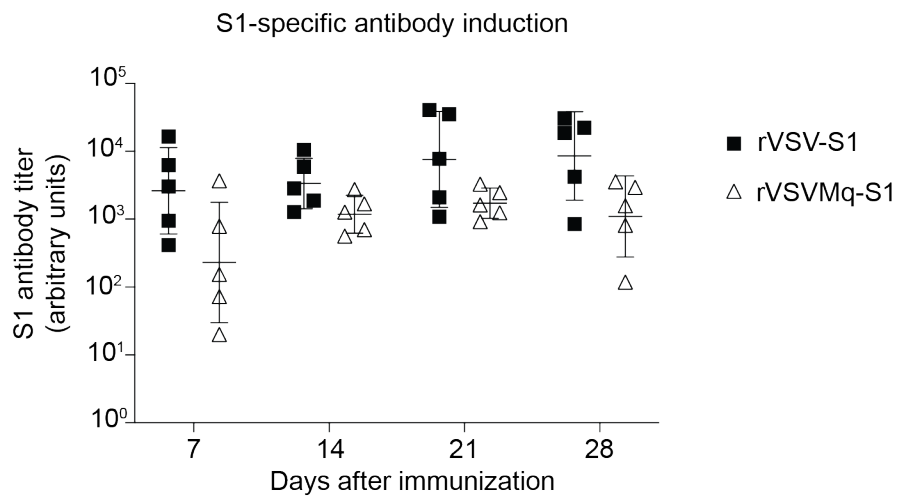
Supplementary Figure 1. Mice were immunized i.v. with  $1E+08$  RLU of snLuc, and blood was collected to determine luciferase activity in serum. Half-life of snLuc in serum was 0.7 hours, as determined by one phase decay analysis with non-linear regression in Prism Graphpad.



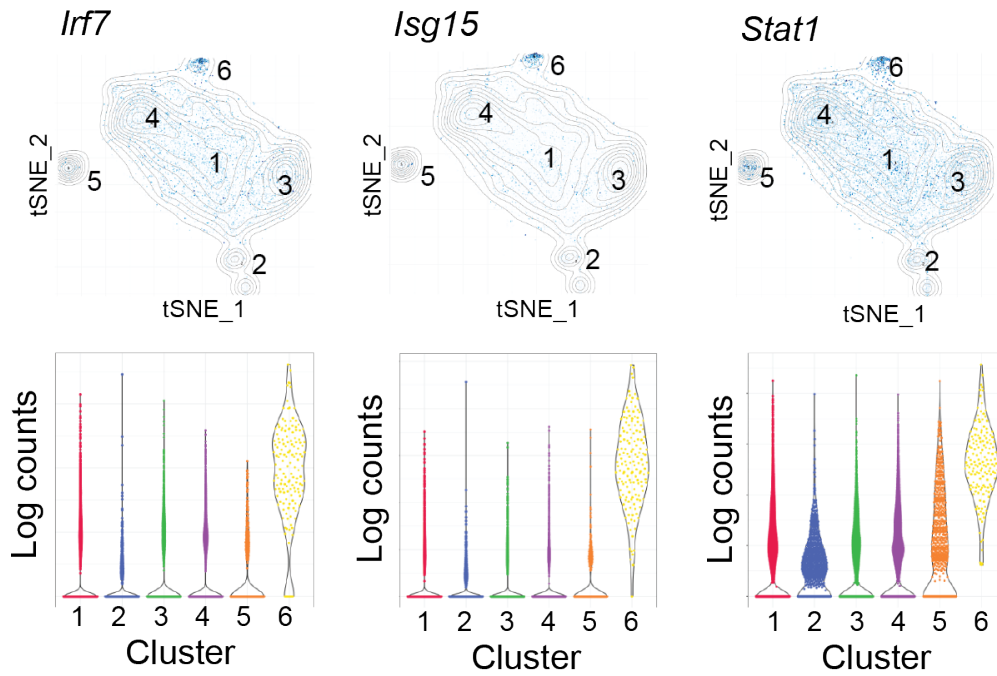
Supplementary Figure 2. (A) Experimental design. Mice were immunized intravenously with  $1E+05$  PFU of rLCMV, or  $1E+06$  PFU of rVSVMq or rVSV expressing OVA, and blood was collected for MHC-I tetramer staining. (B) Frequencies of MHC-tetramer binding CD8 T cells in blood over time after immunization with rLCMV-OVA, rVSVMq-OVA or rVSV-OVA. (C) Mice were immunized with rLCMV-S1, rVSVMq-S1 or rVSV-S1 and spleens were collected at days 7 and 14. Total numbers of S1-specific CD8 T cells were determined by tetramer staining. Statistical analyses were performed with two-way ANOVA with Bonferroni's posttest for multiple comparisons (B and C); \*  $P < 0.01$ .



A



Supplementary Figure 3. Mice were immunized i.v. with 1E+06 PFU of rVSV-S1 or rVSVMq-S1, and blood was collected at different time points to determine S1-binding antibodies in serum.



Supplementary Figure 4. Gene expression levels of *Irf7*, *Isg15* and *Stat1*; visualized by color intensity in the t-SNE plot and their respective violin plots.

# **Homologous mRNA prime-boost vaccination promotes clonal continuity in germinal centers and breadth of neutralizing antibody responses**

Matias Ciancaglini<sup>1</sup>, Mirela Dimitrova<sup>1</sup>, Denice Weklak<sup>2</sup>, Ingrid Wagner<sup>3</sup>, Doron Merkler<sup>3</sup>, Florian Kreppel<sup>2</sup>, Daniel Pinschewer<sup>1\*</sup>.

<sup>1</sup> Department of Biomedicine, University of Basel, Petersplatz 10, 4051 Basel, Switzerland.

<sup>2</sup> Institute for Biochemistry and Molecular Medicine, Center for Biomedical Education and Research (ZBAF), Department of Human Medicine, Faculty of Health, Witten/Herdecke University, Witten, 58453, Germany.

<sup>3</sup> Department of Pathology and Immunology, University of Geneva, Geneva, Switzerland.

\*Corresponding author: Daniel D. Pinschewer, M.D., Department of Biomedicine-Haus Petersplatz, Division of Experimental Virology, 4009 Basel, Switzerland. E-Mail: [daniel.pinschewer@unibas.ch](mailto:daniel.pinschewer@unibas.ch).

Phone: +41 79 543 39 70

## **Abstract**

The generation of affinity-matured plasma and memory B cells, induced by the germinal center response to Severe Acute Respiratory Syndrome Coronavirus 2 (SARS-CoV-2) vaccination, is essential for the prevention of symptomatic infection. In this study, we examined how mRNA- and adenovirus-based vaccination regimens differ in their ability to induce and maintain these germinal center responses. Both homologous mRNA and heterologous adenovirus/mRNA vaccinations induced similar levels of spike-specific B cells and neutralizing antibodies. However, mRNA immunization led to longer-lived germinal center reactions that further expanded with a booster dose. By fate-mapping of germinal center B cells during primary immunization, we aimed to assess their participation in secondary germinal centers upon homologous or heterologous boost immunizations. Notably, larger numbers of primary activated B cells within secondary germinal centers, induced by RNA homologous prime-boost, were associated with better neutralization of SARS-CoV-2 Beta and Omicron variants. These findings highlight the differential ability of SARS-CoV-2 vaccine regimens to sustain germinal center reactions and its impact on the breadth of neutralizing antibody responses.

## Introduction

Vaccinations activate the adaptive immune system and establish, predominantly through germinal center (GC) reactions, long-lasting and protective antibody responses<sup>189</sup>. These GC reactions are critical for generating high-affinity and durable antibodies, as well as memory B cells (MBCs). Upon antigen re-encounter, MBCs proliferate and differentiate into antibody secreting cells (ASCs) or re-enter GCs to undergo new rounds of antigen-driven selection and affinity maturation<sup>190</sup>. The mutational load of MBCs is commonly lower than the one in ASCs<sup>191</sup>, and they tend to have broader reactivity allowing them to recognize a broader range of pathogen variants<sup>192</sup>. Their ability to enter secondary GCs enables them to further refine their affinity and adapt to antigenic variants<sup>193</sup>. These two characteristics are of critical importance to promptly mount high-affinity antibody responses to rapidly evolving viruses, as is the case of SARS-CoV-2<sup>194</sup>.

Vaccination against SARS-CoV-2 has been a global success involving a diverse collection of novel vaccine technologies mainly including mRNA and adenoviral vector-based platforms<sup>195</sup>. These vaccines express the full-length spike protein of SARS-CoV-2 and are able to elicit virus-neutralizing antibodies, a main correlate of protection from symptomatic infection<sup>196</sup>. mRNA-1273 and ChAdOx-1 nCoV-19 vaccines are able to induce GC reactions that are critical for serum antibody and MBC formation, and can be boosted upon secondary immunization<sup>197,198</sup>. Since ChAdOx1 vaccination was later associated with immune thrombotic thrombocytopenia, many individuals that had received a ChAdOx1 prime were subsequently boosted with an mRNA vaccine<sup>199,200</sup>. This combination ChAdOx1/mRNA prime-boost regimen showed somewhat enhanced immunogenicity<sup>88,201</sup>. However, there are no studies directly comparing the ability of these vaccination regimens to induce and boost the germinal center reaction, leaving the relative contributions of each regimen to the GC response unclear.

In this study we used mouse models to determine antigen-specific GC B cell induction by mRNA or adenoviral vector vaccines and their capacity to re-engage previously activated B cells into secondary GC upon homologous or heterologous boost immunizations. Fate-mapping experiments showed that mRNA homologous prime-boost elicited GCs with higher numbers of cells that were the progeny of the primary GC B cell response than ChAdOx-1/mRNA or ChAdOx-1/ChAdOx-1 immunizations did. More importantly, reactivated secondary GCs elicited by mRNA/mRNA correlated with elevated breadth, i.e. a higher proportion of variant cross-reactive neutralizing antibodies.

## Results

### Primary antigen specific B cell responses to mRNA-1273 immunization are longer-lived than those to ChAdOx-1

To compare the spike-specific B cell response elicited by primary immunization with mRNA-1273 and ChAdOx-1 in intramuscularly (i.m.) immunized C57BL/6 mice (Figure 1A). Inguinal lymph nodes (iLNs) were collected and stained with spike protein tetramers to quantify antigen-specific B cells. Both vaccines induced a spike-specific B cell response at 14 days after immunization, yet the mRNA-induced response was 10 times higher in terms of spike-binding B cell count (Figures 1B and 1C). Among the spike-specific B cells, both vaccines induced similar proportions of class-switched (IgM-IgD<sup>-</sup>) cells. Analysis of GL7 on GC B cells and CD38 expression on MBCs revealed that on day 14 the response to mRNA vaccination consisted mostly of GC B cells with a small proportion of MBCs, while ChAdOx-1 induced these two subsets of spike-specific B cells in approximately equivalent proportions (Figures 1D and 1E). Surprisingly and even though mRNA immunization elicited higher numbers of spike-specific B cells, the total number of GC B cells was similar in the two vaccination settings (Figure 1F). Accordingly, the proportion of spike-binding B cells within the total GC B cell response was significantly higher in mRNA-1273 than ChAdOx-1 vaccination (Figures 1G and 1H). Indirectly, these data suggest that a substantial part of the ChAdOx-1 induced GC B cell compartment is directed against antigens other than spike. Likely, at least some portion thereof represented the well-known response to adenoviral backbone antigens<sup>116,117,202</sup>.

mRNA vaccination has been shown to induce GC reactions that are sustained for months after primary immunization<sup>203</sup>. When comparing the spike-specific B cell response at day 14 to day 28 after immunization, responses to mRNA as well as to ChAdOx-1 had contracted. Spike-binding B cells remained, however, readily detectable after mRNA-1273 vaccination while responses of most ChAdOx-1-immunized animals were in the range of non-vaccinated controls (Figure 1I). Moreover, and irrespective of the vaccine administered, the proportion of germinal center B cells amongst spike-specific B cells had declined (Figure 1J and 1K). Altogether these data showed that mRNA-1273 induced a longer-lived spike-specific B cell response than ChAdOx-1, and that the latter response comprises a substantial proportion of non-spike-specific B cells, which likely comprised adenoviral backbone-directed B cells.

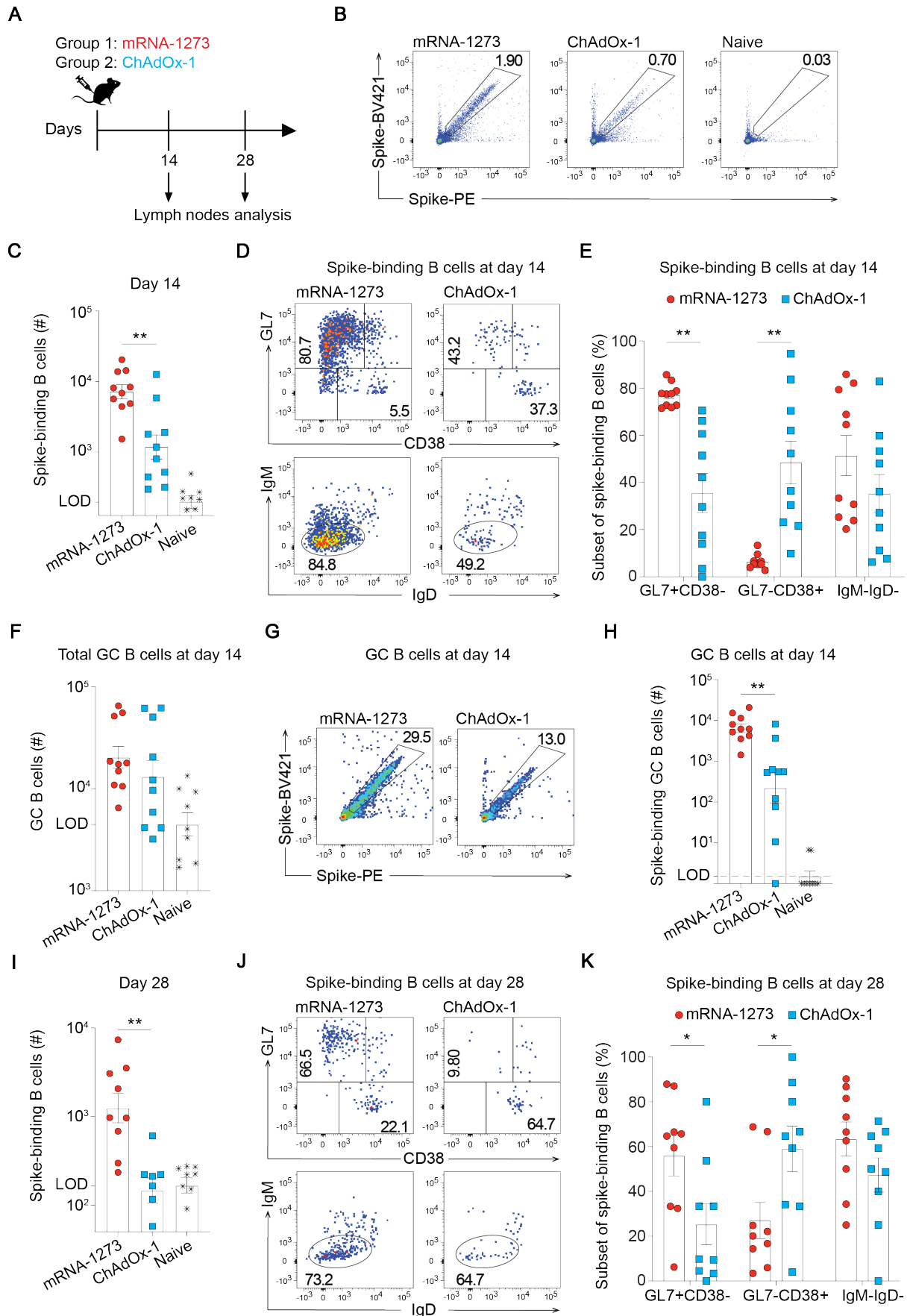


Figure 1. (A) Experimental design. Mice received mRNA-1273 or ChAdOx-1 i.m. on day 0. iLNs were collected at 14 and 28 days. (B) Representative FACS plots of spike-binding B cells in inguinal lymph nodes from mice immunized with mRNA-1273 or ChAdOx-1 after 14 days (C) Spike-binding B cell numbers in inguinal lymph nodes from mice immunized with mRNA-1273 or ChAdOx-1 at day 14. (D) Representative FACS plots of GC (GL7<sup>+</sup> CD38<sup>-</sup>) and memory (GL7<sup>-</sup> CD38<sup>+</sup>), or class-switched (IgM<sup>-</sup> IgD<sup>-</sup>) spike-binding B cells at day 14. (E) Percentages of GC (GL7<sup>+</sup> CD38<sup>-</sup>), memory (GL7<sup>-</sup> CD38<sup>+</sup>) or class-switched B cells (IgM<sup>-</sup> IgD<sup>-</sup>) among spike-binding B cells at day 14. (F) Total numbers of GC B cells in inguinal lymph nodes at day 14. (G) Representative FACS plots of spike-binding B cells within the GC compartment at day 14. (H) Total numbers of spike-binding GC B cells in inguinal lymph nodes at day 14. (I) Spike-binding B cells in inguinal lymph nodes at day 28 after immunization. (J) Representative FACS plots of GC (GL7<sup>+</sup> CD38<sup>-</sup>) and memory (GL7<sup>-</sup> CD38<sup>+</sup>), or class-switched (IgM<sup>-</sup> IgD<sup>-</sup>) spike-binding B cells at day 28. (K) Percentages of GC (GL7<sup>+</sup> CD38<sup>-</sup>), memory (GL7<sup>-</sup> CD38<sup>+</sup>) or class-switched B cells (IgM<sup>-</sup> IgD<sup>-</sup>) among spike-binding B cells at day 28. Statistical analysis was performed with one-way ANOVA with Tukey's post-tests. P values <0.05 were considered significant (\*), P < 0.01 as highly significant (\*\*), and P > 0.05 was considered as not statistically significant (not indicated).



### **mRNA-1273/mRNA-1273 and ChAdOx-1/mRNA-1273 vaccination regimens induce secondary GC B cell responses of similar magnitude**

Next, we compare the immunogenicity of mRNA-1273 or ChAdOx-1 homologous prime-boost immunization to ChAdOx-1/mRNA-1273 heterologous prime-boost as clinically employed in several countries and yielding higher antibody titers than the respective homologous vaccination regimens<sup>201,204</sup>. Prime and boost were conducted i.m. on the ipsilateral side with at 4-week interval (Figure 2A). At two weeks after secondary immunization, the two mRNA-boosted groups had comparable numbers of spike-binding B cells, while the response to homologous ChAdOx-1 boost was about 10-fold lower (Figure 2B). Most of the spike-specific B cells in mRNA-boosted mice had a GC phenotype and were class-switched, while MBCs were rare. In two separate experiments about half of the ChAdOx-1/ChAdOx-1-immunized animals exhibited a fairly low percentage of spike-specific class-switched and GC B cells, with a correspondingly increased fraction of MBCs (Figures 2C and 2D). This virtually binary distribution within the experimental group remains currently unexplained.

Unlike in primary immunization, where mRNA-1273 and ChAdOx-1 had elicited similar total numbers of GC B cells, mRNA-1273 boost, either homologous or heterologous, resulted in significantly higher total numbers of GC B cells than those elicited by the homologous ChAdOx-1 prime-boost regimen (Fig. 2E, compare Fig. 1F). Likewise, the spike-binding GC B cell response to ChAdOx-1/ChAdOx-1 was significantly lower than the one elicited by either mRNA-1273/mRNA-1273 or ChAdOx-1/mRNA-1273 immunization (Figures 2F and 2G).

Spike-specific CD8 and CD4 T cell responses were analyzed by MHC class I tetramer staining and by antigen-induced marker (AIM) assays, respectively. Primary immunization with ChAdOx-1 induced significantly higher numbers of splenic tetramer-binding CD8 T cells than mRNA-1273, whereas spike-specific CD4 T cell responses were inconsistently detected irrespective of the immunization (supplementary Figure 1A and B). Analogously to the B cell response, mRNA-1273 homologous prime-boost and ChAdOx-1/mRNA-1273 heterologous prime-boost induced similar numbers of spike-specific CD8 and CD4 T cells, both of which were significantly higher than those elicited by ChAdOx-1 homologous prime-boost, respectively (supplementary Figure 1A-D). These results documented that homologous mRNA-1273/mRNA-1273 and heterologous ChAdOx-1/mRNA-1273 prime-boost induced spike-specific CD8 and CD4 T cell responses of similar magnitude, both of which were significantly higher than those elicited by homologous ChAdOx-1 vaccination.

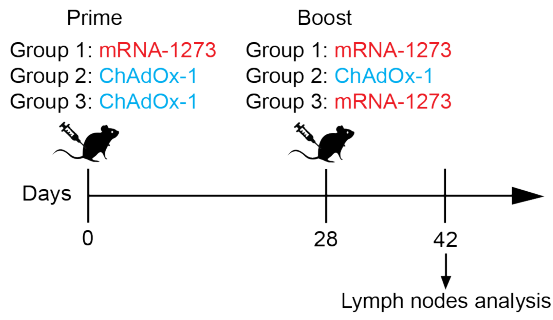
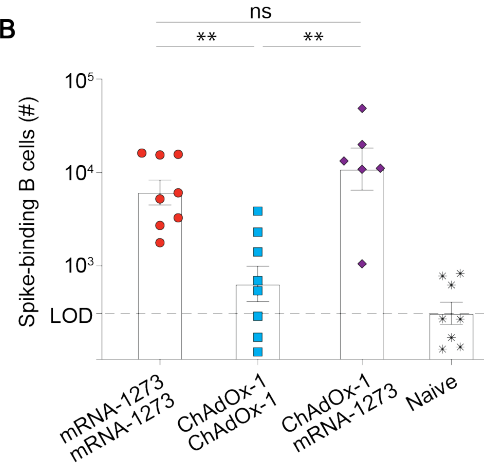
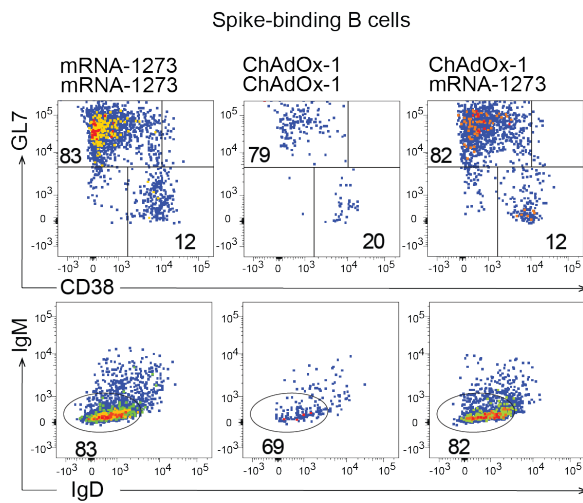
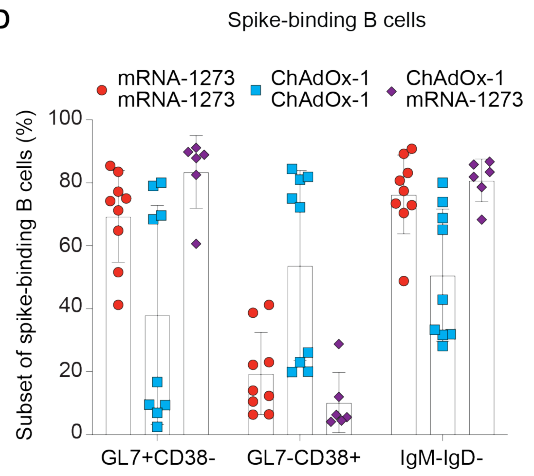
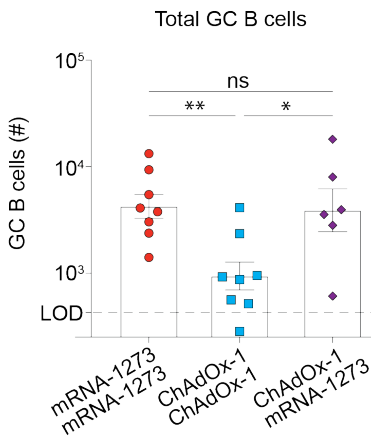
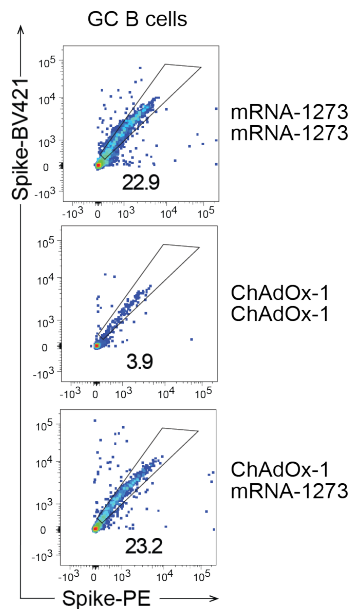
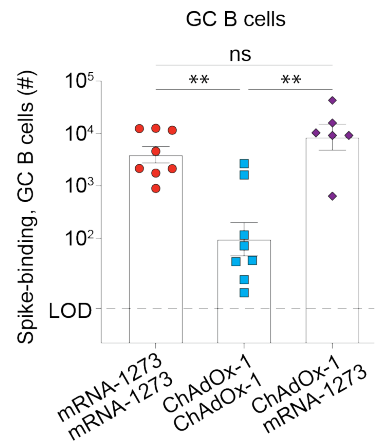
**A****B****C****D****E****F****G**

Figure 2. (A) Experimental design. Mice received i.m. immunizations with mRNA-1273 or ChAdOx-1 at day 0 and a boost with mRNA-1273 or ChAdOx-1 as indicated. iLNs were collected at day 42 and analyzed by flow cytometry. (B) Total numbers of spike-binding B cells in inguinal lymph nodes at day 42. (C) Representative FACS plots of GC (GL7<sup>+</sup> CD38<sup>-</sup>) and memory (GL7<sup>-</sup> CD38<sup>+</sup>), or class-switched (IgM<sup>-</sup> IgD<sup>-</sup>) spike-binding B cells at day 42. (D) Percentages of GC (GL7<sup>+</sup> CD38<sup>-</sup>), memory (GL7<sup>-</sup> CD38<sup>+</sup>) or class-switched B cells (IgM<sup>-</sup> IgD<sup>-</sup>) among spike-binding B cells at day 42. (E) Total numbers of GC B cells in inguinal lymph nodes at day 42. (F) Representative FACS plots of spike-binding GC B cells at day 42. (G) Total numbers of spike-binding GC B cells in inguinal lymph nodes at day 42. Statistical analysis was performed with one-way ANOVA with Tukey's post-tests. P values <0.05 were considered significant (\*), P < 0.01 as highly significant (\*\*), and P > 0.05 was considered as not statistically significant (ns).

## Homologous mRNA-1273 prime-boost vaccination results in superior clonal continuity of GC B cell responses

Booster vaccination can augment humoral immunity by re-fueling ongoing GC reactions with new antigen. Moreover, it can recruit previously primed MBC but also naïve antigen-specific B cells into the secondary GC response<sup>205,206</sup>. To determine the capacity of different vaccination regimens to recruit and/or retain vaccination-primed spike-specific B cells in secondary germinal centers, we exploited activation-induced cytidine deaminase (AID) fate mapping reporter mice (AID<sup>rep 207</sup>). Administration of tamoxifen to AID<sup>rep</sup> mice results in the irreversible EYFP-labeling of B cells expressing AID in a specific time window of the immune response. This EYFP label is transmitted to all labelled cells' progeny, allowing their tracing in the context of subsequent responses. We primed AID<sup>rep</sup> mice with either mRNA-1273 or ChAdOx-1 and administered tamoxifen to label activated B cells during the first five days of the response (Figure 3A). At day 14 after primary vaccination ~30% of GC B cells were EYFP-labelled irrespective of the vaccine administered (Figure 3A-C). Furthermore, both vaccines induced similar numbers of EYFP-expressing germinal center B cells (Figure 3D). Notably, however, and in line with the results reported in Fig. 1, the proportion of spike-specific B cells amongst EYFP<sup>+</sup> GC B cells as well as these cells' total number was higher in animals undergoing mRNA vaccination than in those receiving ChAdOx-1 (Figure 3B,E). This observation indicated that ChAdOx-1-induced GCs contained a higher proportion of spike non-reactive B cells than mRNA vaccination, whereas AID labeling was comparable. Next, we performed mRNA-1273/mRNA-1273 or ChAdOx-1/mRNA-1273 prime-boost, again administering tamoxifen during the first days of prime immunization, to determine the proportion of EYFP<sup>+</sup> secondary GC B cells that had previously participated in the prime response. While the total number of GC B cells as well as the number of spike-binding GC B cells was comparable in the two vaccination regimens (Figs. 3H, compare also Fig. 2E), mRNA-1273/mRNA-1273-vaccinated animals harbored 12-fold higher numbers of EYFP<sup>+</sup> GC B cells than mice undergoing heterologous ChAdOx-1/mRNA-1273 or ChAdOx-1/ChAdOx-1 prime-boost (Figure 3F). Strikingly also, more than half of the spike-specific GC B cells in mRNA-1273/mRNA-1273-immunized animals consisted in EYFP<sup>+</sup> secondary GC B cells that had emerged from prime vaccination, whereas only about ~5% such cells were obtained upon ChAdOx-1/mRNA-1273 vaccination (Fig. 3G). This difference was also reflected in 9.3-fold higher EYFP<sup>+</sup> spike-binding secondary GC B cell numbers (Fig. 3I). Both the number as well as the proportion of EYFP<sup>+</sup> spike-binding secondary GC B cells was even lower when animals underwent homologous ChAdOx-1/ChAdOx-1 prime-boost. These results indicated that homologous mRNA-1273 prime-boost immunization resulted in a high degree of clonal continuity between prime and boost GC responses whereas the spike-specific GC response upon heterologous ChAdOx-1/mRNA-1273 or homologous ChAdOx-1/ChAdOx-1 vaccination contained a higher proportion of clones recruited *de novo* during the boost.

To complement our flow cytometric assessment, we performed immunohistochemistry on draining lymph nodes from prime-boost vaccinated mice (Figure 4A). As revealed by a combined staining of the GC marker GL7 and of EYFP fate-mapped cells, mRNA/mRNA prime-boost vaccination resulted in GC responses that were densely populated by EYFP<sup>+</sup> secondary GC B cells (Figure 4B). In remarkable contrast, secondary GC in draining LNs of mice undergoing ChAdOx-1/mRNA or ChAdOx-1/ChAdOx-1 immunization exhibited a paucity of EYFP<sup>+</sup> B cells (Figure 4B and C). EYFP<sup>+</sup> cells were also found in the medullary region of draining LNs, supposedly representing MBCs that had been activated during prime immunization and upon boost had differentiated into ASCs. These cells were particularly abundant in animals undergoing ChAdOx-1/mRNA prime-boost. These results corroborate and extend the conclusion that mRNA/mRNA prime-boost vaccination promotes clonal continuity in GCs between prime and boost to an extent that cannot be matched by ChAdOx-1/mRNA or ChAdOx-1/ChAdOx-1 vaccination.

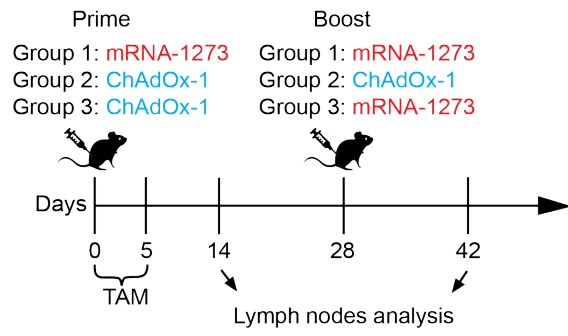
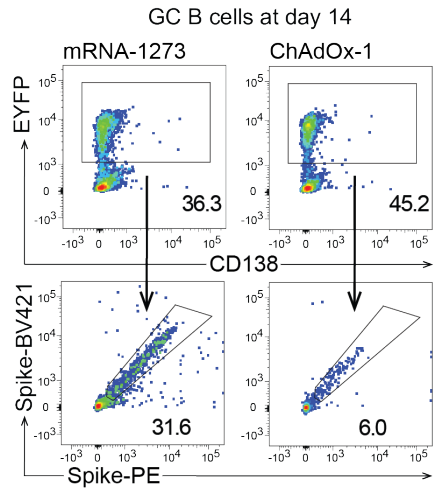
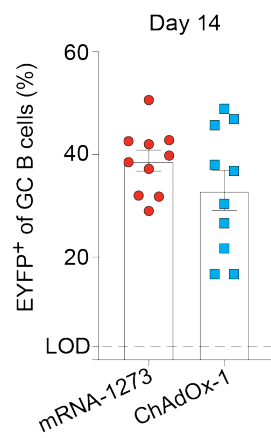
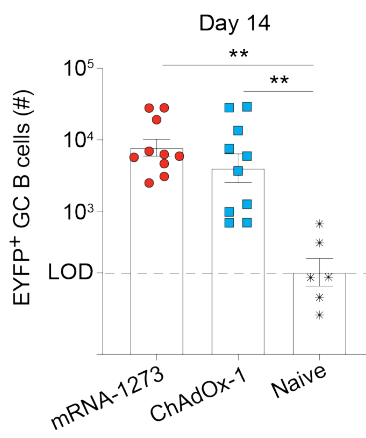
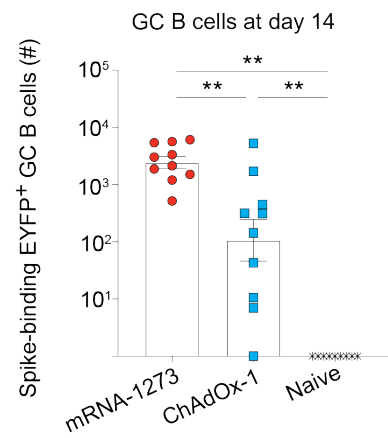
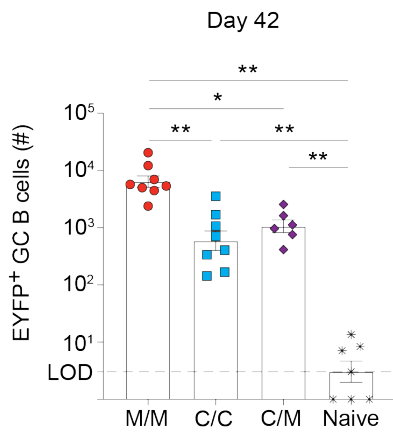
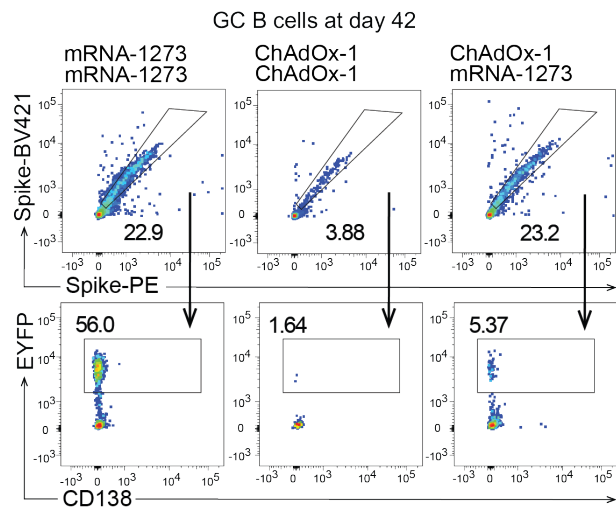
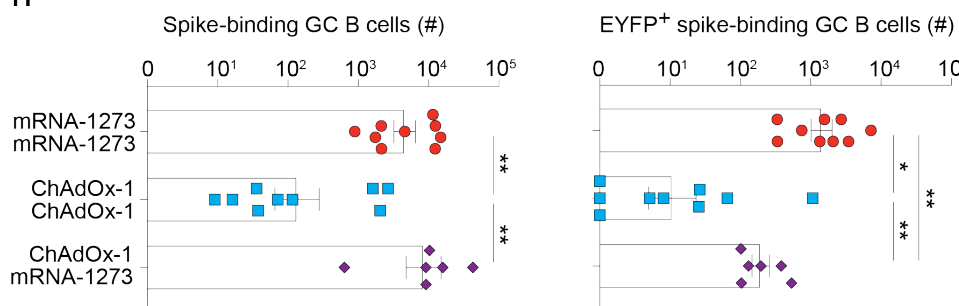
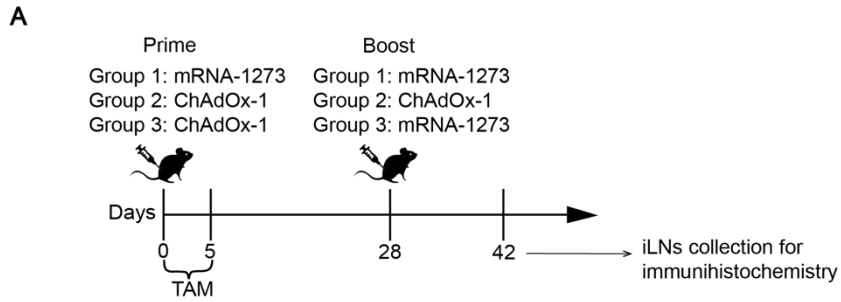
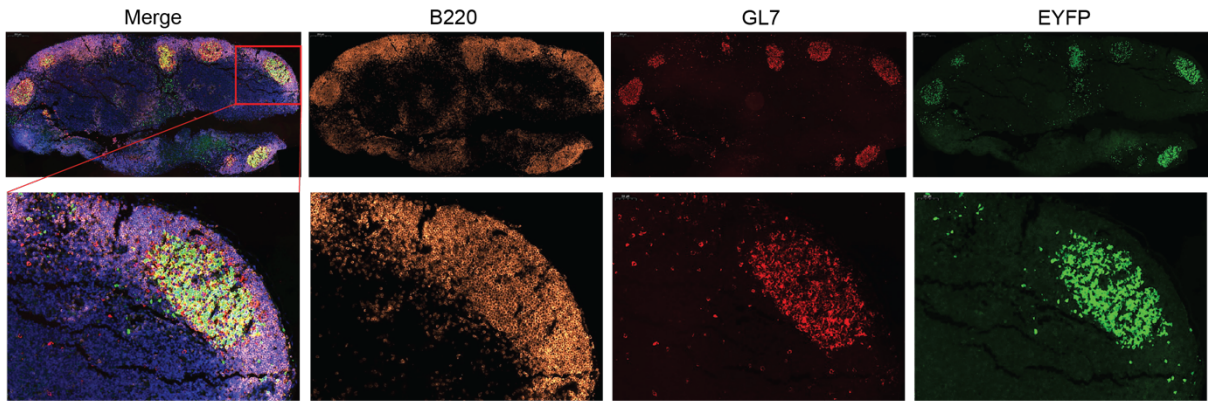
**A****B****C****D****E****F****G****H**

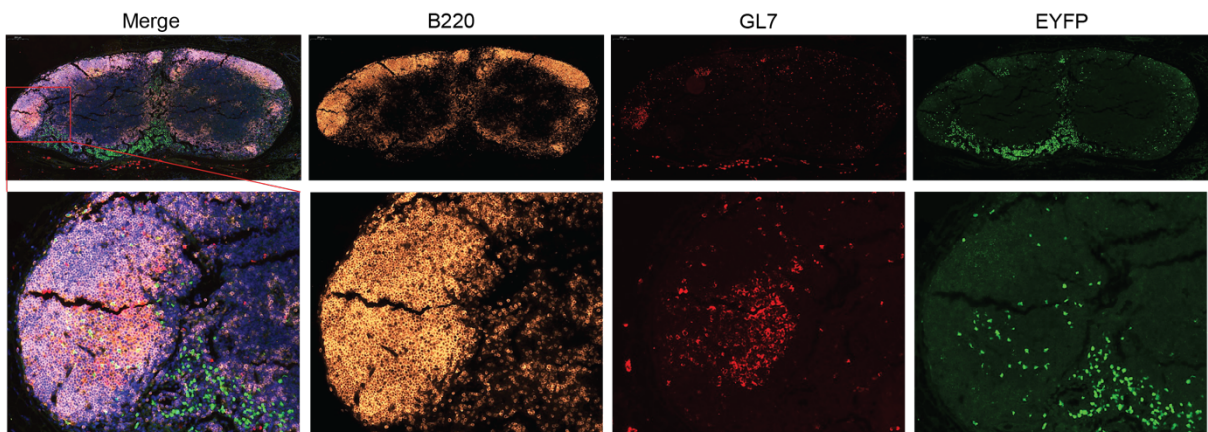
Figure 3. (A) Experimental design. AID<sup>rep</sup> mice were immunized at day 0 i.m. and treated with tamoxifen i.p. for the first 5 days. Secondary immunization was performed at day 28 and iLNs were analyzed at days 14 and 42. (B) Representative FACS plots of fate-mapped GC B cells (EYFP<sup>+</sup> GL7<sup>+</sup> CD38<sup>-</sup>, upper row) and spike-binding B cells within this population (lower row) at day 14. (C) Percentages of fate-mapped cells among GC B cells at day 14. (D) Total numbers of fate-mapped GC B cells at day 14. (E) Total numbers of spike-binding fate-mapped GC B cells at day 14. (F) Total numbers of fate-mapped GC B cells at day 42. (G) Representative FACS plots of fate-mapped GC B cells (EYFP<sup>+</sup> GL7<sup>+</sup> CD38<sup>-</sup>, upper row) and spike-binding B cells within this population (lower row) at day 42. (H) Numbers of spike-binding GC B cells and fate-mapped spike-binding GC B cells at day 42 after immunization. Statistical analysis was performed with one-way ANOVA with Tukey's post-tests. P values <0.05 were considered significant (\*), P < 0.01 as highly significant (\*\*), and P > 0.05 was considered as not statistically significant (not indicated).



**B** mRNA-1273/mRNA1273



**C** ChAdOx-1/mRNA1273



**D** ChAdOx-1/ChAdOx-1

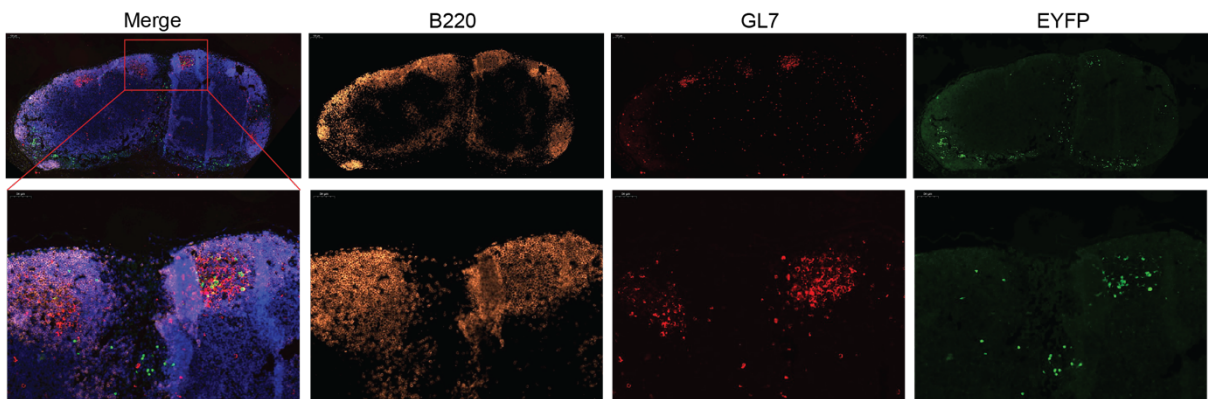




Figure 4. (A) Experimental design. AID<sup>rep</sup> mice were immunized at day 0 i.m. and treated with tamoxifen i.p. for the first 5 days. Secondary immunization was performed at day 28 and iLNs were collected for immunohistochemistry at day 42. (B) iLNs sections from mice immunized with mRNA-1273/mRNA-1273. (C) iLNs sections from mice immunized with ChAdOx-1/mRNA-1273. (D) iLNs sections from mice immunized with ChAdOx-1/ ChAdOx-1. All sections were stained for DAPI, B220, GL7 and EYFP.

### **Antibody responses to homologous mRNA-1273 prime-boost exhibits broader variant coverage than those to heterologous ChAdOx-1/mRNA-1273**

Neutralizing antibodies (nAbs) represent a main correlate of protection against symptomatic SARS-CoV-2 infection<sup>196</sup>. We compared the kinetics of nAb induction in mice immunized with mRNA-1273/mRNA-1273, ChAdOx-1/mRNA-1273 or ChAdOx-1/ChAdOx-1. While mRNA-1273 prime resulted in higher nAb titers at week one after immunization, ChAdOx-1-vaccinated animals reached similar titers by week two, albeit followed by a more pronounced decay until week four (Fig. 5A). Irrespective of these differences, mRNA-1273 homologous or heterologous boost resulted in comparable nAb titers at week 5, which was in line with the comparable numbers of spike-specific B cells in these two groups (Fig. 5A, compare Fig. 2B). Homologous ChAdOx-1/ChAdOx-1 prime-boost yielded lower nAb titers than the other two vaccination regimens.

A comparably modest increase and resultingly low titers of SARS-CoV-2 nAbs after homologous ChAdOX-1 boost were in line with reduced spike-specific and total GC B cell numbers (Figs. 5A, 2E). Yet, these findings contrasted with peak nAb titers and GC B cell numbers after ChAdOX-1 prime that were comparable to those induced by a first dose of mRNA-1273 (Fig. 1C), suggesting the intrinsic immunogenicity of ChAdOX-1 was comparable to mRNA-1273. We considered that anti-vector antibody responses to prior ChAdOX-1 immunization have the potential to diminish the efficacy of subsequent booster doses<sup>116,117,208</sup>. Accordingly, we found that ChAdOx-1 vector backbone-binding antibodies were readily induced within two weeks after prime and increased 34-fold within 2 weeks after homologous ChAdOx-1 boost (Fig. 5B). In contrast, SARS-CoV-2 spike-specific antibody responses were augmented 2.6-fold only. This predominant boosting of ChAdOx-1 backbone-specific antibodies instead of the desired anti-spike response may represent a serological correlate to the low percentage of spike-binding B cells amongst AID<sup>rep</sup> fate-mapped secondary GC B cells (compare Figs. 3D, 3E).

Besides neutralizing titers as a quantitative readout, the breadth of vaccine-induced nAb responses is of interest as a readout of antibody quality and can represent a correlate of protective efficacy against SARS-CoV-2 antigenic variants of concern<sup>209</sup>. Somatic hypermutated spike-specific B cells exhibit higher neutralizing breadth than those from their predecessors, suggesting the germinal center response augments the antigenic breadth of B cells over time<sup>203</sup>. To compare the antigenic breadth of nAb responses elicited by the different vaccination regimens we tested the neutralizing activity of mouse sera against the Beta and Omicron BA.5 variants of SARS-CoV-2, which are resistant to a majority of monoclonal nAbs induced by the original Wuhan-Hu-1 spike protein<sup>152,210</sup>. Accordingly and as expected, the nAb titer of mouse sera against Beta or Omicron was lower than against Wuhan-Hu-1 (Fig. 5 C,D), but the relative reduction in neutralizing potency, i.e. the breadth of the response, varied greatly between different vaccination regimens. As noted above, the Wuhan-Hu-1-specific nAb titer was comparable after mRNA-1273/mRNA-1273 homologous and ChAdOx-1/mRNA-1273

heterologous prime-boost. mRNA-1273/mRNA-1273-induced sera exhibited on average a 16-fold reduction in neutralizing activity when tested against the Beta variant instead of Wuhan-Hu-1, whereas in the ChAdOx-1/mRNA-1273 group the respective difference was 324-fold i.e. a good order of magnitude higher. Analogously, the relative loss in neutralizing potency of mRNA-1273/mRNA-1273- and ChAdOx-1/mRNA-1273-induced sera against Omicron vs. Wuhan-Hu-1 was 52-fold vs. 477-fold, respectively. Sera of mice undergoing ChAdOx-1/ChAdOx-1 homologous prime-boost exhibited a substantially lower Wuhan-Hu-1-specific titer and Beta variant-neutralizing titers were 43-fold lower while neutralizing activity against Omicron was inconsistently detected, rendering our assessment of neutralizing breadth in this group less conclusive.

These studies showed that mRNA-1273/mRNA-1273 homologous prime-boost immunization elicited serum antibodies of higher antigenic breadth than those induced by heterologous ChAdOx-1/mRNA prime-boost, reflecting a differential ability to cover viral antigenic variants of concern.

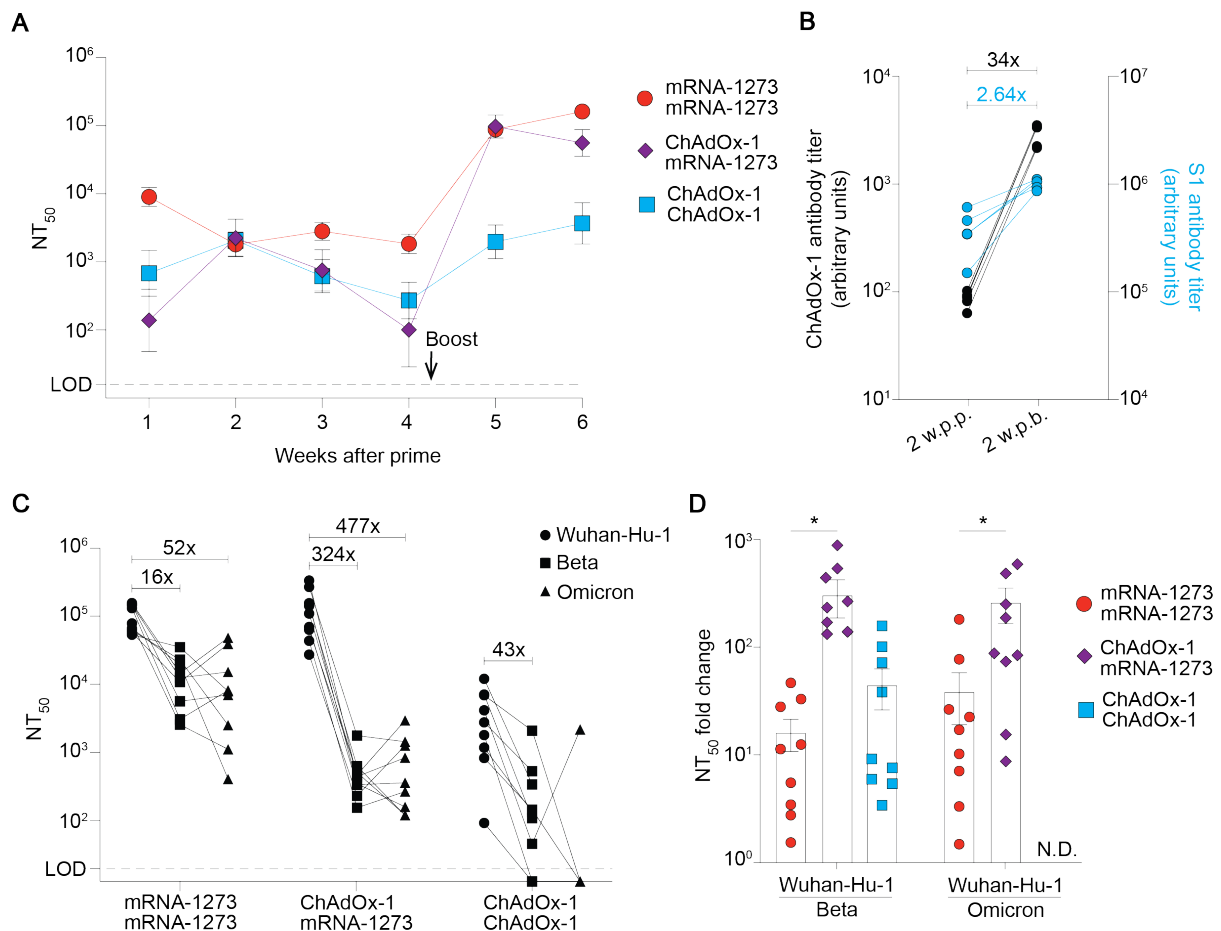


Figure 5. (A) SARS-CoV-2 neutralizing activity to Wuhan-Hu-1 strain was determined by pseudovirus neutralization assay as the reciprocal dilution of sera required to inhibit viral infection by 50% (NT<sub>50</sub>). (B) Antibody titers in serum samples from mice immunized with ChAdOx-1 at 2 weeks after prime and 2 weeks after boost. Titters were calculated against ChAdOx-1 viral particles (vector backbone) and S1 protein (vector transgene). (C) NT<sub>50</sub> from serum samples collected at one week after boost, against viruses pseudotyped with Wuhan-Hu-1, Beta or Omicron BA.5 variants of SARS-CoV-2 spike protein. (D) Ratio of NT<sub>50</sub> against Wuhan-Hu-1 SARS-CoV-2 spike over NT<sub>50</sub> against Beta or Omicron BA.5 variants, from serum samples collected at 1 week after boost. Statistical analysis was performed with two-tailed unpaired Student's *t* test. P values <0.05 were considered significant (\*), and P > 0.05 was considered as not statistically significant (not indicated).

## Discussion

This study explored the dynamics of GC responses following vaccination with mRNA and adenoviral vector-based platforms currently in clinical use. Our results demonstrate that both vaccine types are capable of initiating robust GC reactions, which are crucial for the development of long-lasting immunity and high-affinity antibodies against SARS-CoV-2<sup>144,209</sup>. Our research focused on the capacity of these vaccines to re-engage previously activated B cells into secondary GCs upon homologous or heterologous boost immunizations. Fate-mapping of prime-activated B cells by means of the AID<sup>rep</sup> mouse model revealed that mRNA re-vaccination induced the secondary expansion of this population to a higher extent than ChAdOx-1 homologous or ChAdOx-1/mRNA heterologous prime-boost. Most importantly we found that this enhanced reactivation of spike-specific B cells, i.e. the clonal continuity in GC reactions correlated with an increase in the breadth of neutralizing antibodies. Our findings highlight, therefore, the importance of a continued GC-based evolutionary trajectory of B cells for vaccine efficacy against evolving pathogens. Moreover, they document the preferential utility of mRNA-based prime boost to ascertain clonal continuity and antigenic breadth of serological responses.

In addition to these key observations, we found that double immunization with ChAdOx-1 elicited lower numbers of spike-specific B cells and SARS-CoV-2 neutralizing antibodies compared to heterologous ChAdOx-1/mRNA or mRNA/mRNA vaccinations. This result is supported by prior findings that showed enhanced immunogenicity of mRNA-containing vaccine regimens compared to homologous ChAdOx-1<sup>86,87,201,204,211</sup>. We also found that a larger part of EYFP<sup>+</sup> primary activated B cells by ChAdOx-1 was not able to bind to our spike probes, which suggest that their specificity differed from the transgene and could be directed against adenoviral antigens. Furthermore, we detected vector-binding antibodies at 2 weeks after prime that were further boosted by a second ChAdOx-1 immunization. Notably, the relative increase of these anti-vector antibodies was higher than that of the spike-binding antibodies after homologous boost. This pre-existing immunity has been demonstrated to reduce the immunogenicity of adenovirus vector-based vaccines, and the generation of anti-vector immunity following initial priming impairs the efficiency of subsequent homologous boost immunizations<sup>116,117,212</sup>. Therefore, it is likely that the relative lower immunogenicity of ChAdOX-1/ChAdOx-1 compared to ChAdOx-1/mRNA is caused, at least in part, by vector-specific B cell and antibody responses interfering with secondary homologous immunizations.

A major difference we observed between mRNA and ChAdOx-1 priming was the longevity of the GC reaction. In mice that received an mRNA prime, spike-binding GC B cells persisted until the booster dose, unlike those given ChAdOx-1. This persistent GC reaction induced by mRNA immunization has been documented previously in humans, lasting for months after vaccination and correlating with high levels of somatic hypermutation<sup>197,203,213</sup>. More importantly, it has been shown that mRNA boosts with the original spike protein generate robust B cell and antibody responses against the Omicron variant<sup>214</sup>. In line with these reports, we observed<sup>214</sup> that the presence of EYFP<sup>+</sup> B cells in secondary GCs correlated with increased neutralization to virus escape variants Beta and Omicron.

This indicates that the engagement and continuous evolution of primary activated B cells within the GC reaction allows them to increase their breadth of variant neutralization, and suggests that the antibodies encoded by these B cells are targeting more conserved epitopes in the spike protein. Furthermore, since this effect was most prominent in the mRNA/mRNA regimen, it is likely that the primary persistent GCs were already seeded with more EYFP<sup>+</sup> B cells at the time of boost. This would allow a better expansion of this local population within the GC compartment upon secondary immunization, compared to the regimens that involved ChAdOx-1 priming. Our results suggest that persistent mRNA-primed GCs can get re-filled with antigen during ipsilateral boosts, as it has been shown previously with other vaccines<sup>205,215</sup>.

In summary, our findings highlight the critical role of sustained GC reactions and retention of primed B cells in enhancing antibody responses to vaccines. While both mRNA and adenoviral vector-based vaccines effectively initiate GC reactions, the differences in how they sustain these reactions and re-engage B cells upon boosting are notable. The persistence of GC responses, especially observed in mRNA priming, facilitates a more robust activation and expansion of antigen-specific B cells. This research emphasizes the significance of GC longevity and dynamic B cell responses in developing effective immunization strategies.

## Limitations of the study

In this study we employed a fate-mapping mouse model to show how the progeny of vaccine-primed antigen-specific B cells are re-engaged into secondary GCs after boost. It is likely that we underestimated the numbers of primary activated cells that contributed to secondary GC reaction. The AID<sup>rep</sup> system used in this study is reported to be inefficient<sup>216</sup>. Accordingly, we labeled approximately 30% of primary antigen-specific B cells within GCs. Secondly, we were unable to label B cells that were recruited to GCs after tamoxifen wash-out. Additional limitations include the differences of prime and boost intervals used in this study compared to clinical settings. Homologous ChAdOx-1 and heterologous mRNA/ChAdOx-1 vaccinations have been used mostly with 3 months in between first and second dose<sup>208</sup>, while mRNA homologous regimens comprise 1 month interval between prime and boost<sup>217</sup>. These dosing interval differences can impact the immunogenicity and dynamics of GC responses to vaccination<sup>208,218</sup>. Therefore, we maintained a one-month interval for all regimens tested. Furthermore, distinct antigenic properties of the full-length wild-type SARS-CoV-2 spike protein lacking prefusion-stabilizing mutations in the ChAdOx1 vaccine<sup>219</sup>, the precise biochemistry of the antigen and its presentation may also contribute to the differences in immunogenicity observed in this study.

## Methodology

### Animal experiments, immunizations and tamoxifen administration

C57BL/6 wt mice were purchased from Charles River laboratories and were kept under specific-pathogen-free conditions for colony maintenance and experiments. The AID<sup>rep</sup> mice, which have been previously described, possess a tamoxifen-inducible Cre recombinase (Cre-ERT2) targeted in the *aicda* locus, and a floxed EYFP reporter gene located at the ROSA26 locus. Experimental groups were sex- and age-matched. Mice were bred at the ETH Phenomics Center Zurich (EPIC), and experiments performed at the University of Basel in accordance with the Swiss law for animal protection and with permission by the Cantonal Veterinary Office of Basel City.

Leftovers from mRNA-1273 Moderna, Inc. were kindly provided by the Medical Polyclinic of Basel University Hospital and kept at -80°C until use<sup>220</sup>. Immunizations were performed at a dose of 5ug per mouse and administered i.m. in a volume of 40  $\mu$ l into both rear hind limbs. ChAdOx-1 was administered i.m. at 5E+08 vp/mouse in a volume of 40  $\mu$ l into both rear hind limbs.

Tamoxifen was dissolved in corn oil at 20mg/ml by shaking overnight at 37°C, protected from light. AID<sup>rep</sup> mice were injected 100ul of the tamoxifen corn oil mix intraperitoneally to induce expression of the Cre recombinase.

### Flow cytometry

Spleens or iLNs were mechanically disrupted and counted with a Immunospot S6 device (C.T.L.). For surface staining of B cells, iLNs derived cells were incubated with spike probes conjugated to PE or BV421 for 1h at 4°C. Samples were washed and subsequently stained for surface markers with the following antibodies: CD45R/B220 (RA3-6B2), CD138 (281-2), anti MU/HU GL7 Antigen (GL7), CD38 (REA616), IgM (II/41) and IgD (11-26c.2a). For detection S1-specific CD8 T cells, H2-Kb tetramers were conjugated to PE and loaded with the SARS-CoV-2 spike epitope (VNFNFNGL). Peptide-MHC tetramers were prepared by the University of Lausanne Tetramer core facility. The tetramers were added to the antibody mix for staining. The antibody mix included the following antibodies: CD45R/B220 (RA3-6B2), CD8 (53-6.7), CD44 (IM7), CD62L (MEL-14), CD127 (A7R34), Klrg1 (2F1), CX3CR1 (SA011F11), CD27 (LG3A10) and CD43 (1B11) purchased from BioLegend. For detection of spike-specific CD4 T cells, splenocytes were resuspended in RPMI media containing BD FcBlock and anti-CD154 (CD40L) antibody (BioLegend, clone: MR1) and incubated for 6 hr at 37 °C with no peptide stimulation or stimulation with the S1 and S2 peptide pools purchased from GenScript (Cat. #RP30020). Peptide pools were used at a final concentration of 2 mg/ml each peptide. Following stimulation, cells were washed with FACS buffer (PBS supplemented with 2% FCS) and resuspended in BD FcBlock (clone 2.4G2) for 5 min at RT prior to staining with a surface stain cocktail containing the following antibodies purchased from BioLegend: CD3 (145-2C11), CD4 (RM4-5), I-A/I-E (M5/114.15.2) PE, CD44 (IM7), CD62L (MEL-14), CXCR5 (L138D7), PD-1 (29F.1A12), CD69 (H1.2F3). Dead cells were stained with Zombie-UV Fixable Viability Kit (BioLegend, Cat: #423107). All Samples were fixed by incubation



with 2% paraformaldehyde for 15 minutes at room temperature and measured on a LSRFortessa flow cytometer (Becton Dickinson). Data were analyzed with FlowJo Software (BD Biosciences).

### **Sample collection and processing**

Sample collection: Every 7 days post-immunization, blood was collected from the mouse tail vein using Multivette 600 Serum gel tubes (Starstedt). Following collection, blood was centrifuged at 10000 rpm for 5 minutes. Serum was recovered and stored at -20 C for neutralization assays and ELISAs. Inguinal lymph nodes and spleens were harvested and placed in cold complete Dulbecco's Modified Eagle's Medium (DMEM, Corning, T10014CV) containing 10% heat inactivated FCS. All organs were kept on ice and immediately processed after collection. Organs were homogenized with a syringe plunger and filtered through a 40 mm cell strainer on ice. Cells from iLNs and spleens were resuspended in ice cold complete RPMI and immediately used for counting, culture, or staining.

### **Fluorescent SARS-CoV-2 spike probe generation**

Biotinylated full spike proteins used for flow cytometry experiments were independently conjugated to both PE and BV421 using streptavidin-PE (BioLegend, 405203) or streptavidin BV421 (BioLegend, 405226), at a 1:4 molar ratio. Streptavidin-conjugated fluorophores were added sequentially in 4 steps with 15 minutes incubation at 4°C between each step. Fluorescent spike proteins were used directly after conjugation.

### **SARS-CoV-2 pseudovirus neutralization assays**

Microtainer tubes (Becton-Dickinson) were used for serum collection. SARS-CoV-2 neutralizing antibodies in blood were measured by diluting serum samples from naive or immunized mice in MEM supplemented with 2% FCS, starting with a 1:10 dilution followed by three-fold serial dilutions in 96-well plates. Each dilution of serum or monoclonal antibody S309<sup>221</sup>, serving as a positive control, was incubated with an equal volume of replication-deficient rVSV-EGFP pseudotyped with SARS-CoV-2 spike protein WA1/2020 strain (Wuhan/WIV04/2019, GISAID accession ID: EPI\_ISL\_402124), B.1.351 variant (Beta, GISAID accession ID: EPI\_ISL\_712096) or Omicron BA.5 variant (GISAID accession ID: EPI\_ISL\_12029894) containing approximately 100 infectious units for 1 hour at 37°C. Subsequently, the mixture was incubated with Vero E6 cells (2x10<sup>4</sup> cells/well) for 16 hours and fixed with 2% paraformaldehyde. The number of green spots was quantified using an Immunospot S6 device (C.T.L.). The 50% neutralization titer (NT50) was calculated as the half-maximal inhibitory concentration values using four-parameter nonlinear regression in GraphPad Prism.

### **Spike protein and adenovirus vector ELISAs**

High-binding 96-well flat bottom plates (Sarstedt AG & Co.KG) were coated with 1E+08 viral particles of ChAdOx-1 or 50 ng of spike protein per well in 50  $\mu$ L coating buffer over night at 4 °C. Plates were washed twice with PBS-T (0.05% Tween-20/PBS), then blocked with 200  $\mu$ L 5% BSA/PBS-T at room

temperature for 45 min. 2-fold serial dilutions of serum samples in blocking solution were performed after washing five times with PBS-T. Plates were incubated at 37 °C for 1 h and washed five times with PBS-T. Peroxidase-conjugated polyclonal anti-mouse antibody (1:2000 in blocking solution; Jackson, 115-035-062) was added and the plates were incubated at 37 °C for 60 min. After washing five times with PBS-T, HRP activity was detected using ABTS as a chromogen (Pierce) and the absorbance was measured at 405 nm using the Sapphire plate reader (Tecan). Arbitrary units are computed as  $\ln(1000 \times A_{491\text{nm}})$ ; the limit of detection corresponds to the maximum value reached by negative controls.

### **Immunohistochemistry**

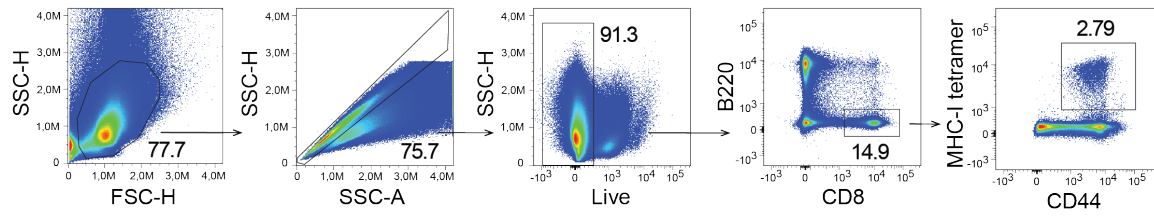
For immunofluorescence analysis of lymph node sections, animals were sacrificed at the indicated time points and iLNs were fixed in PBS containing 4% paraformaldehyde (Merck) overnight at 4°C, then washed with PBS and embedded in paraffin. Immunostaining was performed on 3 µm-thick sections using antibodies against GFP (ICL lab), Alexa Fluor 647-directly labeled B220 (eBioscience) and GL7 Alexa Fluor 550 Conjugate (ThermoFisher). Immunostained slides were incubated with the Vector® TrueVIEW Autofluorescence Quenching Kit to remove autofluorescence signal (Vector Laboratories). Stained sections were scanned using a Panoramic Digital Slide Scanner 250 FLASH II (3DHISTECH) at 200 x magnification.

### **Acknowledgements**

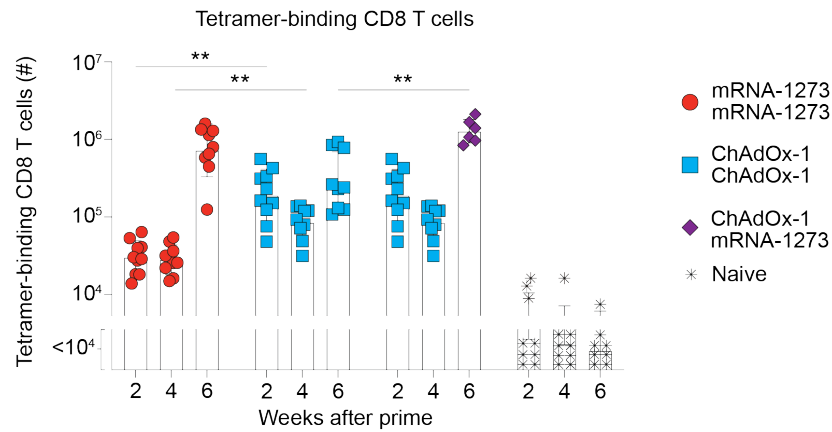
We wish to thank Karsten Stauffer for exceptional animal handling and care. Min Lu and Karen Cornille for excellent technical support. We thank Sabine Egli and Bertha Menigoz from the Medical Polyclinic of Basel University Hospital for providing mRNA-1273 vaccine leftovers. We also thank Ilena Vicenti and Cynthia Saadi for their assistance with immunohistochemistry. We acknowledge the DBM flow cytometry core facility and Morgane Hilpert for their help with cell sorting. Lastly, we are grateful to the entire Experimental Virology group for their helpful discussions.

## Supplementary figures

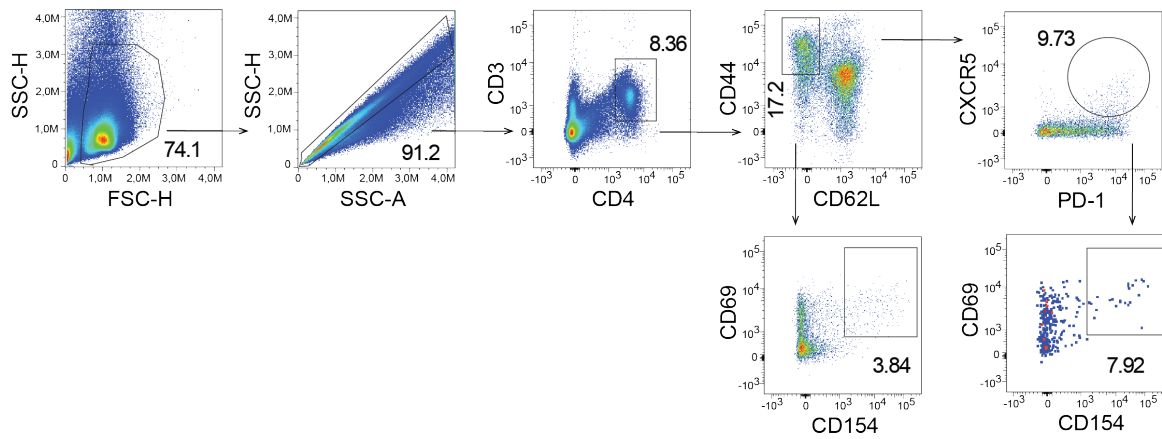
**A**



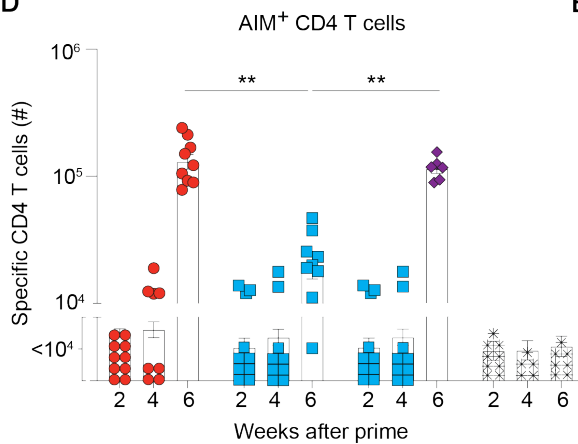
**B**



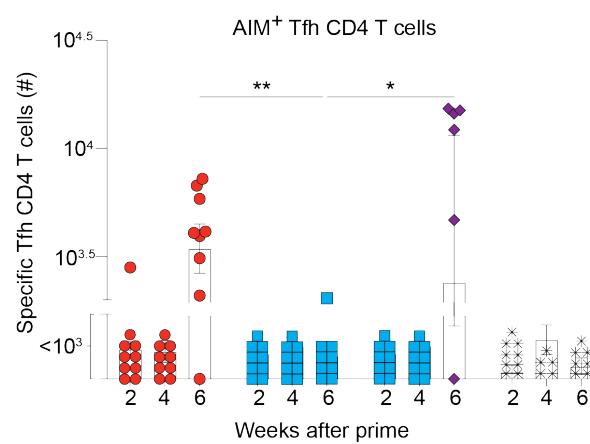
**C**



**D**



**E**



Supplementary Figure 1. (A) Gating strategy for analysis of spike-specific CD8 T cells in spleen by MHC-I tetramer and surface markers staining. (B) Total numbers of spike-specific CD8 T cells in spleens of animals vaccinated with different regimens at the indicated weeks after vaccination. (C) Gating strategy for AIM assay analysis for the identification of spike-specific CD4 T cells. (D) Total numbers of spike-specific CD4 T cells or (E) spike-specific Tfh CD4 T cells in spleens of mice immunized with different regimens at the indicated weeks after vaccination.

# Novel adenovirus vaccine vectors lacking thrombosis-associated interactions with Platelet Factor 4

Erwan Sallard<sup>1</sup>, Daniel Pembaur<sup>2</sup>, Matias Ciancaglini<sup>3</sup>, Lucie Bouard<sup>4</sup>, Denice Weklak<sup>2</sup>, Franziska Jönsson<sup>2</sup>, Chun Kit Chan<sup>5,6</sup>, Elise Chabot<sup>1,7</sup>, Sebastian Schellhorn<sup>1</sup>, Nissai Beaudé<sup>1,8</sup>, Katrin Schröder<sup>1</sup>, Daipayan Sarkar<sup>5,9</sup>, Georgia Koukou<sup>2</sup>, Xiaoyan Wang<sup>11</sup>, Natascha Schmidt<sup>2</sup>, Wibke Bayer<sup>11</sup>, Malik Aydin<sup>1,10</sup>, Dirk Grimm<sup>12</sup>, Abhishek Singharoy<sup>5</sup>, Alexander T. Baker<sup>4,5,13</sup>, Wenli Zhang<sup>1</sup>, Daniel Pinschewer<sup>3</sup>, Florian Kreppel<sup>2,†,\*</sup>, Anja Ehrhardt<sup>1,†,\*</sup>

<sup>1</sup> Virology and Microbiology, Center for Biomedical Education and Research (ZBAF), Department of Human Medicine, Faculty of Health, Witten/Herdecke University, Witten, 58453, Germany.

<sup>2</sup> Institute for Biochemistry and Molecular Medicine, Center for Biomedical Education and Research (ZBAF), Department of Human Medicine, Faculty of Health, Witten/Herdecke University, Witten, 58453, Germany.

<sup>3</sup> Division of Experimental Virology, Department of Biomedicine, University of Basel, 4051 Basel, Switzerland.

<sup>4</sup> Accession Therapeutics Limited, Oxford, OX4 2JZ, UK.

<sup>5</sup> Biodesign Institute Center for Applied Structural Discovery & Biosense Network, School of Molecular Science, Arizona State University, Tempe, AZ.

<sup>6</sup> NIH P41 Biotechnology Resource Center for Macromolecular Modeling and Bioinformatics, Beckman Institute for Advanced Science and Technology, University of Illinois at Urbana Champaign.

<sup>7</sup> École Normale Supérieure de Lyon, Lyon 1 Claude Bernard University, France.

<sup>8</sup> AgroParisTech, Paris-Saclay University, Saclay, France.

<sup>9</sup> MSU-DOE Plant Research Laboratory, East Lansing, MI.

<sup>10</sup> Laboratory of Experimental Pediatric Pneumology and Allergology, Center for Biomedical Education and Research (ZBAF), Department of Human Medicine, Faculty of Health, Witten/Herdecke University, Witten, 58453, Germany.

<sup>11</sup> Institute for Virology, University Hospital Essen, University Duisburg-Essen, Essen, Germany.

<sup>12</sup> Department of Infectious Diseases/Virology, Section Viral Vector Technologies, Medical Faculty, University of Heidelberg, BioQuant, Heidelberg, Germany.

<sup>13</sup> Division of Cancer and Genetics, School of Medicine, Cardiff University, Cardiff CF14 4XN, UK.

† These authors contributed equally to this work.

\* Corresponding authors: [florian.kreppel@uni-wh.de](mailto:florian.kreppel@uni-wh.de); [anja.ehrhardt@uni-wh.de](mailto:anja.ehrhardt@uni-wh.de)

## **Abstract**

The adenoviral vector-based AstraZeneca and Janssen COVID-19 vaccines have been associated with rare cases of thrombosis, believed to be triggered among other factors by vector binding to the blood protein platelet factor 4 (PF4). To identify vectors with lower thrombosis risk, we screened 44 natural and hexon-modified human adenoviruses (Ad). Unlike the applied COVID-19 vaccines and most tested vectors, Ad11, Ad13, Ad34, Ad80, and Ad5 vectors with deleted or chemically shielded hexon hypervariable region 1 (HVR1) did not bind to PF4. Furthermore, interactions with PF4 substantially modified Ad5 infectivity in numerous immortalized or primary cell types, suggesting that PF4 may influence existing vector tropism and toxicity profile beside thrombosis cases. Finally, Ad11, Ad34 and HVR1-deleted Ad5 vectors expressing SARS-CoV-2 spike S1 domain were tested as vaccine candidates in mice and induced relatively strong cellular immune responses. Therefore, the identified PF4 non-binding vectors may represent safe and efficient candidates for clinical applications.

## Introduction

Adenoviruses (Ads) are non-enveloped viruses with a linear double-stranded DNA genome comprising between 26 and 48 kb<sup>222,223</sup>. There are currently 115 known Ad types infecting humans<sup>224</sup>, classified into seven species, in addition to an even larger diversity of non-human Ads infecting other species including primates. Adeno-associated viruses (AAV) are parvoviruses with an approximately 5 kb long single-stranded DNA genome, which in nature depend on adenoviral or herpesviral coinfections to replicate<sup>225</sup>. Due to their high manufacturability, gene delivery efficiency and genetic stability, recombinant AAVs and Ads are the most prominent type of viral vectors used in gene therapy and vaccine development<sup>226</sup>, respectively. Notably, the AstraZeneca (ChAdOx-1 nCoV19, derived from chimpanzee Ad type Y25) and Janssen (Ad26.COVS, derived from human Ad26) COVID-19 vaccines have already been administered well over 2 billion times<sup>227</sup>, and established Ad vaccines as one of the most powerful tools against pandemics. Despite the concomitant success of mRNA vaccines, Ad COVID-19 vaccines remained critical in regions with unstable cold storage logistics<sup>228</sup> and tended to induce stronger T cell immunity<sup>160,229</sup>.

However, clinical applications of Ad vectors still face several obstacles, among which the ability of certain Ad types to interact with blood proteins after systemic administration or local injection, including with prothrombin, the most abundant coagulation factor<sup>230</sup>. Moreover, Ad type 5 (Ad5) displays a strong and potentially pathological liver tropism due to its binding to the coagulation factor X<sup>231</sup> on the fifth and seventh hypervariable regions (HVR) of its hexon protein<sup>232</sup>, the most abundant Ad capsid protein. Likewise, the ChAdY25 and Ad26 vaccines have been associated with very rare cases of vaccine-induced immune thrombotic thrombocytopenia (VITT, also termed TTS), with an incidence in the order of magnitude of 1 case per 100,000 vaccinated persons<sup>84</sup>. This disorder usually occurs within 5 to 20 days after the first vaccine injection, involves thrombosis in the cerebral venous sinus, the splanchnic vein or other unusual thromboembolic events<sup>233</sup>, and is lethal in 23-40% of cases<sup>234,235</sup>. VITT is thought to be initiated by the binding of the vectors to platelet factor 4<sup>85,233</sup> (PF4, also known as CXCL4), which could activate a cascade of immune reactions, notably the production of auto-antibodies, and lead to severe adverse effects in a small subset of patients. PF4 is a 7.8 kDa cationic protein secreted by activated thrombocytes, whose physiological functions include the recruitment of thrombocytes on glycosaminoglycans exposed in vascular injuries and the opsonization of the negatively charged surfaces of pathogens<sup>236</sup>. PF4 blood concentration is usually around 10 ng/mL, but can reach 3-15  $\mu\text{g/mL}$  in case of platelet activation<sup>237,238</sup>. Certain AAV vectors have also been associated with a thrombotic disorder termed thrombotic microangiopathy (TMA) that occurred in several patients enrolled in high dose AAV gene therapy trials, although no link with PF4 has been established to date<sup>239,240</sup>.

The development of safer vaccine and gene therapy vector platforms may protect patients from rare but fatal side effects and improve public trust in medical treatments and prophylaxes. Therefore, we aimed to identify Ad and AAV types with low or absent PF4 binding. Here we established new

techniques for higher-throughput study of protein-virus interactions and screened a collection of 38 natural human Ad types, 6 Ad5 hexon-modified variants and 12 AAV serotypes. Several vectors lacked detectable PF4 binding including Ad5 variants with HVR1 deletion or shielding and Ad34. This confirmed the hypothesis that PF4 binds adenoviruses on the hexon protein, and identifies the HVR1 hexon loop as one critical interaction site. Moreover, we found that PF4 substantially modified Ad5 attachment and infection levels in numerous immortalized or primary cell types. Finally, we showed that several PF4-negative vectors can be used as vaccine vectors *in vivo*, and in particular that an HVR1-deleted Ad5 vaccine vector displayed an advantageous immunogenicity profile.



## Results

### Screenings of AAV and natural Ad collections identified vectors lacking PF4 binding

In order to rapidly screen large vector collections, we established the ELISA-qPCR technique (Fig. 1a, Supplementary Fig. 1). Briefly, virus particles are incubated with proteins of interest coated on a microtiter plate; following washes, vectors that specifically bound to the proteins remain in the wells and can be quantified by qPCR. We confirmed the specificity of ELISA-qPCR in the case of a few known interactors of Ad5 (Supplementary Fig. 1a) and were able to replicate preexisting results<sup>85</sup> by detecting PF4 binding to Ad5 and Ad vectors carrying the same capsids as the AstraZeneca and Janssen vaccines, hereafter termed ChAdY25 and Ad26 respectively (Fig. 1b). We then screened for PF4 binding a collection of 38 natural human Ad types drawn from all known human Ad species<sup>241</sup> and found that Ad11, Ad13, Ad34 and Ad80 were the only tested types for which PF4 binding could not be detected in any of the experimental repeats, as indicated by a consistently negative binding index (Fig. 1c, Supplementary Fig. 2). Likewise, a screening of 12 AAV serotypes recapitulated the previous finding<sup>242</sup> that AAV8 and 9, but not 1 and 6, bound to PF4 (Fig. 1d, Supplementary Fig. 3). Among the other tested AAV vectors, only AAV7 did not display detectable PF4 binding using the same criterium.

We sought to confirm the observed lack of PF4 binding by Ad11, Ad13, Ad34 and Ad80 with independent techniques. We established the Aggregate Pull-Down (APD) technique to quantify Ad vector particles (VP) aggregates that may form upon interaction with PF4 and be segregated from free VPs by low speed centrifugation (Fig. 2a). As expected, we observed PF4-induced aggregation of Ad5, ChAdY25 and Ad69, but not Ad13, Ad34 and Ad80, confirming the lack of PF4 binding of the latter Ad types (Fig. 2b). However, Ad11 displayed PF4-induced aggregation, contradicting ELISAqPCR observations.

In order to test for PF4 binding in more physiologically relevant contexts, we studied PF4 impact on Ad infectivity. Incubation of Ad5 or Ad69 particles with PF4 increased VP uptake in A549 cells by around 3 fold in average. On the other hand, PF4 did not influence Ad34 and Ad80 internalization, further confirming their lack of PF4 binding (Fig. 2c). In order to differentiate productive infections from abortive VP internalizations, we measured Ad-driven GFP fluorescence levels in cells infected with Ad5 and Ad69 and detected an increase for both Ads (Fig. 2d). For Ad34, PF4 did not modify the mean GFP fluorescence intensity but was associated with a 14% increase in the proportion of GFP-positive cells. To test if this was due to PF4 binding on Ad34 or to cellular responses to PF4 independent from direct PF4 – VP interactions, we added to the infectivity assays a sample whereby cells were cultivated in presence of PF4 prior to infection, then washed extensively and infected after PF4 removal. This treatment prompted an increase in Ad34-expressed GFP fluorescence level even higher than PF4 incubation simultaneously with infection (Fig. 2e). In the case of Ad5, cultivation of cells in presence of PF4 prior to infection also induced an increase in the percentage of GFP-positive cells, but this time significantly weaker than PF4 incubation simultaneous with infection, showing that both PF4

interactions with VPs and VP-independent interactions with target cells increase Ad5 gene expression in infected cells.

Finally, the validated surface plasmon resonance (SPR) technique confirmed that Ad34 fully lacks detectable PF4 binding (Fig. 2f).

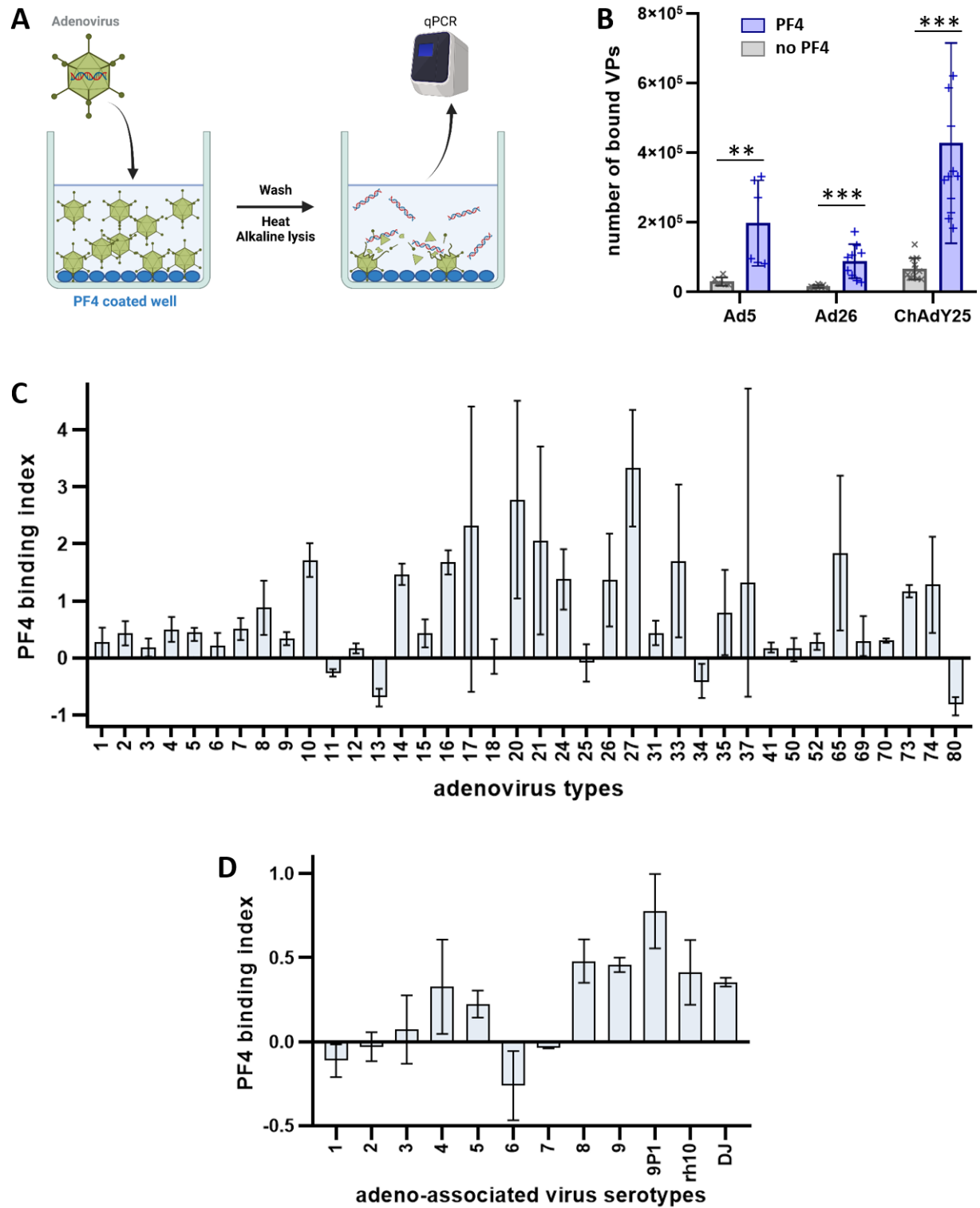


Fig. 1. Identification of adenovirus and adeno-associated virus vectors lacking binding to PF4 by ELISA-qPCR screening.

**A:** Principle of the ELISA-qPCR technique. Adenovirus (Ad) VPs are allowed to interact with proteins, e.g. PF4, coated on an ELISA plate. After washes, the genomes of VPs which specifically interacted with the proteins are released by heating and alkaline treatment and quantified by qPCR. Figure created with BioRender. **B:** PF4 binding of vaccine-equivalent vectors. Ad5 was obtained from the Ad-GLN collection.  $N \geq 6$ , two independent repeats. **C, D:** Screening of the Ad-GLN and Ad-WT collections (**C**) and AAV collection (**D**) for PF4 binding by ELISA-qPCR. For each experiment repeat, the PF4 binding index is computed as described in Methods (Statistics), with positive values indicating significant binding to PF4 and negative values corresponding to overlap in the number of bound VPs in PF4-coated versus control samples. Averages and minimum/maximum range of the PF4 binding index from two to four (Ad5, 11, 13, 34, 80) independent repeats are displayed.

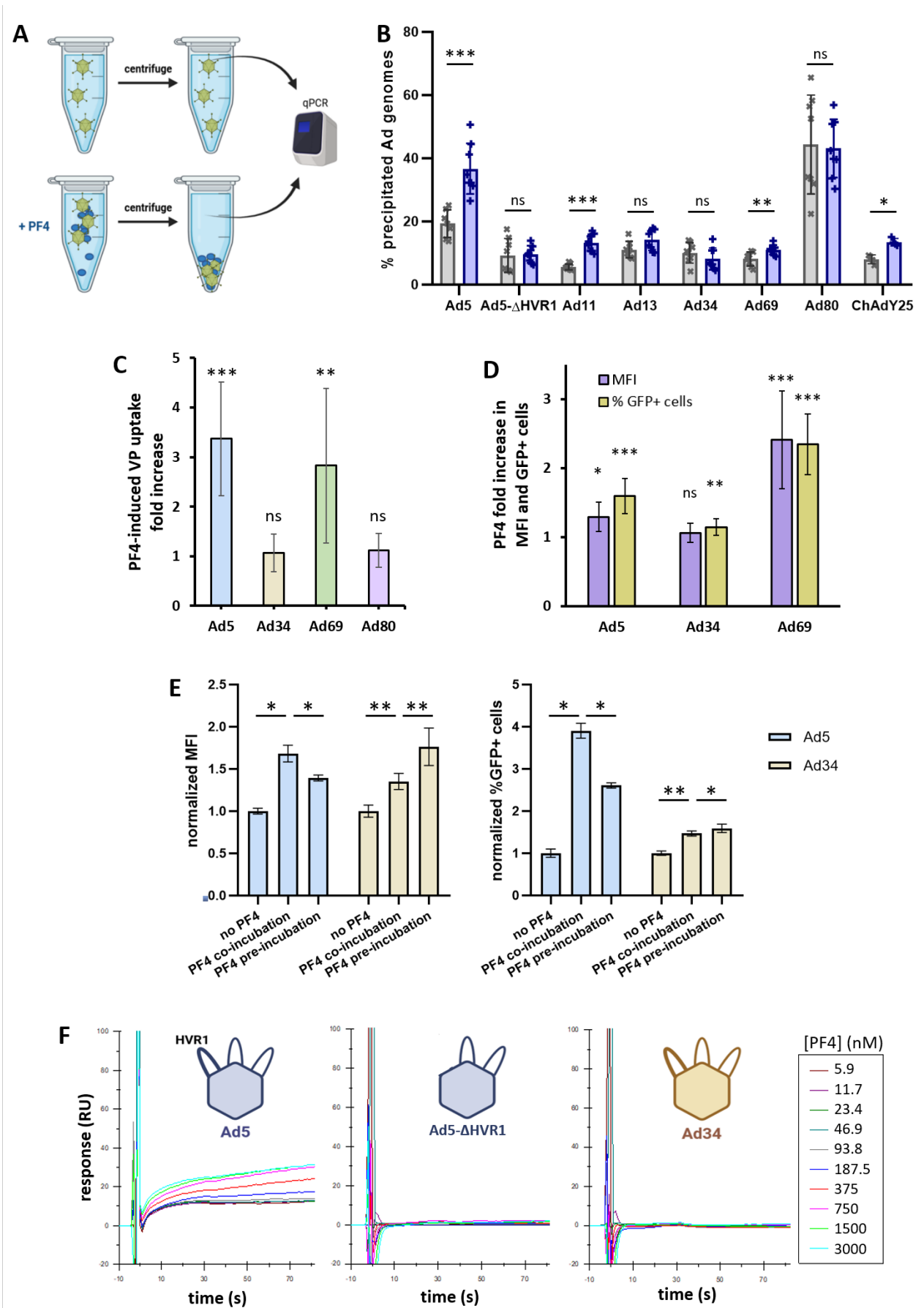


Fig. 2. A panoply of independent techniques confirms that Ad34 and Ad5- $\Delta$ HVR1 lack of binding to PF4.

**A:** Principle of the Aggregate Pull-Down technique. Aggregates forming upon interaction with PF4 are separated from free VPs by low speed centrifugation and titrated by qPCR. Figure created with BioRender. **B:** Aggregate pull-down of selected Ads in absence or presence of PF4. Ad5, Ad69 and Ad34 were obtained from the Ad-GLN collection; Ad11, Ad13 and Ad80 from the Ad-WT collection. N=8, two independent repeats. **C, D:** Fold change in Ad infectivity in A549-derived cells following Ad incubation with PF4. VPs were incubated 10 min. at 37°C in optiMEM with or without 10 µg/mL of PF4, before being allowed to infect cells at 20 vpc. Internalized Ad genomes were titrated by qPCR 3 hours post infection (hpi) (**C**), or Ad-expressed GFP mean fluorescence intensity (MFI) and proportion of GFP-positive cells (% GFP+ cells) were measured by flow cytometry at 24 hpi (**D**). Ads belonged to the Ad-GLN (Ad5, Ad34, Ad69) or the Ad-WT (Ad80) collections. **C:** N≥6, two to five independent repeats. **D:** N≥9, three to four independent repeats. **E:** PF4 cell-mediated and vector-mediated effects on Ad gene expression in A549 cells. A549 cells that had been cultivated in presence of 10 µg/mL PF4 during 3 hours (PF4 pre-incubation) or not were submitted to infectivity assays using Ad5 or Ad34 co-incubated with PF4 (PF4 co-incubation) or not (no PF4) at 20 vpc. At 24 hpi, Ad-expressed GFP mean fluorescence intensity (MFI) and proportion of GFP-positive cells (% GFP+ cells) were measured by flow cytometry and values were normalized on the average of the “no PF4” condition. All Ads belong to the Ad-GLN collection. N≥5. **F:** Surface plasmon resonance (SPR) measurements of PF4 binding to Ad vectors. Ad5 and Ad34 were obtained from the Ad-GLN collection. Representative traces are displayed.

### **Ad5 binding to PF4 is dependent on its hexon HVR1 loop**

Baker *et al.* predicted by Brownian dynamics modeling that PF4 binds to hexon HVRs, with HVR1 being the most likely candidate for the ChAdY25 vaccine<sup>85</sup>. In order to gather further information on the location of PF4 binding site(s), we compared by ELISA-qPCR the PF4 binding of Ad5 variants with chemically or genetically modified hexons (Fig. 3a). Point mutations in HVR1, HVR5 and HVR7 did not prevent PF4 binding, contrary to deletion of the full HVR1 loop. PEGylation of HVR1 and HVR5, i.e. covalent linking of a large inert polymer which sterically prevents interactors to bind near its linkage site, also inhibited PF4 binding (Fig. 3b). The lack of PF4 binding by the HVR1-deleted Ad5 was confirmed by APD (Fig. 2b) and SPR (Fig. 2f).

We constructed Ad5H34, an Ad5-derived vector whose HVR1 loop sequence had been replaced by that of Ad34, and the reciprocal chimeric vector Ad34H5, derived from Ad34 and carrying Ad5 HVR1 loop (Fig. 3c). Both Ad34H5 and Ad5H34 displayed significant binding to PF4 in ELISA-qPCR (Fig. 3d).

Since Ad34H5 showed that the Ad5 HVR1 loop is sufficient to confer PF4 binding and this loop is one of the immunodominant epitopes for neutralizing antibodies of Ad5 capsid<sup>243</sup>, we tested whether PF4 modified Ad5 susceptibility to neutralizing antibodies, and observed that it partially protected Ad5 against human serum immunoglobulins (Fig. 3e).

On the other hand, the observation that the HVR1 loop of Ad34 did not ablate Ad5H34 PF4 binding appears at odds with Ad5- $\Delta$ HVR1 lack of PF4 binding. To investigate PF4-hexon interactions, we conducted Brownian Dynamics (BD) simulations (Supplementary Fig. 4a) which predicted that close interactions with PF4 were substantially rarer in the case of HVR1-deleted Ad5 and Ad34 than of Ad5 (Fig. 4a), fitting experimental data. Although it had been proposed that PF4-Ad binding may be driven by electrostatic interactions between the negative hexon protein and the positive PF4<sup>85</sup>, the similar surface electrostatic profiles between Ad5 and Ad34 (Fig. 4b) suggest that surface charge is not the driving parameter in determining whether a vector binds PF4 or not. The models instead pointed towards the HVR1 loop's structure as a more likely explanatory factor, with the less protruding HVR1 loop of Ad34 disfavoring interactions (Fig. 4c). Accordingly, the HVR1 loops of Ad5H34 and Ad34H5 were predicted to be sterically closer to that of Ad5 than that of Ad34 (Supplementary Movie 1), while electrophoretic light scattering (ELS) measurements showed that Ad34 had a net surface potential equally or more negative than the PF4-binder Ad types tested (Fig. 4d). Finally, the hexon residues that interacted most frequently with PF4 in BD simulations are clustered in the HVR1 loop, with HVR5 and HVR7 appearing as potential secondary binding sites (Supplementary Fig. 4b). Those locations match with concentrations of residues unique to PF4 non-binder types (Supplementary Fig. 4c), while HVR1 is predicted to be the only hexon site with substantially different conformation in Ad34 and Ad11 compared with their PF4-binder relatives Ad35 and Ad14 (Supplementary Movie 2). On PF4 proteins, residues of the equatorial ring are predicted to be the ones most frequently involved in interactions (Supplementary Fig. 4d).

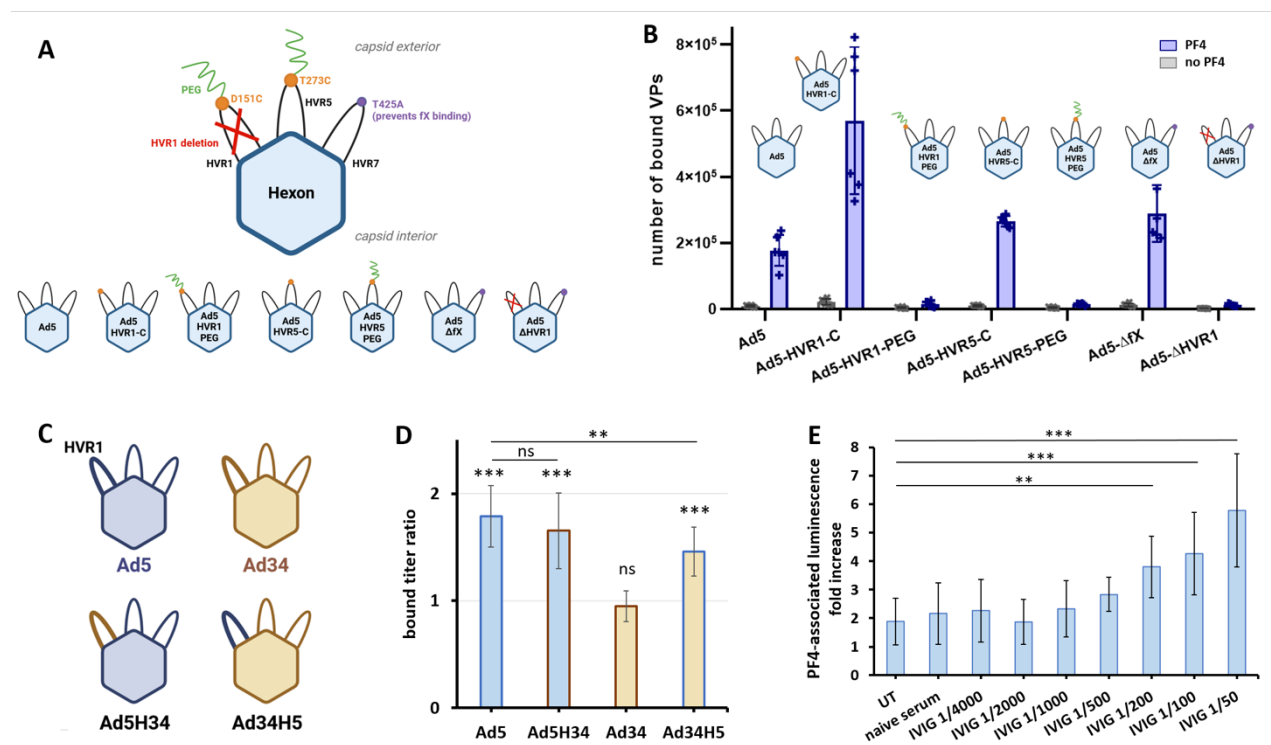


Fig. 3. PF4 likely binds to Ad5 hexon HVR1 loop and partially protects Ad5 against neutralizing antibodies.

**A:** Schematic representation of the Ad5 hexon genetic and chemical variants studied. These variants include: D151C and T273C point mutations; covalently linking a cysteine residue with a 5kDa polyethylene-glycol (PEG) polymer, which prevents binding on part of the hexon surface by steric competition; deletion of the HVR1 loop; and T425A substitution, which ablates the binding of fX. The E1-deleted, GFP-expressing Ad5 vector was used as control (Ad5). HVR: hyper-variable region. PEG: poly-ethylene glycol. Figure created with BioRender. **B:** ELISA-qPCR of the Ad5 hexon variants for PF4 binding. N=6, two independent repeats. **C:** Schematic representation of the HVR1 exchange performed to construct the Ad5H34 and Ad34H5 vectors. Figure created with BioRender. **D:** ELISA-qPCR of the Ad5H34 and Ad34H5 variants for PF4 binding. Numbers of bound VPs in PF4 coated wells were normalized on the average number from the three non-coated wells of the same experiment repeat. Ad5 and Ad34 were obtained from the Ad-GLN collection. N=8, three independent repeats. **E:** PF4 interference assay with Ad5 human serum neutralizing antibodies. Ad5 vectors from the GLN collection were incubated with or without 10  $\mu\text{g}/\text{mL}$  PF4 and 1/50 diluted human seronegative serum (“naive serum”) or pooled human intravenous immunoglobulins (“IVIG”) at varying dilutions. A549 cells were then infected with the suspensions at 500 vpc and vector-expressed luciferase luminescence was measured at 24 hpi. The ratio of luminescence levels between samples with and without PF4 and identical serum or immunoglobulin treatment is displayed. UT: untreated, without human serum or antibodies. N=12, four independent repeats. ANOVA test of displayed results yielded  $p < 0.0001$ , and the Dunnett post-hoc tests against the “UT” sample not displayed on the figure yielded non-significant p-values.

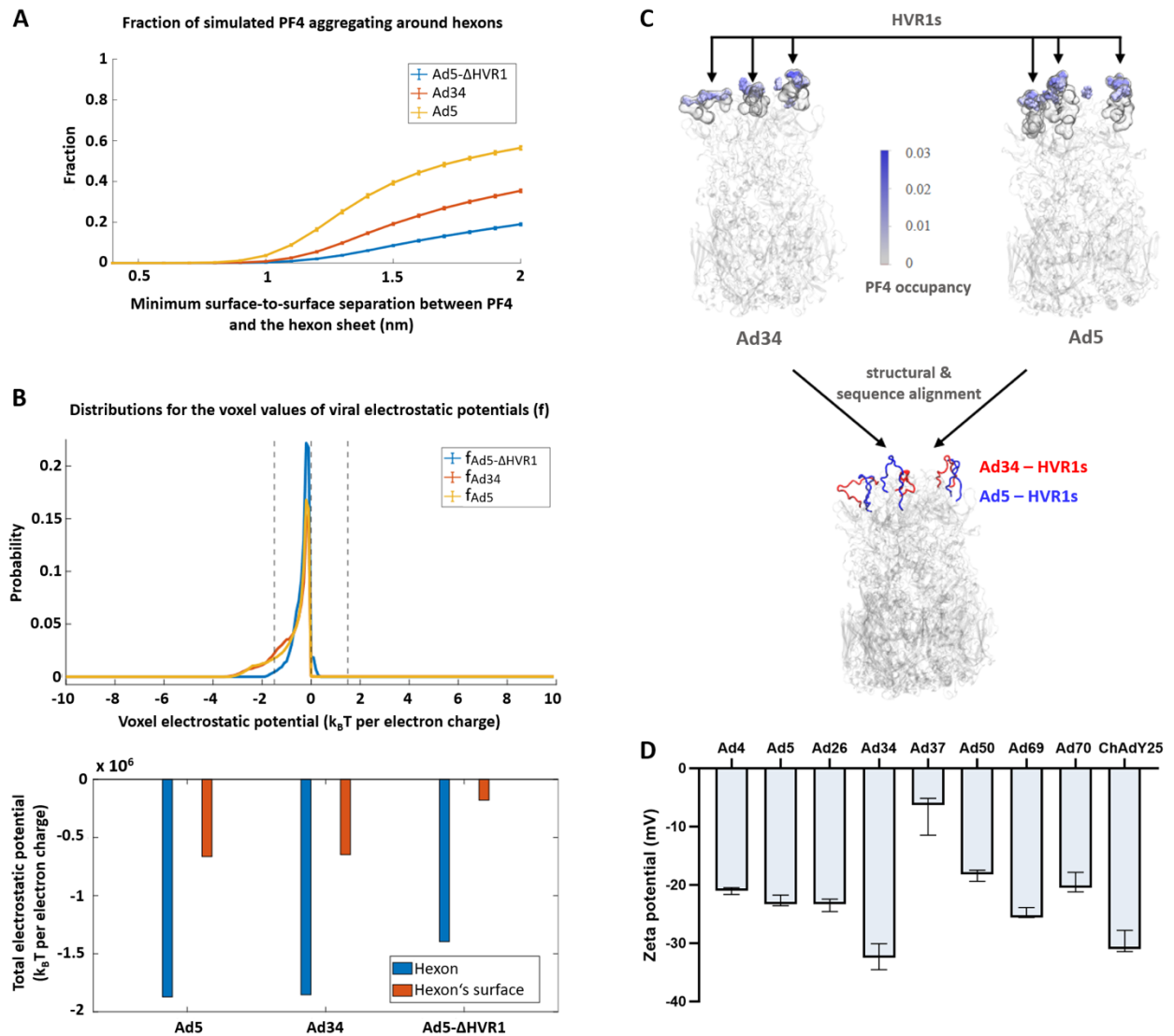


Fig. 4. Vector surface negative potential is not sufficient to explain PF4 binding.

**A:** Fraction of PF4 found at given surface-to-surface distance from adenovirus hexons, as sampled from Brownian dynamics (BD) simulations. **B:** Distribution of computed surface electrostatic potential as well as integrated values across whole hexons or hexon surface. **C:** BD simulations of popular regions for PF4 occupancy on hexons. Structural alignments of Ad34's hexon and Ad5's hexon suggest that Ad5's HVR1 loops protrude more than those of Ad34, potentially enhancing their likelihood to interact with PF4 in the bulk solvent. Detail molecular images in mapping popular PF4 interacting residues to their molecular positions in either Ad34's hexon or Ad5's hexon are given in Supplementary Fig. 4b. **D:** Surface potential of Ad particles measured by electrophoretic light scattering (ELS). Except ChAdY25 and Ad26, vectors belong to the Ad-GLN collection.  $N=3$ .



## **Ad5 infection levels in multiple immortalized or primary cell types were strongly influenced by PF4**

With the aim of better understanding how PF4 may affect Ad-host interactions, we extended Ad5 infectivity assays to a wide array of human immortalized cell lines and primary cells, in presence or absence of Ad5 seronegative human serum. Extensive differences were observed between cell types and between samples treated with and without serum, and no general rule could be identified about the amplitude and direction of the infectivity change induced by PF4 (Fig. 5a-c, Supplementary Fig. 5a,b). In particular, primary human nasal epithelium responded very strongly to the presence of PF4 both with and without serum, although in opposite directions (Fig. 5b). PF4 effects on blood leukocytes infectivity were more modest (Fig. 5c).

Ads are able to bind to erythrocytes<sup>244</sup>, which can result in substantial vector sequestration or retargeting following systemic administrations. We adapted the APD technique to study docking to human erythrocytes (Fig. 5d) of a fiber-modified Ad5 with ablated CAR tropism (Ad5- $\Delta$ CAR), whose ability to bind PF4 had been verified by ELISA-qPCR (Supplementary Fig. 2). PF4 increased Ad5- $\Delta$ CAR precipitation to a higher degree with compared to without erythrocytes (Fig. 5e), showing that PF4 increased erythrocyte docking. PF4 had no influence on Ad34 docking on erythrocytes (Supplementary Fig. 5c), suggesting that PF4 effects on Ad5- $\Delta$ CAR depend on direct interactions with VPs. We also tested Ad34 and its close relative but PF4-binder type Ad35 in infectivity assays with primary leukocytes, and PF4 did not substantially affect their infectivity (Supplementary Fig. 5b).

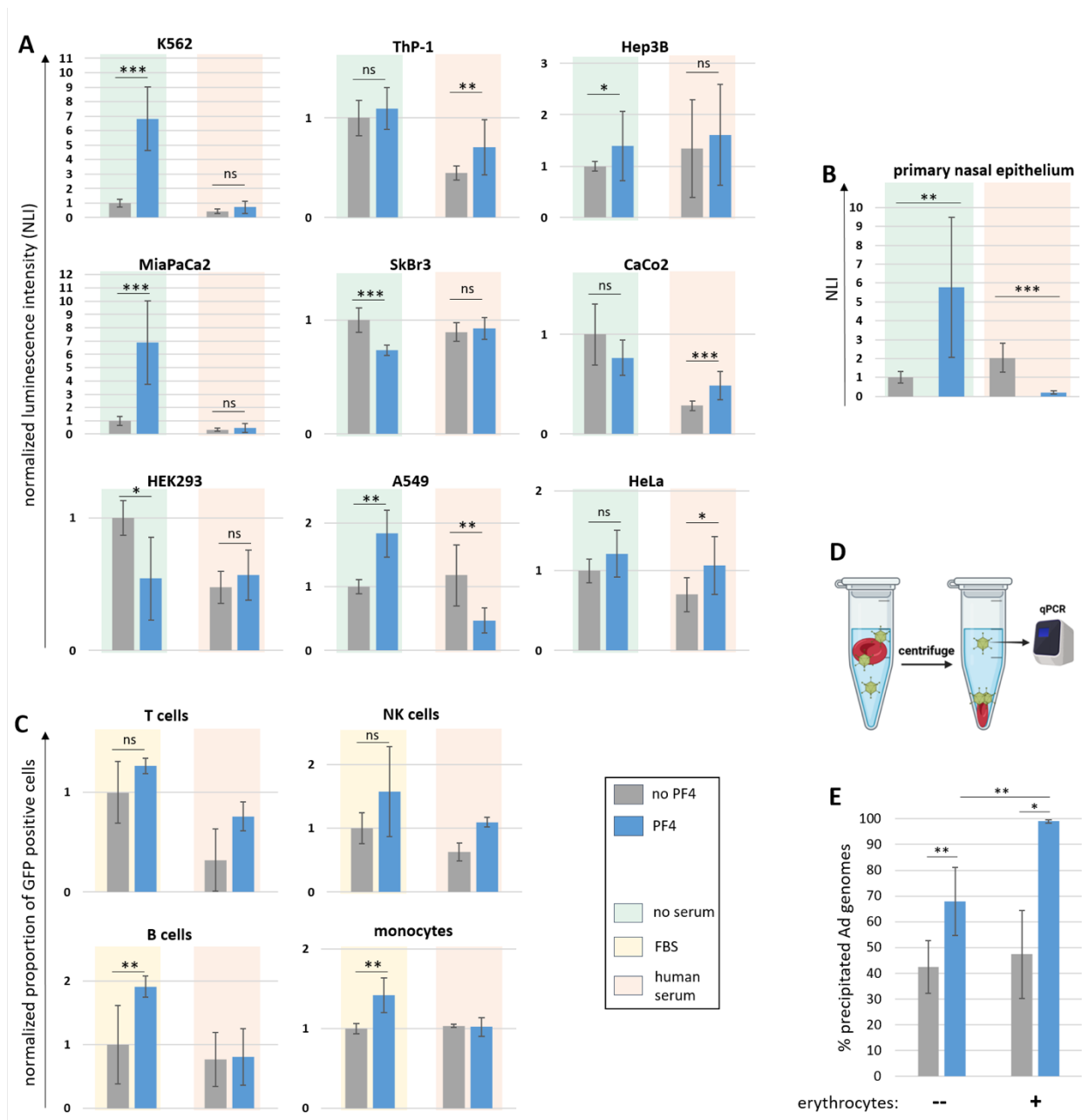


Fig. 5. PF4 effects on Ad5 infectivity are serum and cell type dependent. Cells were infected with Ad5 VPs incubated for 10 min. at 37°C in presence or absence of 10  $\mu\text{g}/\text{mL}$  PF4, 10% fetal bovine serum (FBS), or human serum seronegative for Ad5. **A**: Immortalized cells were infected with 20 vpc of Ad5 vector from the Ad-GLN collection. Ad-expressed luciferase luminescence was quantified 24 hpi and normalized to the average of the “no PF4, no serum” condition for each cell line.  $N \geq 6$ , two or three independent repeats. **B**: Primary human nasal epithelium cells were infected with 20 vpc of Ad5 vector from the Ad-GLN collection. Ad-expressed luciferase luminescence was quantified 24 hpi and normalized to the average of the “no PF4, no serum” condition. NLI: normalized luminescence intensity.  $N \geq 7$ . **C**: Primary peripheral blood mononuclear cells were infected with 2000 vpc of Ad5 vector from the Ad-GLN collection. Ad-expressed GFP fluorescence was quantified 48 hpi and the proportions of GFP-positive cells were normalized to the average of the “no PF4, FBS” condition for each cell type.

$N \geq 3$ , one or two independent repeats. **D:** Principle of the Erythrocyte Pull-Down technique. VPs aggregated or docking on erythrocytes are separated from free VPs by low speed centrifugation and titrated by qPCR. Figure created with BioRender. **E:** Erythrocyte pull-down of a fiber-modified Ad5 with ablated CAR tropism (Ad5- $\Delta$ CAR) in absence or presence of PF4.  $N=8$ .

### **PF4 non-binding model COVID-19 vaccine vectors induced cellular immune responses in mice**

In order to assess the clinical applicability of PF4-negative vectors, the E1 genes of Ad5, Ad5- $\Delta$ HVR1, Ad11 and Ad34 were replaced by a cassette encoding SARS-CoV-2 spike protein S1 domain to generate model COVID-19 vaccine vectors. Groups of mice were immunized intravenously with 5E8 VP of either one of these Ad vectors or vehicle (Fig. 6a) and S1-specific CD8<sup>+</sup> T cells were enumerated and characterized in blood 14 and 28 days later using MHC class I tetramers. On day 14, the response elicited by Ad5- $\Delta$ HVR1-S1 was somewhat higher than those triggered by Ad5-S1, and the latter exceeded the responses to Ad11-S1 and Ad34-S1 (Fig. 6b,c). By day 28 the response to Ad5-S1 had caught up with the one induced by Ad5- $\Delta$ HVR1-S1, while the responses to Ad11-S1 and Ad34-S1 remained about 2-fold lower. A similar hierarchy was also noted when MHC class I tetramers were used to enumerate S1-specific CD8<sup>+</sup> T cells in the spleen 30 days after immunization (Fig. 6d). When studying the cells' differentiation, minor differences between vectors were noted in the early (day 14) expression levels of the effector / memory markers CX3CR1 and CD27 (Supplementary Fig. 6c), but these differences mostly levelled out by day 28 and were not reflected in a differential repartition of S1-specific CD8<sup>+</sup> T cells into short-lived effector cells (KLRG1<sup>+</sup> CD127<sup>-</sup>) and memory-precursor cells (KLRG1<sup>-</sup> CD127<sup>+</sup>; Supplementary Fig. 6b, c). Splenic T cell responses were analyzed on day 30, both by MHC class I tetramer and intracellular cytokine assays (Fig. 6d). Only minor differences between groups were noted in the total number of tetramer-binding or S1-specific IFN- $\gamma$ -producing CD8<sup>+</sup> T cells, with a hierarchy following the one previously observed in blood. No major differences between vaccination groups were noted in terms of splenic CD8<sup>+</sup> T cell effector/memory profiles elicited (Supplementary Fig. 6e, f). S1-specific IFN $\gamma$ -producing CD4<sup>+</sup> T cells were highest in the Ad5-S1 immunized group, closely trailed by the Ad5- $\Delta$ HVR1-S1-immunized animals, while CD4<sup>+</sup> T cell responses to Ad11-S1 and Ad34-S1 were significantly lower than those elicited by Ad5-S1. These rather subtle differences became somewhat more clear-cut when enumerating IFN- $\gamma$ /TNF- $\alpha$ -coproducing and thus more polyfunctional CD8 and CD4 T cells (Fig. 6e, f). Taken together the cellular immune responses induced by Ad5-S1 and Ad5- $\Delta$ HVR1-S1 were of similar magnitude and phenotype, whereas those induced by Ad11-S1 and Ad34-S1 exhibited a similar phenotype, too, but were of slightly reduced magnitude. To determine the induction of humoral responses, we quantified serum vector-binding antibodies and neutralizing antibodies directed against spike-decorated pseudoviral particles. Ad5-S1 was the only vector to consistently induce anti-spike neutralizing antibodies, and neutralization titers decreased close to ten-fold between days 14 and 28 after immunization (Fig. 6g). Meanwhile, the

anti-vector humoral response was higher in Ad11-S1 and Ad34-S1 vaccinated animals than in mice receiving Ad5 vectors (Fig. 6h). In the Ad5- $\Delta$ HVR1-S1 immunized group only one out of five animals had detectable anti-Ad5- $\Delta$ HVR1-S1 antibodies, and only at low level.

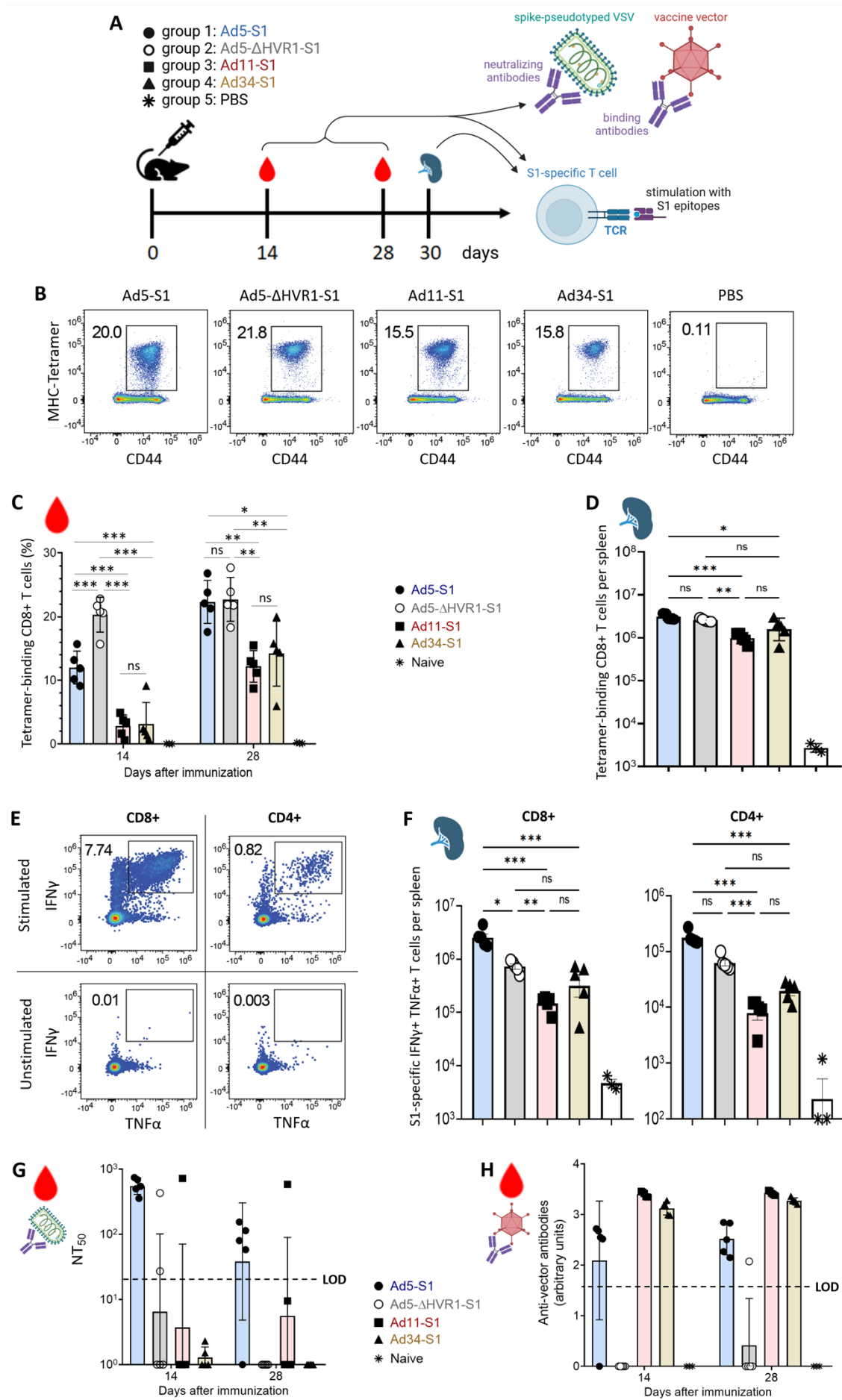


Fig. 6. Assessment of PF4-negative candidate SARS-CoV-2 vaccines for mouse immunization.

**A:** Experiment design. Five 10-12 weeks old C57BL/6JCrI male mice per group were immunized intravenously with 5E8 VP of E1-deleted or E1/E3-deleted vectors expressing the S1 domain of the SARS-CoV-2 spike protein (Hu-1 strain). Blood was drawn at 14 and 28 days after immunization (dai) and mice were sacrificed at 30 dai for splenocyte collection. **B:** Representative FACS plots showing the frequencies of peripheral blood S1-epitope specific CD8 T cells in the different groups **C, D:** Percentages of S1-epitope specific CD8 T cells in blood (**C**) and numbers in spleen (**D**) as determined by MHC tetramer staining. Time-course analysis using a mixed model two-way ANOVA was performed in (**C**). **E:** Representative FACS plots of stimulated or unstimulated IFN- $\gamma$  and TNF- $\alpha$  secreting CD8 and CD4 T cells. **F:** Numbers of S1-specific IFN- $\gamma$  and TNF- $\alpha$  secreting CD8+ (left) and CD4+ (right) T cells in spleen upon peptide stimulation. Numbers of IFN- $\gamma$  and TNF- $\alpha$  secreting cells in non-stimulated controls were subtracted. **G:** SARS-CoV-2 neutralizing antibody titer (NT<sub>50</sub>) in mouse serum. **H:** Vector particle binding antibodies in the serum of immunized mice were determined by ELISA. Symbols represent individual mice. LOD: limit of detection.

## Discussion

Here we identified several AAV and Ad vectors lacking VITT-associated interactions with PF4 and may thus represent safer candidates for gene therapy, oncolytic virotherapy as well as vaccination. The identified natural Ad types, namely Ad13, 34, 80 and possibly Ad11, share a low to very low seroprevalence<sup>245</sup> that strengthens their potential safety profile. We also showed that genetic or chemical capsid engineering of Ad5 could lead to the loss of pre-existing binding to PF4 through deletion or polymer shielding of the hexon HVR1 loop. Future developments on polymer modification of non-Ad5 types will be required to assess the full potential of this method, notably in the context of repeated Ad delivery as often required by vaccination or therapy regimens.

Moreover, AAV and Ad types not included in this study, notably simian Ads, may be screened for PF4 binding using SPR and/or the panoply of user-friendly, scalable and affordable techniques established in this article (ELISA-qPCR, infectivity assays and Ad-PF4 aggregates or erythrocytes pull-down) in order to identify novel candidates.

ELISA-qPCR and APD displayed a relatively high sensitivity, as exemplified by the significant detection of PF4-Ad5 binding even at low VP concentration (Supplementary Fig. 1b) and despite the relatively low affinity of this interaction ( $K_D = 789 \text{ nM}^{85}$ ). Our assays almost systematically yielded concordant results and constitute a panoply of independent techniques facilitating the screen of large Ad and AAV collections for PF4 binding with results robust across experimental conditions. However, these assays remain so far only qualitative and levels of unspecific binding to uncoated surfaces were variable (Supplementary Fig. 2). Further experiments using varying concentrations of VPs and proteins are warranted to elucidate their sensitivity cut-offs. Finally, additional tests should assess the range of

applications of our new techniques, which in theory extend to all virus-protein interactions in the case of ELISA-qPCR.

APD and ELISA-qPCR yielded contradicting results regarding Ad11, therefore it is still unknown whether this serotype is able to bind PF4. Measurements with independent and validated techniques including SPR are underway and will hopefully solve the uncertainty as well as indicate how reliable APD and ELISA-qPCR are respectively. It is possible that the disagreement between both techniques stems from the use of different buffers, however this did not appear to affect the other tested serotypes. We complemented our screenings with infectivity assays that confirmed that Ad34 and Ad80 do not bind to PF4 (Fig. 2c-e). In order to test if the PF4-mediated infectivity increase of Ad5 and Ad69 is explained only by the formation of VP aggregates (as observed by APD) or if PF4 also increased the infectivity of free VPs, we quantified Ad-driven GFP fluorescence in infected A549 cells (Fig. 2d). Since not only the mean fluorescence intensity (MFI) but also the proportion of GFP-positive cells was increased by pre-incubation of Ad5 and Ad69 with PF4, we favor the second hypothesis. PF4 increased GFP fluorescence levels not only by increasing the infectivity of PF4-binder Ad types, but also through VP-independent effects on the tested cells (Fig. 2e) which may consist in a response to chemokine signaling affecting GFP expression. Ad34-driven GFP fluorescence levels were even higher when target cells had been cultivated in presence of PF4 before infection rather than simultaneously. Since the duration of exposure to PF4 was identical, this may be explained by the longer time of cultivation after removal of PF4 in the former case. VP-independent effects of PF4 on cell viability and gene expression patterns have already been reported in different populations of human leukocytes<sup>246</sup> and may have enhanced or dampened PF4 influence on Ad-driven GFP expression in infected primary leukocytes (Fig. 5c, Supplementary Fig. 5b). They could explain the slight PF4-mediated increase of Ad34-driven GFP expression observed in T and B cells (Supplementary Fig. 5b). On the other hand, PF4 effects on Ad gene expression dependent on PF4-VP interactions likely explains at least part of the strong permissivity changes in presence of PF4 in several of the tested human cell types (Fig. 5a-c). Moreover, PF4 may increase Ad sequestration on erythrocytes (Fig. 5e), a known cause of vector inactivation and toxicity<sup>244,247</sup>, but on the contrary could protect vectors from neutralizing antibodies and thereby increase bioavailability. Altogether, these results highlight that PF4 binding may modify the tropism of clinical Ad vectors and raise additional safety concerns beside thrombosis. Interestingly, substantial and cell type specific Ad5 infectivity modifications have been reported not only after binding with PF4, but also with the defensin HNP1, another small cationic antimicrobial protein<sup>248</sup>.

The inhibition of PF4 binding by HVR1 deletion (Fig. 3b) and PEGylation of HVR1 and HVR5 (which is spatially very close to HVR1) but not by fiber protein modification (Ad5- $\Delta$ CAR and Ad5F35 vectors, Supplementary Fig. 2) proved that PF4 binds to the hexon of Ad5. Moreover, these results added to Brownian dynamics simulations (Fig. 4b-d), the comparison of hexon structures and sequences of PF4 binder versus non-binding Ad types (Fig. 4a, Supplementary Movies 1,2), the PF4-mediated partial protection against neutralizing antibodies (Fig. 3e) and especially the acquisition of PF4 binding capability by Ad34 upon insertion of Ad5 HVR1 loop (Fig. 3d) all point to HVR1 as the most likely binding site. This loop, protruding at the apex of the hexon, is already known as the binding site

on the Ad5 capsid of several proteins including lactoferrin<sup>249</sup> and the SR-A6 scavenger receptor<sup>250</sup>. The fact that the Ad5H34 vector, whose HVR1 loop was exchanged with that of Ad34, does bind to PF4 (Fig. 3d), suggests that the precise amino acid sequence and surface electronegativity of the HVR1 loop are not determining factors in PF4 binding. We instead favor the hypothesis that occupancy of the interhexon space by the HVR1 loop plays an important role in PF4 binding. Indeed, structural models predicted that Ad5's and Ad5H34's, but not Ad34's HVR1 loops, protrude towards the interhexon space (Supplementary Movie 1). Furthermore, given the flexibility of hexon HVRs, it can be envisioned that PF4 does not have a unique binding site. It is also possible that the binding site(s) differs between Ad types, which is suggested by our observation that Ad4 binds PF4 (Fig. 1c) despite its very short HVR1 loop. The structural alignment algorithms used here may also be poorly predictive of flexible loops structures, while Brownian Dynamics models indicate interaction probability but not affinity, explaining the mild PF4 binding predicted for Ad34 contrary to experimental data. A more detailed experimental study of additional Ad types and hexon variants is therefore warranted to fully elucidate PF4 binding site(s).

Like other *in vitro* studies, our investigation of PF4 binding to Ads either in optiMEM, RPMI, PBS or immobilized on an ELISA plate may not fully recapitulate the interactions occurring in the blood or in tissues, which are more complex environments in which other interaction partners can be involved. In particular, understanding the immunological consequences of the modified Ad cell binding and infection patterns observed here will require dedicated investigation. Still, we can reasonably expect that the Ad types for which we detected no PF4 binding would at least display lower binding *in vivo* than other Ads and may present a lower risk of causing thrombosis.

Adenoviral vaccines, gene therapy vectors and oncolytic vectors without VITT risk may prevent a number of patients' deaths and even more non-fatal complications, as well as improve the public trust in medical treatments and adherence to epidemics containment measures. We therefore tested the applicability of several PF4-negative Ads as proof-of-concept vaccine vectors. We chose Ad5- $\Delta$ HVR1 and Ad34, which did not display PF4 binding according to several independent techniques and using three different virus preparations of confirmed quality. We also included Ad11 despite the uncertainty regarding its ability to bind PF4 or not, due to its already validated use as a vaccine vector. Indeed, E1/E3-deleted Ad11 vectors encoding HIV gag protein had been used to immunize mice and had proven immunogenic in heterologous administrations alongside Ad35-based vectors<sup>251</sup>.

Our mouse immunization study revealed S1-specific cellular immune responses induced by all tested vectors (Fig. 6b-f, supplementary Fig. 6). As demonstrated with COVID-19 vaccines, cell mediated immune responses are a main correlate of variant cross-reactive vaccine protection<sup>164</sup> and are far more durable than antibody titers<sup>160</sup>. Hence T cells may represent the most important arm of immunity to induce when it comes to prevention of severe disease<sup>155</sup>. Ad5- $\Delta$ HVR1-S1 induced T cell responses comparable to Ad5-S1, while Ad11-S1 and Ad34-S1 were somewhat less immunogenic. In terms of humoral responses, only Ad5-S1 induced SARS-CoV-2 neutralizing antibodies (Fig. 6g). However, the S1 subunit used as an antigen here seems to be a poor inducer of SARS-CoV-2 neutralizing antibodies<sup>252</sup>, unlike the full-length S protein. Finally, anti-vector antibodies can impede



adenoviral vector-based immunization<sup>42,114,116,117</sup>. The low to undetectable anti-vector responses in Ad5- $\Delta$ HVR1-S1 vaccinated mice therefore hold promise for HVR1 deleted vectors in homologous prime boost vaccination.

Since the validated ChAdY25 type proved suitable for human vaccination in a pandemic context despite also displaying lower immunogenicity in mice than Ad5<sup>253</sup>, in our opinion our study does not exclude Ad11 and Ad34 as potential vaccine platforms. The immunogenicity of species B human Ad vaccines in mice was already reported to be inferior to other Ad species<sup>81,254</sup>, and previous studies of Ad vaccine vectors encoding the HIV gag protein in macaques reported a relatively low immunogenicity of Ad34 (T cell IFN- $\gamma$ ) secretion levels around 8 times lower than Ad5<sup>81,255</sup>, but also found that Ad34-induced cellular responses were strongly boostable<sup>255</sup>. Even if the low immunogenicity of Ad34 vectors also applied to humans and to other antigens, various approaches of antigen design and adjuvanting can be implemented to increase the immunogenicity of a vaccine despite possible limitations of the vector platform<sup>253</sup>, while the manufacturability and very low seroprevalence of Ad11 and Ad34 add arguments in favor of their consideration for clinical use. Likewise, the vectors NG-641 and Enadenotucirev (previously known as EnOncoAd or ColoAd1) carrying Ad11 hexon<sup>256</sup> have already been used in several clinical trials for oncolytic virotherapy, supporting the safety profile and high biological activity in humans of species B Ad vectors<sup>257,258</sup>. Furthermore, species D types Ad13 and Ad80 have recently been predicted to be relatively immunogenic as vaccine platforms based on mouse innate immune responses to wild-type viruses<sup>254</sup> and may therefore deserve consideration despite problematic manufacturability in our hands.

Alternatively, it may be possible to readily improve the safety of existing adenovirus vaccine platforms by HVR1 deletion. It has already been shown that HVR1-deleted Ad5 vectors are substantially less hepatotoxic and less sensitive to serum neutralizing antibodies than wild-type Ad5<sup>259</sup>. If these advantages as well as the loss of PF4 binding and the conservation of efficiency as vaccines could be translated to other Ad types, HVR1 deletion could represent a potent and simple engineering method to increase vector safety and facilitate repeated administration.

A limitation of our study is that the extreme rarity of VITT and lack of a fully representative animal model have precluded until now the drawing of firm conclusions on whether PF4 binding to Ad VPs is a trigger of VITT. Alternative and not mutually exclusive hypotheses involve Ad VPs interactions with platelets leading to their activation and phagocytosis<sup>260</sup>, or vaccine impurities<sup>233</sup>. However, the latter hypothesis is not sufficient to explain why VITT was associated with both anti-COVID-19 adenovirus-based vaccines despite extensive differences in formulation<sup>261</sup> and not to mRNA-based vaccines, and the former why VITT auto-antibodies are directed specifically against PF4 and not other platelet proteins. On the contrary, the involvement of PF4 interactions with adenovirus proteins or full VPs in VITT is supported by the observations that antibodies can be elicited against PF4 proteins adopting a new conformation upon binding to pathogen surfaces<sup>236,262</sup>, and that VITT symptoms very closely match those of spontaneous heparin-induced thrombosis (HIT), which can be elicited by bacterial or viral infections<sup>263,264</sup>. Therefore, the currently most supported and accepted hypothesis regarding the origin of VITT is that a subset of pre-sensitized individuals exposed to Ad-PF4 complexes undergo epitope

spreading leading to the secretion of highly reactive anti-PF4 auto-antibodies<sup>261</sup>. This would explain why spontaneous HIT and VITT present an early onset following immunization and usually involve oligoclonal antibodies, suggesting they result from secondary immune responses against PF4-particle complexes. A similar hypothesis proposes that anti-PF4 auto-antibodies derive by epitope spreading from antibodies recognizing adenovirus particles independently of PF4 binding<sup>265</sup>, but this appears unlikely because of the apparent lack of adenovirus capsid structures highly similar to the epitope of VITT antibodies on PF4 that may permit epitope spreading. Worryingly, if Ad-PF4 complexes were indeed one of the triggers of VITT, it could be expected that a large number of COVID-19 vaccinees would now be primed for acute secondary immune response and potentially thrombosis in case of future exposure to PF4-binding vectors. This would mean that there is a crucial medical need for the development of PF4-negative viral vectors.

Thrombotic disorders have been associated not only with adenoviral vaccines, but also adeno-associated virus gene therapy vectors<sup>239</sup>. Even though the AAV-associated TMA syndrome differs from the Ad-related VITT in its clinical presentation, it is striking that the AAV9 type associated with most identified cases binds to PF4<sup>242</sup>. Other cases have been linked to the C102 and LK03 vectors<sup>240</sup>, whose ability to complex PF4 has not yet been tested. Furthermore, pathogens such as HIV-1 are able to bind to PF4<sup>266</sup> and associate with deep vein thrombosis and thrombocytopenia<sup>267,268</sup>, and a VITT case was reported following papillomavirus vaccination<sup>269</sup>. Thus, investigations on other vectors and virus families for interactions with PF4 and the potential pathologic consequences are warranted.

To conclude, we established here a novel technique armamentarium facilitating fast, affordable, sensitive and specific assessment of virus-protein interactions. We identified several vectors, namely AAV1, 6 and 7, Ad13, 34 and 80, and Ad5- $\Delta$ HVR1, which lack PF4 binding. In particular, Ad34 showed applicability and Ad5- $\Delta$ HVR1 non-inferiority as preclinical vaccine platforms. These results may represent a milestone in the development of safer Ad vectors.

## Methods

### Vector acquisition

The Ad-WT collection has already been described in Wang *et al.*<sup>245</sup>. The Ad-GLN collection, already described in Zhang *et al.*<sup>241</sup>, contains vectors from different types that express TurboGFP, NanoLuc luciferase and the selection marker kanamycin/neomycin under a synthetic CAG promoter in the deleted E3 region. The CAG promoter consists of the human cytomegalovirus early enhancer element, the chicken beta-actin promoter including parts of the first exon and intron, and parts of the second intron and third exon of the rabbit beta-globin gene.

The hexon-modified Ad5 vectors were produced similarly as described elsewhere<sup>270</sup>. Briefly, genetic capsid modifications were introduced using pRed/ET homologous recombination (Gene Bridges, Heidelberg, Germany) in a bacmid carrying an Ad5 genome (AY339865) with the E1 locus (bp

441-3534) replaced by a CMV-promoter driven eGFP expression cassette. Vector PEGylation was conducted with 5 kDa mono-activated maleimide polyethylene glycol as described elsewhere<sup>270</sup>.

The CAR-ablated Ad5 (previously described<sup>271</sup>) was generated by introducing the point mutation Y477A (AAQ19310.1) in the fiber gene of the GFP-expressing, E1-deleted Ad5 backbone with the pRed/ET recombination kit. The Ad5F35 vector contains Ad35 fiber (positions 30954 to 31794) replacing the original Ad5 fiber (positions 31169 to 32782). The Ad5- $\Delta$ HVR1 vector was constructed by incorporating the T425A hexon mutation which ablates binding to factor X, and substituting the 22 amino acids at the positions 141 to 162 of the hexon protein by the neutral peptide GGSG, as described elsewhere<sup>259</sup>. The Ad5H34 vector was constructed from the HVR1-deleted Ad5 as backbone using the pRed/ET recombination kit, by substituting the 22 amino acids at the positions 141 to 162 of Ad5's wild-type hexon for the 17 amino acids at the positions 141 to 157 of Ad34's hexon protein. Likewise, Ad34's hexon amino acids 141 to 157 were replaced by Ad5's hexon amino acids 141 to 162 by recombineering<sup>241</sup> to generate the Ad34H5 vector.

To generate the model S1 vaccine vectors, the human codon-optimized S1 domain of SARS-CoV-2 Wuhan strain (pUC57-2019-nCoV-S plasmid, GenScript Biotech Corporation) was subcloned under a CMV promoter and before a SV40 poly-A terminator. This expression cassette was then inserted in left-to-right orientation in *lieu* of the E1 gene (genomic positions 441 to 3521) of an E3-deleted Ad5 genome, as well as Ad11 (468 to 3271) and Ad34 (469 to 3272) backbones carrying Ad5 E4-ORF6 (PCR-amplified from Ad5 genomic positions 32958 to 34072) instead of their own homologous ORFs (genomic positions 31875-32973 for Ad11 and 31861-32959 for Ad34) so that the resulting Ad11-S1 and Ad34-S1 vectors can be rescued in HEK293 cells despite their lack of E1 gene. The Ad5- $\Delta$ HVR1-S1 vector was obtained from Ad5-S1 by substituting the 22 amino acids at the positions 141 to 162 of the hexon protein by the neutral peptide GGSG.

All adenovirus vectors produced for this study, including ChAdY25 and Ad26 vectors with capsids equivalent to the COVID-19 vaccines, were grown on HEK293 cells and purified by double CsCl banding and subsequent desalting with PD-10 columns (SE Healthcare). Ad vectors were titrated by optical density measurements<sup>272</sup> and silver staining of VP proteins after polyacrylamide gel electrophoresis in reducing conditions.

Adeno-associated vectors were produced, purified and titrated as described previously<sup>273</sup>.

## **ELISA-qPCR**

Proteins used in this study were human platelet factor 4 (PF4-h, Chromatec), which was stored at 4°C in PBS at a concentration of 200  $\mu$ g/mL; human factor X (fX, Cellsystems #HCX-0050-MG); and *S.typhimurium* tRNA-specific adenosine deaminase (tadA, MyBioSource #MBS1445221). Proteins of interest were diluted in coating buffer (0.1 M NaHCO<sub>3</sub>, pH set between 9.2 and 9.6 using 1 M Na<sub>2</sub>CO<sub>3</sub>) to a concentration of 20  $\mu$ g/mL and 75  $\mu$ L were added per well of ELISA plate (Sarstedt #82.1581.200), which was sealed with a transparent film and incubated overnight at 4°C. Wells were washed twice with TBS-Tween (TBST; 0.5% Tween20), blocked with blocking buffer (TBST + 0.5% pork skin gelatin) for 1 h at room temperature (RT), and washed twice with TBST. Vector particles were diluted in blocking

buffer and incubated in the chosen coated wells for 2 h at 37°C. Except stated otherwise, 5E7 VP of adenovirus vectors or 5E8 VP of adeno-associated vectors were used per well with 75  $\mu$ L total volume. After virus incubation, wells were washed four times with TBST in order to eliminate VPs which did not interact specifically with the coated proteins. To quantify the remaining VPs, 75  $\mu$ L of alkaline lysis buffer (25 mM NaOH + 2 mM EDTA) were added per well and the plate was carefully and tightly sealed and heated at 95°C for 10 min. to open capsids and release vector genomes. The plate was then immediately put on ice and 25  $\mu$ L of cold neutralization solution (80 mM Tris-HCl + 0.1% Tween20, pH = 3.2) were added in each well. The virus genome solutions of each well were homogenized by shaking and two 2  $\mu$ L aliquots were taken for qPCR titration using a CFX96 Real-Time System machine (BioRad) and the my-Budget 5x EvaGreen qPCR-Mix II (Bio-Budget) following the manufacturer's instructions, except for vectors of the Ad-WT collection which were quantified using Takyon No ROX Probe 2x MasterMix dTTP blue (Eurogentec) and the universal hexon primer/probe set of Heim *et al.*<sup>274</sup>. See Supplementary Table 1 for primers.

### **Electrophoretic light scattering measurements**

To ensure homogeneous measurement conditions and best visibility of Zeta( $\zeta$ )-potential changes, vectors were submitted to buffer exchange prior to ELS measurement. Buffer exchange was performed using 5E10 VPs and PD-10 MiniTrap G-25 columns (GE Healthcare, Solingen, Germany) following the company's instructions with the "gravity" protocol. Briefly, the column was equilibrated using the measurement buffer (50 mM HEPES, pH 7.2). Afterwards, vectors were added to the column and subsequently, the vector volume was adjusted to 500  $\mu$ L by adding measurement buffer to the column. The column was placed on a 1.5 mL reaction tube and the vector was eluted using 1 mL measurement buffer. Complete sample volume was used to measure "particle concentration" (Zetasizer Advance Serie – Ultra Red, Malvern Panalytical, Kassel, Germany) in a glass cuvette with square aperture (PCS1115). Thereby, size and concentration were determined by multiple angle dynamic light scattering (MADLS) with three measurement repeats (25°C, dispersant scattering mean count rate 179 kcps, dispersant values: R.I. 1.33; viscosity 0.8872 mPa s). For  $\zeta$ -potential measurement, 700  $\mu$ L of the suspension were transferred to a folded capillary cell (DTS1070). To ensure sample integrity, three size measurements in backscatter mode were done before and after the  $\zeta$ -potential measurement (25°C, dispersant values as given above).  $\zeta$ -potential measurement was done in "general purpose" mode with a minimum number of runs of 10, three repeats and 60 seconds pause between each repeat (25°C, dispersant values as given above).

### **Aggregate Pull-Down**

1E7 VPs were incubated for 30 min. at 37°C in 30  $\mu$ L of PBS + 1% BSA with or without 10  $\mu$ g/mL of PF4. After centrifugation for 5 min. at 1000 g, the supernatant was transferred to a new tube containing 30  $\mu$ L of 2x alkaline lysis buffer (50 mM NaOH + 4 mM EDTA), while 30  $\mu$ L of 2x alkaline lysis buffer and 30  $\mu$ L of PBS + 1% BSA were added to the pellet. Both treated supernatant and pellet were mixed

thoroughly and heated at 95°C for 10 min. in order to release Ad genomes, then neutralized with 20  $\mu$ L of cold neutralization solution and titrated by qPCR (see Supplementary Table 1 for primers).

### **Erythrocyte Pull-Down**

This assay was inspired from Carlisle *et al.*<sup>244</sup>. Venous blood was collected into EDTA tubes (Sarstedt, 02.1066.001) from the antecubital vein of a healthy volunteer who gave informed consent. The blood was swiveled at room temperature (RT) for 15 min. then centrifuged for 5 min. at 2000 g in order to isolate erythrocytes, which were then washed three times with PBS, resuspended in PBS + 1% BSA to a concentration of 5.5E9 cells / mL, and kept at 4°C for no more than 3 days. 4E7 VPs were incubated 30 min. at 37°C in 80 $\mu$ L of the erythrocyte suspension with or without 10  $\mu$ g/mL of PF4. The suspension was centrifuged for 5 min. at 1000 g and the supernatant was transferred to a new tube. Both supernatant and pellet were treated with 2x alkaline lysis buffer, mixed thoroughly and heated at 95°C for 10 min. in order to release Ad genomes, then neutralized with neutralization solution and titrated by qPCR (see Supplementary Table 1 for primers).

The study was approved by the ethics committee of the University Witten/Herdecke (approval number 216/2020, December 17<sup>th</sup> 2020; all relevant ethical regulations have been followed and all donors gave informed consent).

### **Cell culture**

Cells were cultivated with Dulbecco's Modified Eagle Medium (DMEM, Pan-Biotech; for A549, CaCo2, EaHy926, HEK293, Hela, Hep3B, HepG2, MiaPaCa2 and SkBr3 cells) or Roswell Park Memorial Institute 1640 Medium (RPMI, Pan-Biotech; for HCC827, Jurkat, K562, SKOV-3 and THP-1 cells), each supplemented with 10% (or 20% in the case of CaCo2 and HCC827 cells) Fetal Bovine Serum (FBS, Pan-Biotech) and 1x Penicillin-Streptomycin (P/S, Pan-Biotech) at 37°C under an atmosphere with 5% CO<sub>2</sub>. ThP-1 cells were additionally supplemented with 50  $\mu$ M  $\beta$ -mercaptoethanol. ThP-1 macrophages were differentiated 72h in presence of 20 ng/mL of phorbol-12-myristat-13-acetate (PMA). Cells were tested for mycoplasma infection using the VenorGeM OneStep kit (Minerva Biolabs).

Peripheral blood mononuclear cells (PBMCs) were isolated from the blood of healthy volunteers collected in EDTA tubes using SepMate tubes (Stemcell technologies) following manufacturer's instructions. PBMCs were counted and cultivated in RPMI + 10% FBS + P/S media for 24 hours in low adherence dishes (Corning, #3471) before infection. The study was approved by the ethics committee of the University Witten/Herdecke (approval number 159/2022, October 10<sup>th</sup> 2022; all relevant ethical regulations have been followed and all donors gave informed consent).

Nasal epithelium cultures were derived from patients samples with chronic rhinosinusitis and nasal polyposis undergoing an operational procedure. Tissue samples were first cut into small portions and placed in collagenized cell culture flasks (Greiner Bio-One, AT) filled with BEGM® medium (Lonza, Switzerland). Portioned tissue pieces were then removed (usually after 1-3 days) from the cell culture flasks and the culture was continued using the outgrowth technique as described previously<sup>275</sup>. After

two to three weeks, a 90% confluence rate was achieved and the culture purity was assessed by flow cytometry using epithelial cell-specific antibodies as described previously<sup>276</sup>. The cells were then seeded into collagenized cell culture plates and used for infection assays. The sample collection and obtaining of consent was conducted under strict observance of relevant ethical regulations and under a positive ethics approval from the Witten/Herdecke University, Germany (approval number: 209/2020).

### **Surface Plasmon Resonance**

A BIAcore T200 (Cytiva, formerly GE Healthcare) equipped with a C1 sensor chip (Biacore) was used to generate binding profile at 25°C in a running buffer of HBS-EP+ (10 mM HEPES, 150 mM NaCl, 3 mM EDTA, and 0.05% (v/v) Surfactant P20).

To prepare the capture surface, viruses were amine-coupled under standard conditions at a flow rate of 10 µL/min, as follows. Each flow cell was activated with a freshly prepared 1:1 v/v mixture of aqueous stocks of 0.4 M 1-ethyl-3-(3-dimethylaminopropyl) carbodiimide (EDC) + 0.1 M N-hydroxysuccinimide (NHS) for 240 s. Viruses were diluted to  $\sim 2.5 \times 10^{10}$  VP/ml in 10 mM acetate 3.5 buffer and coupled for 30 min. Finally, excess reactive esters were blocked with 1 M ethanolamine-HCl pH 8.5 for 1 min.

Human PF4 (PF4-h, ChromaTec) was prepared in PBS + 0.5% BSA + 0.005% P20 at nominal concentrations of 0, 5.9, 11.7, 23.4, 46.9, 93.8, 187.5, 375, 750, 1500 and 3000 nM and injected over all flow cells for 90 s at a flow rate of 10 µL/min.

All sensorgram plots were subtracted from the reference flow cell to remove the nonspecific responses, bulk refractive index changes, and systematic instrument noise.

### **Sequence and protein structure analyses**

Alignments of hexon protein sequences were performed using the Mafft online tool with default parameters. Models of Ad5, Ad5-ΔHVR1, Ad5H34, Ad11, Ad14, Ad34 and Ad35 hexon monomer structures were constructed on SWISS-MODEL with the default parameters, using RCSB Protein Data Bank's 3tg7 structure of Ad5 hexon monomer as template. Graphic visualizations were performed with chimeraX.

### **Structural modellings and Molecular dynamic simulation**

The structural model PDB 6B1T (Ad5 hexon) was employed and compared against the corresponding amino acid sequence from GenBank to identify segments of missing residues. Sequences of these segments of missing residues, termed missing peptides here, were fed to AlphaFold (Web Services) to generate corresponding tentative structures. These missing peptides were then manually adjusted and positioned back to either Ad5 so that the position of the beginning residue of each peptide was within 8 Å of the residue preceding it in the corresponding amino acid sequence and the ending residue of each peptide was within 8 Å of the residue after it in the corresponding amino acid sequence. The structure model of Ad34 hexon was generated entirely from AlphaFold (Web Services).

Molecular dynamics (MD) simulations were applied on the above starting models for Ad34 and Ad5 to prompt each of the grafted missing peptides adopting a conformation that would be in equilibrium with the rest of the hexon trimeric complexes. To do so, 25 hexons were first laid out tightly onto a plane to mimic the tight-packing environment of hexons over the capsid (Supplementary Fig. 4a). These ensembles of hexons were then simulated with explicit solvent for 4  $\mu$ s under a hexagonal periodic boundary condition to equilibrate the starting hexon modes for Ad34 and Ad5. The same model building and simulation strategy were applied to Ad5- $\Delta$ HVR1. PF4 tetramer structure was adopted from PDB 1RHP.

### **Brownian dynamic (BD) simulations and contact analyses**

The last frames of the respective MD simulations for each hexon ensemble were used as the representative structural model for the considered adenovirus. The corresponding mean field descriptions were derived following previous work<sup>85,277,278</sup> using an in-house python module, SimpleARBD (unpublished, Github) and included the charge-electrostatic representation and the contact force profiles. The mean field representations were fed into the Atomic Resolution Brownian Dynamics (ARBD) simulation engine for BD simulations as previously described<sup>85,277-279</sup>. The initial setting for the corresponding BD simulation was to lay the hexon ensemble on the x-y plane with the ensemble's center of mass being located at the origin. Then, 400 copies of PF4 tetramers were scattered randomly on a plane parallel to the x-y plane and was 150 Å vertically above the outermost surface of the hexon ensemble (Supplementary Fig. 4a) and their diffusion was simulated for 4  $\mu$ s. PF4 tetramers were not interacting with one another during the simulations, thus mimicking the docking process of PF4 from a diverse pool of initial locations in the bulk outside the adenovirus' capsid. The distance between each copy of PF4 and the hexon ensemble as well as their contacts were monitored and analysed by the analysis module of SimpleARBD. In this study, a copy of PF4 was considered making contacts with the hexon ensemble if any of the PF4's heavy atoms came within 5Å of the heavy atoms of the hexon ensemble.

### **Infectivity assays**

To test the impact of PF4 on the infectivity of Ad-GLN collection vectors in immortalized cells, 2E7 VP/mL were incubated 10 min. at 37°C in OptiMEM (Gibco) with or without 10  $\mu$ g/mL of PF4. In certain experiments, 10% human serum collected in serum tubes (Sarstedt 01.1601) from a healthy volunteer seronegative for Ad5 and Ad34 were added to the incubation mix. At the end of the incubation time, the culture medium of subconfluent cells was replaced by the virus suspension, resulting in 20 VP/cell (vpc). At 3 hours post infection (hpi), cells were either washed three times and harvested to titrate internalized Ad genomes, or the infection suspension was replaced by culture media and cells were kept in culture until early Ad gene expression was measured by luciferase assay or flow cytometry.

To quantify early infection rates (Fig. 2c), cell DNA was extracted using the Monarch genomic DNA purification kit (NEB #T3010L) or the NucleoSpin Tissue kit (Macherey-Nagel #740952-250)

following manufacturer's instructions. Internalized Ad genomes and cell genomes were titrated by qPCR and the number of Ad genomes per cell was used as an estimator of infectivity (see Supplementary Table 1 for primers).

Luciferase luminescence (Fig. 3e, 5a,b, Supplementary Fig. 5a) was measured 24 hpi using the Nano-Glo® Luciferase Assay (Promega, Madison, USA) kit, a TECAN infinite f plex plate reader and black 96-well luciferase plates (Thermo Fisher Scientific Nunc A/S).

GFP fluorescence intensity (Fig. 2d,e, 5c, Supplementary Fig. 5b) was measured 24 hpi. Cells were harvested, washed twice in PBS, fixated 10 min. in 2% formaldehyde, washed twice in PBS then resuspended in PBS and analysed by flow cytometry (CytoFlex, Beckman Coulter, Munich, Germany) in FITC channel (585/42 nm), excited with a 488 nm laser.

To study potential VP-independent effects of PF4 on infected cells (Fig. 2e), A549 cells were cultivated for 3 hours in optiMEM with or without 10 µg/mL PF4 then washed three times with PBS and submitted to an infectivity assay as described above.

Infectivity assays on PBMCs were conducted similarly to immortalized cell lines except that 2000 vpc were used, VP incubation and infection was not conducted in optiMEM but in RPMI media supplemented with either 10% FBS or 10% human serum, and Ad-expressed GFP fluorescence intensity was measured by flow cytometry at 48hpi. To this end, cells were washed twice in PBS + 0.5% bovine serum albumin (BSA), Fc receptors were blocked by incubation at 4°C for 15 min. in BD Horizon Brilliant stain buffer (BD Biosciences) + 6% human TruStain FcX solution (BioLegend). Cells were then splitted in two equal groups and stained for 25 min. at 4°C with either anti-CD45 (BioLegend #368524), CD8a (BD Pharmingen #555369), CD3 (BD Biosciences #562426) and CD56 (BD Biosciences #557747), or anti-CD45, CD20 (BD Biosciences #340908), CD14 (BioLegend #301830) and CD11b (BioLegend #301322) fluorophore-coupled antibodies to enable cell type identification. Cells were washed twice more in PBS + 0.5% BSA, incubated for 5 min. at 4°C in BD Horizon Brilliant stain buffer + 4% of 7AAD dye in order to stain dead cells. The samples were then diluted 1:1 in PBS and analysed by flow cytometry.

### **Mice and animal experimentation**

C57BL/6 wt mice were purchased from Charles River laboratories and were kept under specific-pathogen-free conditions for colony maintenance and experiments. Experimental groups were sex- and age-matched. Mice were bred at the ETH Phenomics Center Zurich (EPIC), whereas experiments were performed at the University of Basel in accordance with the Swiss law for animal protection and with permission by the Cantonal Veterinary Office of Basel City. For adenoviral vector immunization, 5E8 VP were administered in a volume of 200 µl into the tail vein.

Blood samples were stained immediately after collection with antibodies against CD45R/B220 (RA3-6B2), CD8 (53-6.7), CD44 (IM7), CD62L (MEL-14), CD127 (A7R34), Klrg1 (2F1), CX3CR1 (SA011F11), CD27 (LG3A10) and CD43 (1B11) purchased from BioLegend and subsequently treated with FACS lysing solution (BD Biosciences, Cat. #349202) to remove erythrocytes and fix the cells. For



detection of S1-specific CD8 T cells, H2-K<sup>b</sup> tetramers were conjugated to PE and loaded with the SARS-CoV-2 spike epitope (VNFNFNGL) by the University of Lausanne Tetramer core facility. The tetramers were added to the antibody mix for staining. Spleens were mechanically disrupted and counted with an Immunospot S6 device (C.T.L.). For surface staining, splenocytes were incubated with the same cocktail of antibodies and tetramer as used for blood with the addition of anti-erythroid cells antibody (TER-119). Dead cells were stained with Zombie-NIR Fixable Viability Kit (BioLegend, Cat: #423105). Samples were fixed by incubation with 2% paraformaldehyde for 15 minutes at room temperature. For functional assays, splenocytes were restimulated with overlapping peptide sets spanning the spike protein purchased from GenScript (Cat. #RP30020) and stained by intracellular cytokine assays as described previously<sup>280</sup>. In addition to anti-CD45R/B220 and CD8, antibodies against CD4 (RM4-5), IFN- $\gamma$  (XMG1.2) and TNF- $\alpha$  (MP6-XT22) were used. All samples were measured on a 5-laser Aurora spectral flow cytometer (Cytex Biosciences, Fremont, CA, USA) and analyzed with FlowJo Software (BD Biosciences).

### **Neutralizing antibody assays**

To identify seronegative donors, human sera were collected in serum tubes (Sarstedt 01.1601) from healthy volunteers (the study was approved by the ethics committee of the University Witten/Herdecke with the approval number 159/2022, October 10<sup>th</sup> 2022; all relevant ethical regulations have been followed and all donors gave informed consent), heated at 56°C for 30 min. and diluted 1:10 in pure DMEM. Twofold dilution series up to a serum dilution of 1:2560 were then performed using DMEM + 10% FBS as diluent in order to equalize the total serum concentration, then incubated for 1h at 37°C with 5E7 VP/mL of the chosen vector of the Ad-GLN collection. DMEM + 10% FBS was used as control. The incubation mix was then distributed onto subconfluent A549 cells, resulting in 100 VP/cell (vpc). Media was changed 3 hours post infection (hpi) and luciferase luminescence was measured 24 hpi using the Nano-Glo® Luciferase Assay (Promega, Madison, USA) kit, a TECAN infinite f plex plate reader and black 96-well luciferase plates (Thermo Fisher Scientific Nunc A/S). Sera showing no decrease in luminescence signal even at 1:10 dilution compared with the FBS control were considered seronegative.

To assess the effects of PF4 in presence of Ad5-neutralizing antibodies, Ad5 VPs from the GLN collection were incubated with or without 10  $\mu$ g/mL PF4 in OptiMEM for 30 min. at 37°C. Meanwhile, IVIGs were diluted from 1:5 to 1:400 in FBS, human seronegative serum was diluted 1:5, and an FBS-only sample was prepared for the untreated (“UT”) control. All of these samples were heat-inactivated for 30 min. at 56°C then added to the vector suspensions at 10% final volume. Following further 15 min. incubation at 37°C, the suspensions were added onto subconfluent A549 cells at 500 vpc and luciferase assays were conducted at 24 hpi as described above.

SARS-CoV-2 neutralizing antibodies in blood were measured by diluting serum samples from naive or immunized mice in MEM + 2% FCS, starting with a 1:10 dilution followed by three-fold serial dilutions in 96-well plates. Each dilution of serum or monoclonal antibody S309<sup>221</sup>, serving as a positive

control, was incubated with an equal volume of replication-deficient rVSV-EGFP pseudotyped with SARS-CoV-2 spike protein (Wuhan Hu-1 strain) containing approximately 100 infectious units for 1 hour at 37°C. Subsequently, the mixture was incubated with Vero E6 cells ( $2 \times 10^4$  cells/well) for 16 hours and fixed with 2% paraformaldehyde. The number of green spots was quantified using an Immunospot S6 device (C.T.L.). The 50% neutralization titer (NT50) was calculated as the half-maximal inhibitory concentration values using four-parameter nonlinear regression in GraphPad Prism.

### **Binding antibody assay**

High-binding 96-well flat bottom plates (Sarstedt AG & Co.KG, Nümbrecht, Germany) were coated with  $1 \times 10^8$  viral particles per well in 50  $\mu$ L coating buffer over night at 4 °C. Plates were washed twice with PBS-T (0.05% Tween-20/PBS), then blocked with 200  $\mu$ L 5% BSA/PBS-T at room temperature for 45 min. A 2-fold serial dilution of antibodies in blocking solution was performed after washing five times with PBS-T. Plates were incubated at 37 °C for 1 h and subsequently washed five times with PBS-T. Peroxidase-conjugated polyclonal anti-human antibody (1:2000 in blocking solution; Abcam, Cambridge, United Kingdom) was added and the plates were incubated at 37 °C for 70 min. After washing five times with PBS-T, colorimetric reaction was started by addition of 100  $\mu$ L of a  $\sigma$ -phenylenediamine-dihydrochloride substrate solution (1 tablet in 0.05 M phosphate-citrate buffer; Merck KGaA, Darmstadt, Germany). The reaction was stopped with 1 M sulfuric acid and the absorbance at a wavelength of 491 nm was measured using the SPECTROstar nano (BMG LABTECH GmbH, Ortenberg, Germany). Arbitrary units (Fig. 6h) are computed as  $\ln(1000 \times A_{491\text{nm}})$ ; the limit of detection corresponds to the maximum value reached by negative controls (background); and samples below this limit arbitrarily receive the value of 0 units.

### **Statistical analyses**

In ELISA-qPCR screens of Ad collections (Fig. 1c,d, 3b), usual statistical tests were irrelevant given that our goal was to identify vectors which do not bind to PF4, not those that significantly bind to it. Therefore, non-binding vectors were considered to be those for which the number of bound VPs in PF4-coated wells overlapped with that in non-coated wells in all experiment repeats (Supplementary Fig. 2,3). This corresponds to a PF4 binding index consistently negative. The index was computed as follows for each experiment repeat from the qPCR-measured numbers of VPs bound in PF4-coated or uncoated wells (both conditions in triplicate):

$$\text{PF4 binding index} = (\text{Minimum}_{\text{PF4}} - \text{Maximum}_{\text{uncoated}}) / \text{Average}_{\text{uncoated}}$$

Measurements displayed in different subplot are taken from different samples. When  $N \leq 4$  data points had been acquired, error bars indicate the minimum and maximum range. When  $N \geq 5$ , error bars indicate standard deviation and pairwise comparisons were performed using two-sided Mann-Whitney U tests when applicable. Multiple comparisons were conducted with one-way ANOVA and either post-hoc Tukey tests or, if comparisons were conducted only with a control sample, Dunnett tests. The

significance threshold was set at  $p < 0.05$ . Significance symbols: ns = non-significant, \* =  $p < 0.05$ , \*\* =  $p < 0.01$ , \*\*\* =  $p < 0.001$

Statistical analyses and visualizations were performed with the R software with the packages dplyr and ggplot2.

## **Acknowledgments**

We are grateful to Dr. Inga Seuthe (Sankt-Johannes Hospital, Hagen, Germany) and Merve Torun (then working at Witten/Herdecke University, Witten, Germany) for providing and maintaining the clinical samples used for nasal epithelium culture.

## **Funding**

DFG grant EH 192/5-1 (A.E.)

PhD program Witten/Herdecke University (E.S., D.W.)

## **Author contributions**

Conceptualization: ES, DPi, FK, AE

Methodology: ES, DPe, LB, WB, MA, DG, ATB, WZ, DPi, FK, AE

Investigation: ES, DPe, MC, LB, DW, FJ, EC, SS, NB, KS, MT, GK, XW, NS

Formal analysis: ES, DPe, MC, EC, LB, CKC, DS, AS, ATB

Writing – original draft: ES

Writing – review and editing: ES, DPe, MC, DW, SS, KS, GK, XW, WB, ATB, WZ, DPi, FK, AE

Funding acquisition: ATB, DPi, FK, AE

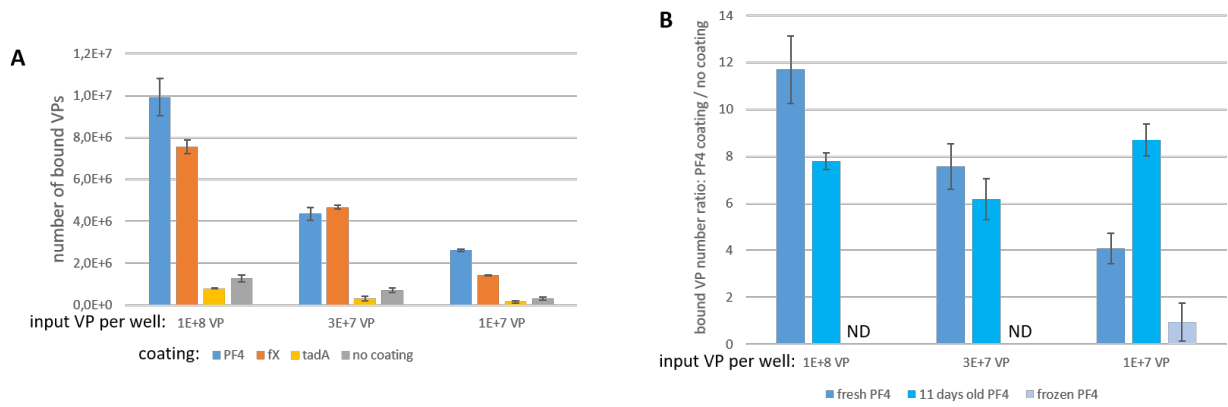
## **Competing interests**

None.

## **Data and materials availability**

All data are available in the main text or the supplementary materials.

## **Supplementary figures**



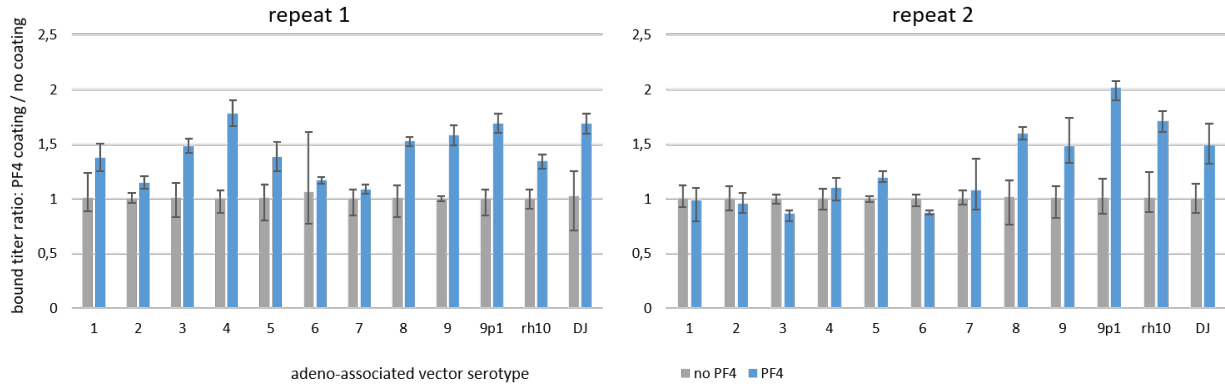
Supplementary Fig. 1.

Establishment of the ELISA-qPCR technique. The ELISA-qPCR technique facilitates specific and sensitive assessment of Ad5-protein interactions (A). ELISA plates were coated with PF4, factor X (fX), *S.typhimurium* tRNA-specific adenosine deaminase (tadA) or buffer only (no coating). Ad5-GLN was allowed to interact with coated proteins at doses of 1e8 (left), 3e7 (center) or 1e7 (right) virus particles (VP) per well. At all doses, the binding of Ad5-GLN to PF4 and fX (positive controls) was clearly detectable, while no increase in VP number in tadA-coated wells (negative controls) could be observed. N=2 data points per sample. The PF4 protein remains stable when conserved at 4°C for several weeks but can not be used for ELISA-qPCR after freezing (B). The ratio of bound Ad5-GLN VP number between PF4-coated wells and non-coated wells was calculated after ELISA-qPCR. PF4 proteins were either used directly after resuspension of the lyophilised powder, after 11 days at 4°C or after freezing. N≥2 data points per sample.



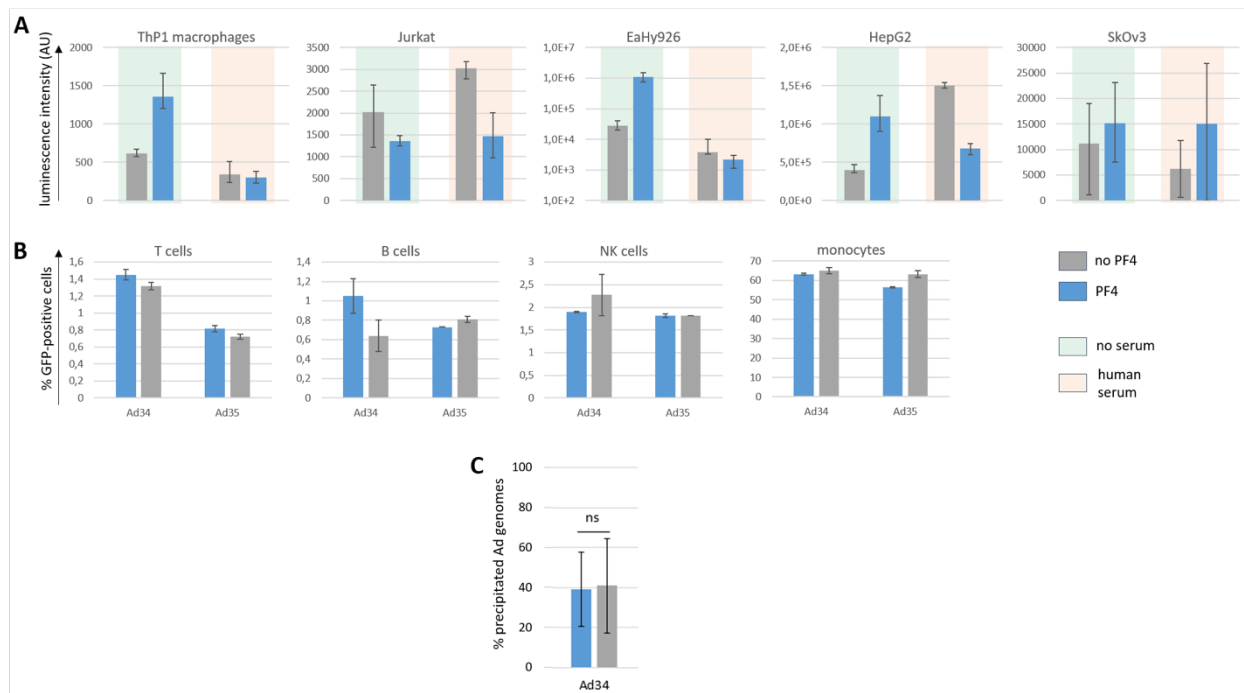
Supplementary Fig. 2.

ELISA-qPCR screening of adenovirus vectors for PF4 binding. Two independent experiments were conducted in triplicates for all vectors, and additional repeats were conducted with different virus suspensions for types of interest or whose results had been unclear. Vectors with no detectable PF4 binding were identified as those with overlap in each experiment between virus genome titrations in PF4-coated and non-coated wells. Since our null hypothesis was that the bound VP numbers are significantly different (PF4 binding), statistical tests could not be applied. Error bars: minimum/maximum.



Supplementary Fig. 3.

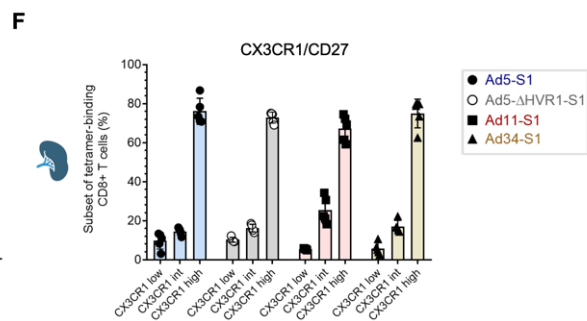
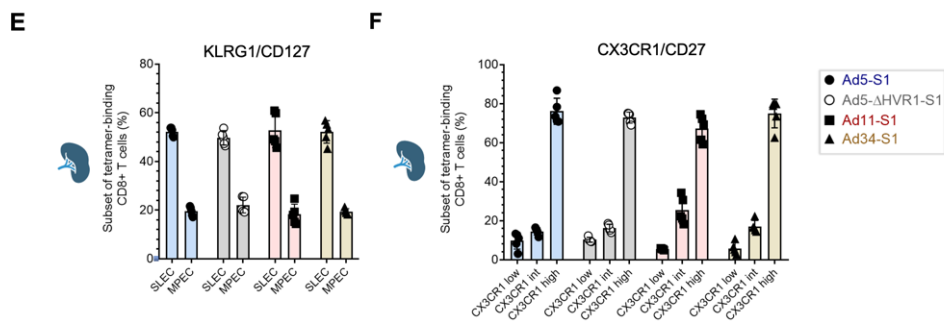
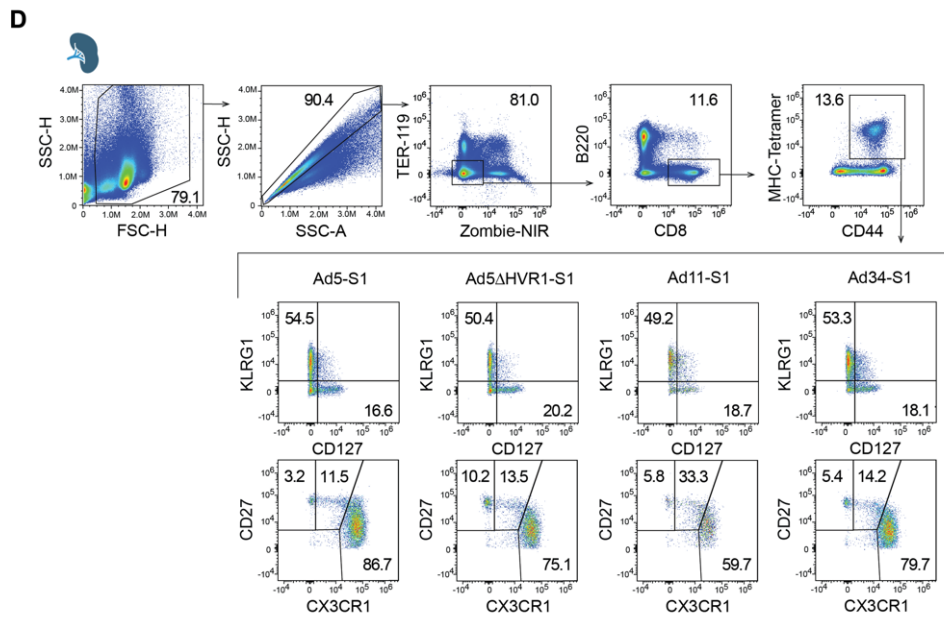
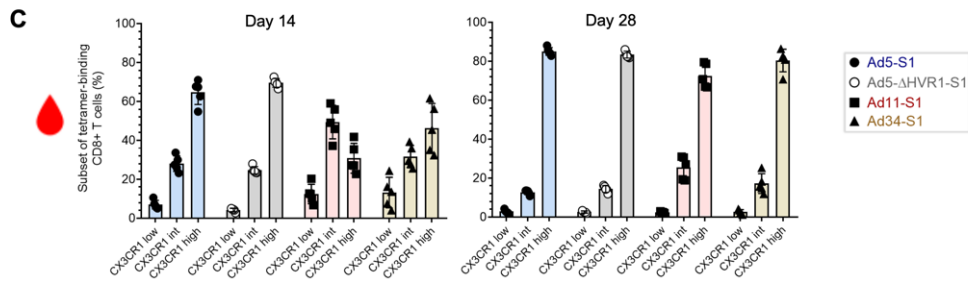
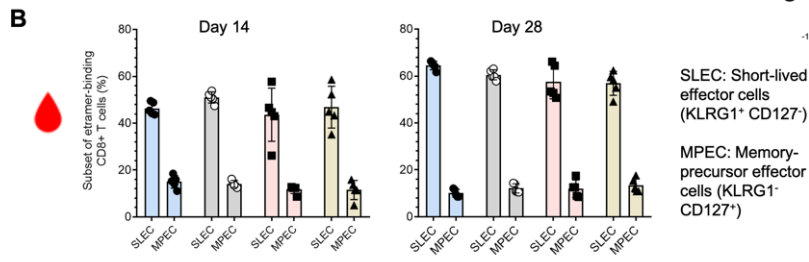
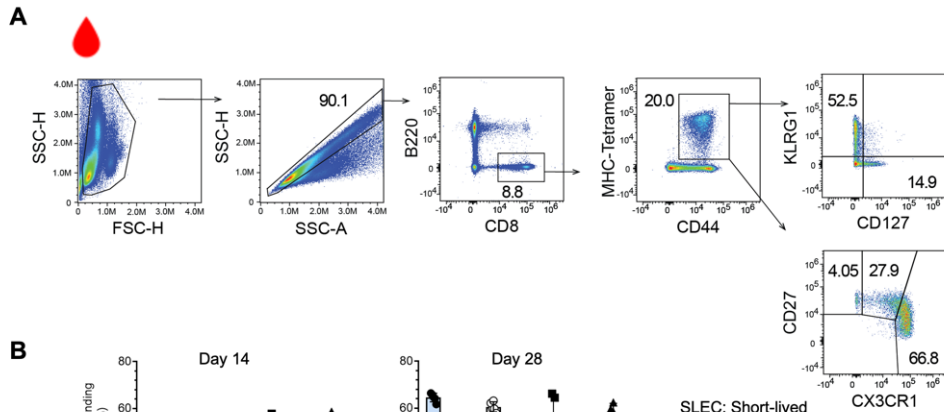
ELISA-qPCR screening of adeno-associated vectors for PF4 binding. Two independent experiments were conducted in triplicates for all serotypes. Vectors with no detectable PF4 binding were identified as those with overlap in each experiment between virus genome titrations in PF4-coated and non-coated wells. Since our null hypothesis was that the bound VP numbers are significantly different (PF4 binding), statistical tests could not be applied. Error bars: minimum/maximum.



Supplementary Fig. 4.

Infectivity assays on an array of immortalized and primary cell lines. Infectivity assays were conducted as in Fig. 5. A: Immortalized cells were infected with 20 vpc of Ad5 vector from the Ad-GLN collection. Ad-expressed luciferase luminescence was quantified 24 hpi and normalized on the average of the “no PF4, no serum” condition for each cell line. N=4. B: Primary peripheral blood mononuclear cells were infected with 2000 vpc of Ad34 or Ad35 vectors from the Ad-GLN collection. Ad-expressed GFP

fluorescence was quantified 48 hpi and the proportions of GFP-positive cells were normalized on the average of the “no PF4, FBS” condition for each cell type. N=2. C: Erythrocyte pull-down of Ad34 from the Ad-GLN collection in absence or presence of PF4. N=10, three independent repeats. Pairwise comparisons were conducted with the Mann-Whitney U test.





### Supplementary Fig. 5.

Phenotyping of S1-specific T cells from immunized mice. A: Gating strategy to determine the frequencies and phenotypes of S1-epitope specific CD8 T cells in peripheral blood. B, C: Frequencies of S1-specific CD8 T cells based on KLRG1 and CD127 (B) or CX3CR1 and CD27 (C) at day 14 or 28 after immunization. D: Gating strategy to determine the frequencies and phenotypes of S1-epitope specific CD8 T cells in spleens. Representative FACS plots of each group phenotype are shown. E, F: Frequencies of S1-specific CD8 T cells based on KLRG1 and CD127 (E) or CX3CR1 and CD27 (F) at day 30 after immunization.

name	sequence	target
GLN-for	accaagcgaaacatcgcacgag	vectors of the Ad-GLN collection
GLN-rev	gcgataccgtaaagcagcaggaag	vectors of the Ad-GLN collection
WT-for	gccccagtggtcttacatgcacatc	vectors of the Ad-WT collection
WT-rev	gccacgggtggggtttctaaactt	vectors of the Ad-WT collection
WT-probe	ccgggtctggtgcagttgccccgc	vectors of the Ad-WT collection
CMV-for	tacatcaatgggctgtgata	vaccine-equivalent vectors
CMV-rev	ggcggagtgttacgacatt	vaccine-equivalent vectors
Fiber-for	accggtttccgtgcatatgg	Ad5 hexon mutants and Ad5- $\Delta$ CAR
Fiber-rev	ggtattgcagcttcctcctgg	Ad5 hexon mutants and Ad5- $\Delta$ CAR
AAV-for	aacgccaatagggactttcc	vectors of the AAV collection
AAV-rev	gggcgtacttggcatatgat	vectors of the AAV collection

Supplementary Table 1. Primers used in this study.

### Supplementary Movie 1.

Superposition of Ad5, Ad34H5, Ad5H34 and Ad34 hexon structures

The structures of Ad5 (green), Ad34H5 (yellow), Ad5H34 (magenta) and Ad34 (blue) monomeric hexons were modelised on SWISS-MODEL and superposed. The inner side of the capsid is located down and the outer side up.

### Supplementary Movie 2.

Superposition of Ad11, 14, 34 and 35 hexon structures.

The structures of Ad11 (green), 14 (orange), 34 (blue) and 35 (magenta) monomeric hexons were modelised on SWISS-MODEL and superposed. The inner side of the capsid is located down and the outer side up.

## General discussion

A deep understanding of the immunological mechanisms induced by vaccination, that lead to protective immunity, is essential for developing new vaccine platforms against current and emerging pathogens. Despite their widespread success, the development of the vast majority of vaccines has historically taken an empirical approach, with minimal understanding of the underlying mechanisms by which they induce protective immunity. This pragmatic approach, while it has led to many effective vaccines, exposes its limitations when it comes to addressing some complex global health challenges. Despite decades of intensive research and relentless effort, we still do not have effective vaccines for pathogens as HIV or HCV, exposing the gap in our scientific knowledge<sup>281,282</sup>. Furthermore, the ever-present threat of emerging pathogens amplifies the urgent need for the development of novel vaccination platforms and the understanding of how they generate immunity.

The present thesis was aimed at gaining a better mechanistic understanding of how vaccines work. In the first part, we focused our study on the molecular determinants of viral vectors that account for long-lived CD8 T cell responses. In the second part, we performed a comparative analysis of COVID-19 vaccine regimens in clinical use, focusing on the induction and maintenance of GC responses. Finally, in the third part, we identified viral vectors that represent safer vaccine platforms, and tested their immunogenic capacity.

Both CD8 T cells and antibodies represent major effector arms of the adaptive immune system that account as vaccine correlates of protection from infection<sup>283</sup> or severe disease<sup>284</sup>. Inflammatory signals as well as antigen expression levels are key factors for proper activation of CD8 T cells by viral vectors<sup>285,286</sup>. However, it is unclear how these components are influenced by the cytolytic nature of viral vectors, especially in the context of replication-deficient platforms. Moreover, prime-boost immunization strategies are often used in vaccinology to provide adequate stimulation of antibody responses<sup>287,288</sup>. Many different approaches have been taken with clinically approved COVID-19 vaccines, most of which consist in mRNA-LNP and adenoviral vectors. Still, the extent to which these platforms, or their combination, can engage primary activated B cell clones into the secondary GC response is unknown. Throughout this thesis, we aimed to address these questions by employing various mouse models, which facilitate the mechanistic understanding of immune processes.

In the first part of the thesis, we were able to highlight how non-cytolytic and replication-deficient viral vectors can trigger IFN-I for the induction of long-lived and effector-differentiated CD8 T cell responses. Our first approach consisted in using two different vectors that differ greatly in their cytopathogenicity: rLCMV a non-cytolytic vector and rVSV, a highly cytolytic vector. While non-cytolytic vectors can persist in the host cell and provide longer stimulation of the immune system<sup>289</sup>, cytolytic vectors can induce cross-presentation by DC uptake of dead cells for CD8 T cell priming<sup>290</sup>. Even though both vectors induced comparable CD8 T cell frequencies initially, responses to rVSV contracted much faster than those to rLCMV. Analysis of transgene expression *in vivo* showed that the decay of antigen produced

by rVSV was more pronounced than that of rLCMV, revealing a positive correlation between the amount of transgene expressed by the vectors and the resulting CD8 T cell response. These observations suggested that cytolytic vector activity in the context of replication-deficient vectors can negatively impact the antigen dose and consequently impair appropriate priming of CD8 T cells. Notably, these results differ from replication-competent platforms, where enhanced cytolytic activity did not influence the induction of CD8 T cells on the long term<sup>168</sup>.

Another experimental approach was taken to understand how vector cellular tropism affects the CD8 T cell response. Given that rLCMV and rVSV glycoproteins interact with different cell surface receptors, we hypothesized that exchanging their glycoproteins would alter their cellular tropism and potentially affect the priming of CD8 T cells. Intriguingly, the resulting CD8 T cell response did not significantly change with the glycoprotein swap. Furthermore, antigen expression levels also did not differ between paired vectors carrying different glycoproteins. A possible explanation for these observations comes from the fact that even though LCMV and VSV glycoproteins interact with different cell surface receptors, they are capable of targeting and infecting DCs with similar efficiency, as shown from *in vitro* studies<sup>65</sup>.

An unexpected finding of this study was that the non-cytolytic rVSVMq failed to induce higher expression levels than the cytolytic rVSV vector *in vivo*. The lack of host shut-off activity by rVSVMq allows longer vector persistence *in vitro* by inhibiting its cytolytic activity<sup>54</sup>. Taking this into account, we initially hypothesized that abrogation of the cytolytic effect in rVSVMq would lead also to increased antigen production *in vivo*. Indeed, rVSVMq showed protracted antigen expression compared to rVSV in mice lacking innate and adaptive immune functions, as interferon receptors and lymphocytes, as demonstrated by our experiments with snLuc-expressing vectors. This strongly suggested that the non-cytolytic nature of a replication-deficient vector can extend vector persistence in the host cell. However, analogous experiments in wild-type mice showed a completely different picture, since antigen expression by rVSVMq compared to rVSV was greatly diminished. Further experiments in IFNAR-deficient mice revealed higher sensitivity of rVSVMq to the IFN-I response, as compared to rVSV. These results are explained, at least in part, by the stronger induction of IFN- $\alpha$  by rVSVMq compared to rVSV. As it has been described, both rVSV and rVSVMq can target and infect DCs<sup>65</sup>. However, the wild-type matrix protein of rVSV can act as an IFN-I antagonist, by binding proteins at the nucleus pore and suppressing cellular activity<sup>56</sup>. This means that IFN- $\alpha$  mRNA transcripts, which expression is induced after viral RNA sensing from RIG-I and other PRRs, cannot be efficiently exported to the cytoplasm to be translated and initiate the IFN response. On the other hand, the mutated matrix protein of rVSVMq lacks the ability to interact with cellular nucleoporins and cannot therefore shut-off the host cell efficiently, losing its IFN-antagonizing function<sup>55</sup>. These observations align with previous *in vitro* studies that found VSV matrix mutant variants to be stronger inducers of IFN-I compared to the wild-type protein<sup>175</sup>. Another factor that could account for rVSVMq lower antigen expression in wild-type mice is CTL-mediated destruction of transduced cells<sup>128</sup>. Although this seems unlikely given that CD8 T cells require time to get primed, expand and differentiate, the histological observation that they engaged with rVSVMq-transduced cells as early as 6 hours after immunization means this possibility cannot be

excluded. This hypothesis of CTL-mediated clearance of vector-transduced cells could be addressed by experiments in mice lacking CD8 T cells, or mice with T cells lacking cytotoxic functions, as in the perforin-deficient model<sup>118</sup>, and snLuc-expressing vectors as a surrogate of vector persistence.

Another important and unexpected finding, was that the induction of long-lived and effector-differentiated CD8 T cells by rVSVMq was linked to its ability to trigger IFN-I. This stimulatory effect of IFN-I on the potency of CD8 T cell responses is well documented in the context of certain viral infections<sup>176,180,181</sup>. At the same time, IFN-I-driven antiviral state greatly suppressed rVSVMq antigen expression, thereby limiting antigen availability at a critical time when the adaptive immune system is being primed. It seems that for this particular case, the positive effect of IFN-I on the CD8 T cells overcame its negative impact on antigen expression. These observations differ from other types of vaccine vectors, as those based on adenoviruses. Immunization with adenoviral vectors elicits higher frequencies of antigen-specific CD8 T cells in mice lacking IFN-I signaling compared to wild-type mice<sup>95</sup>. Furthermore, adenoviral vectors based on serotypes that induce higher IFN-I signaling promote less potent CD8 T cell responses<sup>95</sup>. On the other hand, vaccine vectors based on MVA depend on IFN-I triggering to induce potent CD8 T cell expansion<sup>169</sup>. Taken together, these studies suggest that the interplay between IFN-I induction, antigen expression, and the subsequent CD8 T cell response is highly dependent on the specific type of vaccine vector used.

Even though rVSVMq-induced responses were highly dependent on IFN-I signaling by the CD8 T cells, independent experiments demonstrated that IFN- $\alpha$  induction by rVSVMq is an early and very transient process. Immunization with rVSVMq elicits a peak of IFN- $\alpha$  in blood after 6 hours, and histological analysis indicated that IFN- $\alpha$ -producing cells in the spleen are gone by 18 hours from vector administration. Despite this transient IFN- $\alpha$  wave, antigen-specific CD8 T cells were in contact with vector transduced cells at the specific time of IFN-I induction. This suggests that the short IFN- $\alpha$  wave is imprinting the CD8 T cells at very early stages of the response, inducing long-lasting effects on the expansion and differentiation of these cells. An experimental approach to test this hypothesis could involve adoptive transfers of OVA-specific CD8 T cells prior and after the IFN- $\alpha$  peak induced by immunization with rVSVMq-OVA. Analyses of the expansion and differentiation of the transferred cells would indicate the effect of the IFN- $\alpha$  wave on the CD8 T cells.

Similar to rVSVMq, immunizations with rLCMV also resulted in systemic IFN- $\alpha$  induction, although this peak was at 24 hours after vector administration. Potent antiviral CD8 T cell responses to LCMV infection are greatly dependent on the induction of IFN-I<sup>181</sup>. Further experiments of OT-Ix*Ifnar*<sup>-/-</sup> adoptive transfers will help to assess the dependence of CD8 T cell responses to the rLCMV replication-deficient vector, on direct IFNAR signaling of CD8 T cells, as performed with rVSV-based vectors. Longitudinal histological analyses of the spatio-temporal distribution of antigen-specific CD8 T cells, IFN- $\alpha$  producers, and cells transduced by rLCMV or rVSV will also help to determine the dynamics of IFN-I induction and CD8 T cell engagement, as performed for rVSVMq.

In the second part of the thesis, we wanted assessed the potential of different COVID-19 regimens to recall previously activated B cells into secondary GCs. For this, we employed the AID<sup>rep</sup> mouse model, that allows irreversible labelling of AID-expressing cells upon tamoxifen induction.

Even though priming with mRNA or ChAdOx-1 elicited similar numbers of GC B cells, mRNA immunization was able to recruit higher numbers of spike-specific B cells. This was further confirmed by our experiments with AID<sup>rep</sup> mice, showing that AID-expressing B cells after mRNA priming contained higher proportions of spike-specific B cells compared to ChAdOx-1. Moreover, some of the mRNA-primed B cells persisted in the GC compartment until the second boost. This induction of durable GCs after mRNA immunization has also been observed in human studies<sup>203,209</sup>, and could be related to long-term expression of the spike antigen within the GC<sup>213</sup>.

Secondary immunizations with mRNA to ChAdOx-1- or mRNA-primed animals elicited higher numbers of spike-specific B cells and neutralizing antibodies, compared to ChAdOx-1 homologous prime-boost. This relatively inefficient secondary vaccination in the homologous ChAdOx-1 regimen was associated to the development of responses against the vector backbone. This was suggested by the relatively high induction of vector-specific antibodies after homologous ChAdOx-1 boost, compared to the lower increase in S1-specific antibodies. Another indirect line of evidence suggesting a bias of the B cell response towards the vector backbone, comes from the observation that despite eliciting similar numbers of GC B cells, ChAdOx-1-induced GCs contained a higher proportion of spike non-reactive B cells than mRNA vaccination. These results align with other studies that report the induction of vector-specific responses after adenovirus vaccination<sup>114,116,117,291</sup>, that can compete for the transgene-specific response. It also provides more evidence in favor of heterologous prime-boost combinations when adenoviral vectors are employed. This strategy proved to be particularly effective for adenoviral and inactivated vaccines during the COVID-19 pandemic<sup>292</sup>, and has been used for example by the Sputnik V vaccine, which uses two different adenovirus serotypes for prime and boost<sup>293</sup>.

In the case of mRNA/mRNA and ChAdOx-1/mRNA regimens, the magnitude of both spike-specific B cell and T cell responses were comparable at two weeks after boost. Importantly, also the levels of neutralizing antibodies to the vaccine spike antigen Wuhan-Hu-1 were similar. The main difference observed between these two regimens was the enhanced persistence of primary activated B cell clones within secondary GCs upon boost in mRNA/mRNA compared to ChAdOx-1/mRNA. Notably, this was associated to enhanced variant cross-reactivity of nAbs in mice that received mRNA homologous immunization compared to those that received ChAdOx-1/mRNA. The superior ability of mRNA/mRNA elicited antibodies to neutralize variants Beta and Omicron suggests that these nAbs are targeting more conserved epitopes of the RBD or are of higher quality and able to overcome epitope changes associated with mutations in these variants of concern. These results align with human studies showing that immunization with 2 doses of mRNA vaccine encoding the original Wuhan spike protein induces a population of durable MBC with broad reactivity to SARS-CoV-2 variants including Omicron<sup>214</sup>. One possible scenario is that the persistence of primary activated B cell clones in mRNA/mRNA-induced secondary GCs allows them to undergo further rounds of SHM and

diversification of their BCR, resulting in higher breadth. An experimental approach to test this hypothesis would involve the isolation of EYFP+ and EYFP-, spike-specific GC B cells and determine the neutralizing breadth and levels of SHM in their immunoglobulin genes.

Despite the success of mRNA vaccines during the COVID-19 pandemic, their massive deployment and widespread use in large populations exposed several safety concerns. For instance, mRNA vaccination was associated with higher incidence of anaphylaxis in some groups<sup>294</sup>. Although the specific vaccine component responsible for allergic reactions is unclear, there might be a possible role for the PEGylated lipids and the pre-existence of anti-PEG antibodies<sup>295,296</sup>. Additionally, myocarditis has been described following mRNA vaccination, particularly in younger and primarily male adults<sup>297,298</sup>. Furthermore, a few cases of autoimmune vasculitis were reported following the Pfizer-BioNTech mRNA vaccine<sup>299</sup>. The exact contribution of mRNA vaccination and its components to these side effects requires further longitudinal studies, but the relatively new mRNA vaccine platform still have to overcome several challenges to fully meet the global market needs.

In the third part of the thesis, we were able to identify adenoviral vectors that can avoid binding to human PF4, a process that has been associated to thrombosis cases<sup>84</sup>. Therefore, these vectors represent potentially safer human vaccine, gene therapy and oncolytic platforms. Lack of binding to PF4 was identified by screening of different natural serotypes and capsid-engineered human adenoviruses. Deletion or chemical shielding of the hexon HVR1 loop effectively eliminated detectable PF4 binding of Ad5. These represent two potential methods for designing safer adenoviruses with a reduced or suppressed risk of VITT. Furthermore, serotypes Ad11 and Ad34, naturally lacked the ability to bind to PF4. These two vectors have been reported to have low seroprevalence in the human population<sup>245</sup>. This makes them attractive choices as vaccine vectors since pre-existing immunity can impair adenoviral vector immunogenicity. Finally, immunogenicity studies in mice demonstrated that these vectors are able to induce antigen-specific cellular responses. Even though responses to Ad11 and Ad34 were somewhat lower than Ad5, they still have potential as efficacious vaccine platforms. As shown for ChAdOx-1, which is less immunogenic than Ad5<sup>81,253</sup>, but still represents an effective vaccine platform<sup>300</sup>.

Another important finding of this study was that the hexon-modified Ad5- $\Delta$ HVR1 vector elicited similar transgene-specific cellular responses to the parental Ad5 vector. As shown and discussed during the second part of the thesis, vaccination with adenoviral vectors induce anti-vector responses that compete and are detrimental for the transgene immunogenicity upon secondary vector administration. Notably, the modified Ad5- $\Delta$ HVR1 induced substantially lower and almost undetectable vector-binding antibodies, unlike the Ad5 parental vector. This observation finds support from studies that report Ad5-specific neutralizing antibodies being primarily directed against the hexon major capsid protein<sup>243</sup>. Importantly, these results strongly suggest that the HVR1 deletion in adenoviral vector backbones has the potential to not only improve the safety of the vaccine, by avoiding PF4 binding, but also enhance its immunogenicity upon homologous prime-boost immunizations.

In conclusion, this thesis offers a fundamental understanding of the mechanistic requirements of replication-deficient viral vectors for the induction of long-lived and potent CD8 T cell immunity. We showed that non-cytolytic vectors can drive these responses through triggering of IFN-I, and should be chosen for the induction of durable CD8 T cell immunity. Furthermore, combining COVID-19 mRNA vaccinations in homologous prime-boost regimens favors the continued engagement of B cell clones in germinal centers and enhances the breadth of neutralizing antibodies compared to ChAdOx-1/mRNA or ChAdOx-1/ChAdOx-1 regimens. mRNA/mRNA regimens should be chosen in order to elicit variant cross-reactive antibody responses. Finally, the identification of PF4 non-binding adenoviral vectors offers new vaccine platforms with an improved safety profile.

## References

- 1 Shimizu, Y. *Vaccines and immunization*,  
<[https://web.archive.org/web/20220101135141/https://www.who.int/health-topics/vaccines-and-immunization#tab=tab\\_1](https://web.archive.org/web/20220101135141/https://www.who.int/health-topics/vaccines-and-immunization#tab=tab_1)> (2022).
- 2 *Global Immunization Data coverage in 2013*,  
<[https://web.archive.org/web/20200413171049/https://www.who.int/immunization/monitoring-surveillance/global\\_immunization\\_data.pdf](https://web.archive.org/web/20200413171049/https://www.who.int/immunization/monitoring-surveillance/global_immunization_data.pdf)> (2014).
- 3 Jenner, E. *An Inquiry Into the Causes and Effects of the Variolæ Vaccinæ*. Vol. 1 (Sampson Low, 1798).
- 4 Bunin, K. V. [Work of Louis Pasteur on attenuation of microorganisms and preparation of preventive vaccines (on the 150th anniversary to the birth of L. Pasteur)]. *Zh Mikrobiol Epidemiol Immunobiol* **49**, 15-19 (1972).
- 5 Toor, J. *et al.* Lives saved with vaccination for 10 pathogens across 112 countries in a pre-COVID-19 world. *Elife* **10**, doi:10.7554/eLife.67635 (2021).
- 6 Magner, L. N. *A History of Infectious Diseases and the Microbial World (Healing Society: Disease, Medicine, and History)*. Vol. 1 (Praeger, 2009).
- 7 Mallapaty, S. *et al.* How COVID vaccines shaped 2021 in eight powerful charts. *Nature* **600**, 580-583, doi:10.1038/d41586-021-03686-x (2021).
- 8 Li, Y. D. *et al.* Coronavirus vaccine development: from SARS and MERS to COVID-19. *J Biomed Sci* **27**, 104, doi:10.1186/s12929-020-00695-2 (2020).
- 9 Subbarao, K. The success of SARS-CoV-2 vaccines and challenges ahead. *Cell Host Microbe* **29**, 1111-1123, doi:10.1016/j.chom.2021.06.016 (2021).
- 10 Gotuzzo, E., Yactayo, S. & Cordova, E. Efficacy and duration of immunity after yellow fever vaccination: systematic review on the need for a booster every 10 years. *Am J Trop Med Hyg* **89**, 434-444, doi:10.4269/ajtmh.13-0264 (2013).
- 11 Shinefield, H. R. *et al.* Vaccination with measles, mumps and rubella vaccine and varicella vaccine: safety, tolerability, immunogenicity, persistence of antibody and duration of protection against varicella in healthy children. *Pediatr Infect Dis J* **21**, 555-561, doi:10.1097/00006454-200206000-00014 (2002).
- 12 Macartney, K. Long-term protection against varicella with two-dose combination measles-mumps-rubella-varicella vaccine. *Lancet Infect Dis* **19**, 222-223, doi:10.1016/S1473-3099(18)30797-7 (2019).
- 13 Tatem, J. M. *et al.* Oral poliovirus vaccine in the United States: molecular characterization of Sabin type 3 after replication in the gut of vaccinees. *J Med Virol* **35**, 101-109, doi:10.1002/jmv.1890350206 (1991).



- 14 Macadam, A. J. *et al.* Reversion of the attenuated and temperature-sensitive phenotypes of the Sabin type 3 strain of poliovirus in vaccinees. *Virology* **172**, 408-414, doi:10.1016/0042-6822(89)90183-9 (1989).
- 15 Mas Lago, P. *et al.* Persistence of vaccine-derived poliovirus following a mass vaccination campaign in Cuba: implications for stopping polio vaccination after global eradication. *Int J Epidemiol* **30**, 1029-1034, doi:10.1093/ije/30.5.1029 (2001).
- 16 Simsek, C. *et al.* Rotavirus vaccine-derived cases in Belgium: Evidence for reversion of attenuating mutations and alternative causes of gastroenteritis. *Vaccine* **40**, 5114-5125, doi:10.1016/j.vaccine.2022.06.082 (2022).
- 17 Cherkasova, E. A. *et al.* Spread of vaccine-derived poliovirus from a paralytic case in an immunodeficient child: an insight into the natural evolution of oral polio vaccine. *J Virol* **79**, 1062-1070, doi:10.1128/JVI.79.2.1062-1070.2005 (2005).
- 18 Ljungman, P. *et al.* Vaccination of hematopoietic cell transplant recipients. *Bone Marrow Transplant* **44**, 521-526, doi:10.1038/bmt.2009.263 (2009).
- 19 Boudes, P., Sobel, A., Deforges, L. & Leblic, E. Disseminated Mycobacterium bovis infection from BCG vaccination and HIV infection. *JAMA* **262**, 2386 (1989).
- 20 Turner, G. S., Squires, E. J. & Murray, H. G. Inactivated smallpox vaccine. A comparison of inactivation methods. *J Hyg (Lond)* **68**, 197-210, doi:10.1017/s0022172400028679 (1970).
- 21 Gall, A. J. W. L. S. Studies on the Immunization of Rabbits with Formalinized Vaccine Virus. *J Immunol* **1**, 1-8 (1940).
- 22 Beale, A. J. Efficacy and safety of oral poliovirus vaccine and inactivated poliovirus vaccine. *Pediatr Infect Dis J* **10**, 970-972, doi:10.1097/00006454-199112000-00029 (1991).
- 23 Ghendon, Y. & Robertson, S. E. Interrupting the transmission of wild polioviruses with vaccines: immunological considerations. *Bull World Health Organ* **72**, 973-983 (1994).
- 24 Travieso, T., Li, J., Mahesh, S., Mello, J. & Blasi, M. The use of viral vectors in vaccine development. *NPJ Vaccines* **7**, 75, doi:10.1038/s41541-022-00503-y (2022).
- 25 Ewer, K. J. *et al.* Viral vectors as vaccine platforms: from immunogenicity to impact. *Curr Opin Immunol* **41**, 47-54, doi:10.1016/j.coi.2016.05.014 (2016).
- 26 Bett, A. J., Prevec, L. & Graham, F. L. Packaging capacity and stability of human adenovirus type 5 vectors. *J Virol* **67**, 5911-5921, doi:10.1128/JVI.67.10.5911-5921.1993 (1993).
- 27 Dong, J. Y., Fan, P. D. & Frizzell, R. A. Quantitative analysis of the packaging capacity of recombinant adeno-associated virus. *Hum Gene Ther* **7**, 2101-2112, doi:10.1089/hum.1996.7.17-2101 (1996).
- 28 Kapadia, S. U., Simon, I. D. & Rose, J. K. SARS vaccine based on a replication-defective recombinant vesicular stomatitis virus is more potent than one based on a replication-competent vector. *Virology* **376**, 165-172, doi:10.1016/j.virol.2008.03.002 (2008).
- 29 Farina, S. F. *et al.* Replication-defective vector based on a chimpanzee adenovirus. *J Virol* **75**, 11603-11613, doi:10.1128/JVI.75.23.11603-11613.2001 (2001).

- 30 Draper, S. J. & Heeney, J. L. Viruses as vaccine vectors for infectious diseases and cancer. *Nat Rev Microbiol* **8**, 62-73, doi:10.1038/nrmicro2240 (2010).
- 31 Moskopidis, D. *et al.* Role of virus and host variables in virus persistence or immunopathological disease caused by a non-cytolytic virus. *J Gen Virol* **76 ( Pt 2)**, 381-391, doi:10.1099/0022-1317-76-2-381 (1995).
- 32 de la Torre, J. C. Molecular and cell biology of the prototypic arenavirus LCMV: implications for understanding and combating hemorrhagic fever arenaviruses. *Ann N Y Acad Sci* **1171 Suppl 1**, E57-64, doi:10.1111/j.1749-6632.2009.05048.x (2009).
- 33 Qi, X. *et al.* Cap binding and immune evasion revealed by Lassa nucleoprotein structure. *Nature* **468**, 779-783, doi:10.1038/nature09605 (2010).
- 34 Hastie, K. M., Kimberlin, C. R., Zandonatti, M. A., MacRae, I. J. & Saphire, E. O. Structure of the Lassa virus nucleoprotein reveals a dsRNA-specific 3' to 5' exonuclease activity essential for immune suppression. *Proc Natl Acad Sci U S A* **108**, 2396-2401, doi:10.1073/pnas.1016404108 (2011).
- 35 King, B. R. *et al.* A Map of the Arenavirus Nucleoprotein-Host Protein Interactome Reveals that Junin Virus Selectively Impairs the Antiviral Activity of Double-Stranded RNA-Activated Protein Kinase (PKR). *J Virol* **91**, doi:10.1128/JVI.00763-17 (2017).
- 36 Beyer, W. R., Popplau, D., Garten, W., von Laer, D. & Lenz, O. Endoproteolytic processing of the lymphocytic choriomeningitis virus glycoprotein by the subtilase SKI-1/S1P. *J Virol* **77**, 2866-2872, doi:10.1128/jvi.77.5.2866-2872.2003 (2003).
- 37 Hastie, K. M. *et al.* Crystal structure of the prefusion surface glycoprotein of the prototypic arenavirus LCMV. *Nat Struct Mol Biol* **23**, 513-521, doi:10.1038/nsmb.3210 (2016).
- 38 Cao, W. *et al.* Identification of alpha-dystroglycan as a receptor for lymphocytic choriomeningitis virus and Lassa fever virus. *Science* **282**, 2079-2081, doi:10.1126/science.282.5396.2079 (1998).
- 39 Bakkers, M. J. G. *et al.* CD164 is a host factor for lymphocytic choriomeningitis virus entry. *Proc Natl Acad Sci U S A* **119**, e2119676119, doi:10.1073/pnas.2119676119 (2022).
- 40 Pinschewer, D. D. *et al.* Kinetics of protective antibodies are determined by the viral surface antigen. *J Clin Invest* **114**, 988-993, doi:10.1172/JCI22374 (2004).
- 41 Sommerstein, R. *et al.* Arenavirus Glycan Shield Promotes Neutralizing Antibody Evasion and Protracted Infection. *PLoS Pathog* **11**, e1005276, doi:10.1371/journal.ppat.1005276 (2015).
- 42 Flatz, L. *et al.* Development of replication-defective lymphocytic choriomeningitis virus vectors for the induction of potent CD8+ T cell immunity. *Nat Med* **16**, 339-345, doi:10.1038/nm.2104 (2010).
- 43 Flatz, L., Bergthaler, A., de la Torre, J. C. & Pinschewer, D. D. Recovery of an arenavirus entirely from RNA polymerase I/II-driven cDNA. *Proc Natl Acad Sci U S A* **103**, 4663-4668, doi:10.1073/pnas.0600652103 (2006).

- 44 Schwendinger, M. *et al.* A Randomized Dose-Escalating Phase I Trial of a Replication-Deficient Lymphocytic Choriomeningitis Virus Vector-Based Vaccine Against Human Cytomegalovirus. *J Infect Dis* **225**, 1399-1410, doi:10.1093/infdis/jiaa121 (2022).
- 45 Boopathy, A. V. *et al.* Immunogenic arenavirus vector SIV vaccine reduces setpoint viral load in SIV-challenged rhesus monkeys. *NPJ Vaccines* **8**, 175, doi:10.1038/s41541-023-00768-x (2023).
- 46 Schmidt, S. *et al.* Alternating Arenavirus Vector Immunization Generates Robust Polyfunctional Genotype Cross-Reactive Hepatitis B Virus-Specific CD8 T-Cell Responses and High Anti-Hepatitis B Surface Antigen Titers. *J Infect Dis* **229**, 1077-1087, doi:10.1093/infdis/jiad340 (2024).
- 47 Barton, L. L., Peters, C. J. & Ksiazek, T. G. Lymphocytic choriomeningitis virus: an unrecognized teratogenic pathogen. *Emerg Infect Dis* **1**, 152-153, doi:10.3201/eid0104.950410 (1995).
- 48 Steinman, R. M. Lasker Basic Medical Research Award. Dendritic cells: versatile controllers of the immune system. *Nat Med* **13**, 1155-1159, doi:10.1038/nm1643 (2007).
- 49 Abraham, G. & Banerjee, A. K. Sequential transcription of the genes of vesicular stomatitis virus. *Proc Natl Acad Sci U S A* **73**, 1504-1508, doi:10.1073/pnas.73.5.1504 (1976).
- 50 Clarke, D. K. *et al.* Recombinant vesicular stomatitis virus as an HIV-1 vaccine vector. *Springer Semin Immunopathol* **28**, 239-253, doi:10.1007/s00281-006-0042-3 (2006).
- 51 Rose, J. K. Complete intergenic and flanking gene sequences from the genome of vesicular stomatitis virus. *Cell* **19**, 415-421, doi:10.1016/0092-8674(80)90515-2 (1980).
- 52 Jayakar, H. R., Jeetendra, E. & Whitt, M. A. Rhabdovirus assembly and budding. *Virus Res* **106**, 117-132, doi:10.1016/j.virusres.2004.08.009 (2004).
- 53 Redondo, N., Madan, V., Alvarez, E. & Carrasco, L. Impact of Vesicular Stomatitis Virus M Proteins on Different Cellular Functions. *PLoS One* **10**, e0131137, doi:10.1371/journal.pone.0131137 (2015).
- 54 Hoffmann, M. *et al.* Fusion-active glycoprotein G mediates the cytotoxicity of vesicular stomatitis virus M mutants lacking host shut-off activity. *J Gen Virol* **91**, 2782-2793, doi:10.1099/vir.0.023978-0 (2010).
- 55 Desforges, M. *et al.* Matrix protein mutations contribute to inefficient induction of apoptosis leading to persistent infection of human neural cells by vesicular stomatitis virus. *Virology* **295**, 63-73, doi:10.1006/viro.2001.1329 (2002).
- 56 Quan, B., Seo, H. S., Blobel, G. & Ren, Y. Vesiculoviral matrix (M) protein occupies nucleic acid binding site at nucleoporin pair (Rae1 \* Nup98). *Proc Natl Acad Sci U S A* **111**, 9127-9132, doi:10.1073/pnas.1409076111 (2014).
- 57 Yarbrough, M. L., Mata, M. A., Sakthivel, R. & Fontoura, B. M. Viral subversion of nucleocytoplasmic trafficking. *Traffic* **15**, 127-140, doi:10.1111/tra.12137 (2014).
- 58 Rieder, M. & Conzelmann, K. K. Rhabdovirus evasion of the interferon system. *J Interferon Cytokine Res* **29**, 499-509, doi:10.1089/jir.2009.0068 (2009).

- 59 Marquis, K. A., Becker, R. L., Weiss, A. N., Morris, M. C. & Ferran, M. C. The VSV matrix protein inhibits NF-kappaB and the interferon response independently in mouse L929 cells. *Virology* **548**, 117-123, doi:10.1016/j.virol.2020.06.013 (2020).
- 60 Lawson, N. D., Stillman, E. A., Whitt, M. A. & Rose, J. K. Recombinant vesicular stomatitis viruses from DNA. *Proc Natl Acad Sci U S A* **92**, 4477-4481, doi:10.1073/pnas.92.10.4477 (1995).
- 61 Whelan, S. P., Ball, L. A., Barr, J. N. & Wertz, G. T. Efficient recovery of infectious vesicular stomatitis virus entirely from cDNA clones. *Proc Natl Acad Sci U S A* **92**, 8388-8392, doi:10.1073/pnas.92.18.8388 (1995).
- 62 Haglund, K., Forman, J., Krausslich, H. G. & Rose, J. K. Expression of human immunodeficiency virus type 1 Gag protein precursor and envelope proteins from a vesicular stomatitis virus recombinant: high-level production of virus-like particles containing HIV envelope. *Virology* **268**, 112-121, doi:10.1006/viro.1999.0120 (2000).
- 63 Bukreyev, A., Skiadopoulos, M. H., Murphy, B. R. & Collins, P. L. Nonsegmented negative-strand viruses as vaccine vectors. *J Virol* **80**, 10293-10306, doi:10.1128/JVI.00919-06 (2006).
- 64 Finkelshtein, D., Werman, A., Novick, D., Barak, S. & Rubinstein, M. LDL receptor and its family members serve as the cellular receptors for vesicular stomatitis virus. *Proc Natl Acad Sci U S A* **110**, 7306-7311, doi:10.1073/pnas.1214441110 (2013).
- 65 Pipperger, L. *et al.* Differential infection of murine and human dendritic cell subsets by oncolytic vesicular stomatitis virus variants. *Oncoimmunology* **10**, 1959140, doi:10.1080/2162402X.2021.1959140 (2021).
- 66 Johnson, J. E. *et al.* Neurovirulence properties of recombinant vesicular stomatitis virus vectors in non-human primates. *Virology* **360**, 36-49, doi:10.1016/j.virol.2006.10.026 (2007).
- 67 Huneycutt, B. S. *et al.* Distribution of vesicular stomatitis virus proteins in the brains of BALB/c mice following intranasal inoculation: an immunohistochemical analysis. *Brain Res* **635**, 81-95, doi:10.1016/0006-8993(94)91426-5 (1994).
- 68 Agnandji, S. T. *et al.* Phase 1 Trials of rVSV Ebola Vaccine in Africa and Europe. *N Engl J Med* **374**, 1647-1660, doi:10.1056/NEJMoa1502924 (2016).
- 69 Majid, A. M., Ezelle, H., Shah, S. & Barber, G. N. Evaluating replication-defective vesicular stomatitis virus as a vaccine vehicle. *J Virol* **80**, 6993-7008, doi:10.1128/JVI.00365-06 (2006).
- 70 Publicover, J., Ramsburg, E. & Rose, J. K. A single-cycle vaccine vector based on vesicular stomatitis virus can induce immune responses comparable to those generated by a replication-competent vector. *J Virol* **79**, 13231-13238, doi:10.1128/JVI.79.21.13231-13238.2005 (2005).
- 71 Lo, M. K. *et al.* Single-dose replication-defective VSV-based Nipah virus vaccines provide protection from lethal challenge in Syrian hamsters. *Antiviral Res* **101**, 26-29, doi:10.1016/j.antiviral.2013.10.012 (2014).
- 72 Brister J. R., C. J., Curiel D. T., Heim A., Jones M. S., Kajon A., Lion T., Zhang Q., Seto D. *Human Adenovirus Working Group Adenovirus Classification*, <<http://hadvwg.gmu.edu/>> (

- 73 Zhang, W., Fu, J. & Ehrhardt, A. Novel Vector Construction Based on Alternative Adenovirus Types via Homologous Recombination. *Hum Gene Ther Methods* **29**, 124-134, doi:10.1089/hgtb.2018.044 (2018).
- 74 Kovetsdi, I. & Hedley, S. J. Adenoviral producer cells. *Viruses* **2**, 1681-1703, doi:10.3390/v2081681 (2010).
- 75 Gurwith, M. *et al.* Safety and immunogenicity of an oral, replicating adenovirus serotype 4 vector vaccine for H5N1 influenza: a randomised, double-blind, placebo-controlled, phase 1 study. *Lancet Infect Dis* **13**, 238-250, doi:10.1016/S1473-3099(12)70345-6 (2013).
- 76 Green, C. A. *et al.* Safety and immunogenicity of novel respiratory syncytial virus (RSV) vaccines based on the RSV viral proteins F, N and M2-1 encoded by simian adenovirus (PanAd3-RSV) and MVA (MVA-RSV); protocol for an open-label, dose-escalation, single-centre, phase 1 clinical trial in healthy adults. *BMJ Open* **5**, e008748, doi:10.1136/bmjopen-2015-008748 (2015).
- 77 Antrobus, R. D. *et al.* Clinical assessment of a novel recombinant simian adenovirus ChAdOx1 as a vectored vaccine expressing conserved Influenza A antigens. *Mol Ther* **22**, 668-674, doi:10.1038/mt.2013.284 (2014).
- 78 LaVoy, E. C. *et al.* High adenovirus 36 seroprevalence among a population of Hispanic American youth. *Int J Adolesc Med Health* **33**, doi:10.1515/ijamh-2018-0110 (2018).
- 79 Mennechet, F. J. D. *et al.* A review of 65 years of human adenovirus seroprevalence. *Expert Rev Vaccines* **18**, 597-613, doi:10.1080/14760584.2019.1588113 (2019).
- 80 Duffy, M. R. *et al.* Generation and characterization of a novel candidate gene therapy and vaccination vector based on human species D adenovirus type 56. *J Gen Virol* **99**, 135-147, doi:10.1099/jgv.0.000978 (2018).
- 81 Colloca, S. *et al.* Vaccine vectors derived from a large collection of simian adenoviruses induce potent cellular immunity across multiple species. *Sci Transl Med* **4**, 115ra112, doi:10.1126/scitranslmed.3002925 (2012).
- 82 Sallard, E., Zhang, W., Aydin, M., Schroer, K. & Ehrhardt, A. The Adenovirus Vector Platform: Novel Insights into Rational Vector Design and Lessons Learned from the COVID-19 Vaccine. *Viruses* **15**, doi:10.3390/v15010204 (2023).
- 83 Dicks, M. D. *et al.* A novel chimpanzee adenovirus vector with low human seroprevalence: improved systems for vector derivation and comparative immunogenicity. *PLoS One* **7**, e40385, doi:10.1371/journal.pone.0040385 (2012).
- 84 Abrignani, M. G. *et al.* COVID-19, Vaccines, and Thrombotic Events: A Narrative Review. *J Clin Med* **11**, doi:10.3390/jcm11040948 (2022).
- 85 Baker, A. T. *et al.* ChAdOx1 interacts with CAR and PF4 with implications for thrombosis with thrombocytopenia syndrome. *Sci Adv* **7**, eabl8213, doi:10.1126/sciadv.abl8213 (2021).
- 86 Normark, J. *et al.* Heterologous ChAdOx1 nCoV-19 and mRNA-1273 Vaccination. *N Engl J Med* **385**, 1049-1051, doi:10.1056/NEJMc2110716 (2021).

- 87 Schmidt, T. *et al.* Immunogenicity and reactogenicity of heterologous ChAdOx1 nCoV-19/mRNA vaccination. *Nat Med* **27**, 1530-1535, doi:10.1038/s41591-021-01464-w (2021).
- 88 Hillus, D. *et al.* Safety, reactogenicity, and immunogenicity of homologous and heterologous prime-boost immunisation with ChAdOx1 nCoV-19 and BNT162b2: a prospective cohort study. *Lancet Respir Med* **9**, 1255-1265, doi:10.1016/S2213-2600(21)00357-X (2021).
- 89 Harvie, P., Wong, F. M. & Bally, M. B. Use of poly(ethylene glycol)-lipid conjugates to regulate the surface attributes and transfection activity of lipid-DNA particles. *J Pharm Sci* **89**, 652-663, doi:10.1002/(SICI)1520-6017(200005)89:5<652::AID-JPS11>3.0.CO;2-H (2000).
- 90 Fang, E. *et al.* Advances in COVID-19 mRNA vaccine development. *Signal Transduct Target Ther* **7**, 94, doi:10.1038/s41392-022-00950-y (2022).
- 91 Alameh, M. G. *et al.* Lipid nanoparticles enhance the efficacy of mRNA and protein subunit vaccines by inducing robust T follicular helper cell and humoral responses. *Immunity* **55**, 1136-1138, doi:10.1016/j.immuni.2022.05.007 (2022).
- 92 Milane, L. & Amiji, M. Clinical approval of nanotechnology-based SARS-CoV-2 mRNA vaccines: impact on translational nanomedicine. *Drug Deliv Transl Res* **11**, 1309-1315, doi:10.1007/s13346-021-00911-y (2021).
- 93 Pardi, N., Hogan, M. J. & Weissman, D. Recent advances in mRNA vaccine technology. *Curr Opin Immunol* **65**, 14-20, doi:10.1016/j.coi.2020.01.008 (2020).
- 94 Zinkernagel, R. M. Localization dose and time of antigens determine immune reactivity. *Semin Immunol* **12**, 163-171; discussion 257-344, doi:10.1006/smim.2000.0253 (2000).
- 95 Quinn, K. M. *et al.* Antigen expression determines adenoviral vaccine potency independent of IFN and STING signaling. *J Clin Invest* **125**, 1129-1146, doi:10.1172/JCI78280 (2015).
- 96 Finn, J. D. *et al.* Persistence of transgene expression influences CD8+ T-cell expansion and maintenance following immunization with recombinant adenovirus. *J Virol* **83**, 12027-12036, doi:10.1128/JVI.00593-09 (2009).
- 97 Zhou, S. *et al.* Induction and inhibition of type I interferon responses by distinct components of lymphocytic choriomeningitis virus. *J Virol* **84**, 9452-9462, doi:10.1128/JVI.00155-10 (2010).
- 98 Kato, H. *et al.* Cell type-specific involvement of RIG-I in antiviral response. *Immunity* **23**, 19-28, doi:10.1016/j.immuni.2005.04.010 (2005).
- 99 Kariko, K., Buckstein, M., Ni, H. & Weissman, D. Suppression of RNA recognition by Toll-like receptors: the impact of nucleoside modification and the evolutionary origin of RNA. *Immunity* **23**, 165-175, doi:10.1016/j.immuni.2005.06.008 (2005).
- 100 Suprunenko, T. & Hofer, M. J. Complexities of Type I Interferon Biology: Lessons from LCMV. *Viruses* **11**, doi:10.3390/v11020172 (2019).
- 101 Appledorn, D. M. *et al.* Adenovirus vector-induced innate inflammatory mediators, MAPK signaling, as well as adaptive immune responses are dependent upon both TLR2 and TLR9 in vivo. *J Immunol* **181**, 2134-2144, doi:10.4049/jimmunol.181.3.2134 (2008).

- 102 Lam, E., Stein, S. & Falck-Pedersen, E. Adenovirus detection by the cGAS/STING/TBK1 DNA sensing cascade. *J Virol* **88**, 974-981, doi:10.1128/JVI.02702-13 (2014).
- 103 Barchet, W. *et al.* Virus-induced interferon alpha production by a dendritic cell subset in the absence of feedback signaling in vivo. *J Exp Med* **195**, 507-516, doi:10.1084/jem.20011666 (2002).
- 104 Ivashkiv, L. B. & Donlin, L. T. Regulation of type I interferon responses. *Nat Rev Immunol* **14**, 36-49, doi:10.1038/nri3581 (2014).
- 105 MacMicking, J. D. Interferon-inducible effector mechanisms in cell-autonomous immunity. *Nat Rev Immunol* **12**, 367-382, doi:10.1038/nri3210 (2012).
- 106 Parlato, S. *et al.* Expression of CCR-7, MIP-3beta, and Th-1 chemokines in type I IFN-induced monocyte-derived dendritic cells: importance for the rapid acquisition of potent migratory and functional activities. *Blood* **98**, 3022-3029, doi:10.1182/blood.v98.10.3022 (2001).
- 107 Wiesel, M. *et al.* Type-I IFN drives the differentiation of short-lived effector CD8+ T cells in vivo. *Eur J Immunol* **42**, 320-329, doi:10.1002/eji.201142091 (2012).
- 108 Mercier, S. *et al.* Distinct roles of adenovirus vector-transduced dendritic cells, myoblasts, and endothelial cells in mediating an immune response against a transgene product. *J Virol* **76**, 2899-2911, doi:10.1128/jvi.76.6.2899-2911.2002 (2002).
- 109 Hastie, E., Cataldi, M., Marriott, I. & Grdzlishvili, V. Z. Understanding and altering cell tropism of vesicular stomatitis virus. *Virus Res* **176**, 16-32, doi:10.1016/j.virusres.2013.06.003 (2013).
- 110 Mosaheb, M. M., Brown, M. C., Dobrikova, E. Y., Dobrikov, M. I. & Gromeier, M. Harnessing virus tropism for dendritic cells for vaccine design. *Curr Opin Virol* **44**, 73-80, doi:10.1016/j.coviro.2020.07.012 (2020).
- 111 Freigang, S., Probst, H. C. & van den Broek, M. DC infection promotes antiviral CTL priming: the 'Winkelried' strategy. *Trends Immunol* **26**, 13-18, doi:10.1016/j.it.2004.11.013 (2005).
- 112 Probst, H. C., Lagnel, J., Kollias, G. & van den Broek, M. Inducible transgenic mice reveal resting dendritic cells as potent inducers of CD8+ T cell tolerance. *Immunity* **18**, 713-720, doi:10.1016/s1074-7613(03)00120-1 (2003).
- 113 Rock, K. L. & Shen, L. Cross-presentation: underlying mechanisms and role in immune surveillance. *Immunol Rev* **207**, 166-183, doi:10.1111/j.0105-2896.2005.00301.x (2005).
- 114 Schirmbeck, R., Reimann, J., Kochanek, S. & Kreppel, F. The immunogenicity of adenovirus vectors limits the multispecificity of CD8 T-cell responses to vector-encoded transgenic antigens. *Mol Ther* **16**, 1609-1616, doi:10.1038/mt.2008.141 (2008).
- 115 Kedl, R. M. *et al.* T cells compete for access to antigen-bearing antigen-presenting cells. *J Exp Med* **192**, 1105-1113, doi:10.1084/jem.192.8.1105 (2000).
- 116 Roberts, D. M. *et al.* Hexon-chimaeric adenovirus serotype 5 vectors circumvent pre-existing anti-vector immunity. *Nature* **441**, 239-243, doi:10.1038/nature04721 (2006).

- 117 Sanchez, S., Palacio, N., Dangj, T., Ciucci, T. & Penaloza-MacMaster, P. Fractionating a COVID-19 Ad5-vectored vaccine improves virus-specific immunity. *Sci Immunol* **6**, eabi8635, doi:10.1126/sciimmunol.abi8635 (2021).
- 118 Yang, J., Huck, S. P., McHugh, R. S., Hermans, I. F. & Ronchese, F. Perforin-dependent elimination of dendritic cells regulates the expansion of antigen-specific CD8+ T cells in vivo. *Proc Natl Acad Sci U S A* **103**, 147-152, doi:10.1073/pnas.0509054103 (2006).
- 119 Quirk, E. K. *et al.* HIV seroconversion without infection after receipt of adenovirus-vectored HIV type 1 vaccine. *Clin Infect Dis* **47**, 1593-1599, doi:10.1086/593313 (2008).
- 120 Tober, R. *et al.* VSV-GP: a potent viral vaccine vector that boosts the immune response upon repeated applications. *J Virol* **88**, 4897-4907, doi:10.1128/JVI.03276-13 (2014).
- 121 Swadling, L. *et al.* A human vaccine strategy based on chimpanzee adenoviral and MVA vectors that primes, boosts, and sustains functional HCV-specific T cell memory. *Sci Transl Med* **6**, 261ra153, doi:10.1126/scitranslmed.3009185 (2014).
- 122 Painter, M. M. *et al.* Prior vaccination promotes early activation of memory T cells and enhances immune responses during SARS-CoV-2 breakthrough infection. *Nat Immunol* **24**, 1711-1724, doi:10.1038/s41590-023-01613-y (2023).
- 123 Moutaftsi, M. *et al.* Uncovering the interplay between CD8, CD4 and antibody responses to complex pathogens. *Future Microbiol* **5**, 221-239, doi:10.2217/fmb.09.110 (2010).
- 124 Grant, E. J., Quinones-Parra, S. M., Clemens, E. B. & Kedzierska, K. Human influenza viruses and CD8(+) T cell responses. *Curr Opin Virol* **16**, 132-142, doi:10.1016/j.coviro.2016.01.016 (2016).
- 125 Eickhoff, S. *et al.* Robust Anti-viral Immunity Requires Multiple Distinct T Cell-Dendritic Cell Interactions. *Cell* **162**, 1322-1337, doi:10.1016/j.cell.2015.08.004 (2015).
- 126 Taraban, V. Y., Rowley, T. F. & Al-Shamkhani, A. Cutting edge: a critical role for CD70 in CD8 T cell priming by CD40-licensed APCs. *J Immunol* **173**, 6542-6546, doi:10.4049/jimmunol.173.11.6542 (2004).
- 127 Guarda, G. *et al.* L-selectin-negative CCR7- effector and memory CD8+ T cells enter reactive lymph nodes and kill dendritic cells. *Nat Immunol* **8**, 743-752, doi:10.1038/ni1469 (2007).
- 128 Chen, M., Felix, K. & Wang, J. Critical role for perforin and Fas-dependent killing of dendritic cells in the control of inflammation. *Blood* **119**, 127-136, doi:10.1182/blood-2011-06-363994 (2012).
- 129 Sallusto, F., Lenig, D., Forster, R., Lipp, M. & Lanzavecchia, A. Two subsets of memory T lymphocytes with distinct homing potentials and effector functions. *Nature* **401**, 708-712, doi:10.1038/44385 (1999).
- 130 Joshi, N. S. *et al.* Inflammation directs memory precursor and short-lived effector CD8(+) T cell fates via the graded expression of T-bet transcription factor. *Immunity* **27**, 281-295, doi:10.1016/j.immuni.2007.07.010 (2007).
- 131 Yang, C. Y. *et al.* The transcriptional regulators Id2 and Id3 control the formation of distinct memory CD8+ T cell subsets. *Nat Immunol* **12**, 1221-1229, doi:10.1038/ni.2158 (2011).



- 132 Wherry, E. J. *et al.* Lineage relationship and protective immunity of memory CD8 T cell subsets. *Nat Immunol* **4**, 225-234, doi:10.1038/ni889 (2003).
- 133 Banerjee, A. *et al.* Cutting edge: The transcription factor eomesodermin enables CD8+ T cells to compete for the memory cell niche. *J Immunol* **185**, 4988-4992, doi:10.4049/jimmunol.1002042 (2010).
- 134 Zhou, X. *et al.* Differentiation and persistence of memory CD8(+) T cells depend on T cell factor 1. *Immunity* **33**, 229-240, doi:10.1016/j.immuni.2010.08.002 (2010).
- 135 Plotkin, S. A. Vaccination against the major infectious diseases. *C R Acad Sci III* **322**, 943-951, doi:10.1016/s0764-4469(00)87191-7 (1999).
- 136 Plotkin, S. A. Correlates of protection induced by vaccination. *Clin Vaccine Immunol* **17**, 1055-1065, doi:10.1128/CVI.00131-10 (2010).
- 137 Okada, T. *et al.* Antigen-engaged B cells undergo chemotaxis toward the T zone and form motile conjugates with helper T cells. *PLoS Biol* **3**, e150, doi:10.1371/journal.pbio.0030150 (2005).
- 138 McBride, K. M. *et al.* Regulation of class switch recombination and somatic mutation by AID phosphorylation. *J Exp Med* **205**, 2585-2594, doi:10.1084/jem.20081319 (2008).
- 139 Shinkura, R. *et al.* Separate domains of AID are required for somatic hypermutation and class-switch recombination. *Nat Immunol* **5**, 707-712, doi:10.1038/ni1086 (2004).
- 140 Schwickert, T. A. *et al.* A dynamic T cell-limited checkpoint regulates affinity-dependent B cell entry into the germinal center. *J Exp Med* **208**, 1243-1252, doi:10.1084/jem.20102477 (2011).
- 141 Weisel, F. J., Zuccarino-Catania, G. V., Chikina, M. & Shlomchik, M. J. A Temporal Switch in the Germinal Center Determines Differential Output of Memory B and Plasma Cells. *Immunity* **44**, 116-130, doi:10.1016/j.immuni.2015.12.004 (2016).
- 142 Mesin, L., Ersching, J. & Victora, G. D. Germinal Center B Cell Dynamics. *Immunity* **45**, 471-482, doi:10.1016/j.immuni.2016.09.001 (2016).
- 143 Stab, V. *et al.* HIV-1 neutralizing antibodies provide sterilizing immunity by blocking infection of the first cells. *Cell Rep Med* **4**, 101201, doi:10.1016/j.xcrm.2023.101201 (2023).
- 144 Cho, A. *et al.* Anti-SARS-CoV-2 receptor-binding domain antibody evolution after mRNA vaccination. *Nature* **600**, 517-522, doi:10.1038/s41586-021-04060-7 (2021).
- 145 Scheid, J. F. *et al.* Sequence and structural convergence of broad and potent HIV antibodies that mimic CD4 binding. *Science* **333**, 1633-1637, doi:10.1126/science.1207227 (2011).
- 146 Scheid, J. F. *et al.* HIV-1 antibody 3BNC117 suppresses viral rebound in humans during treatment interruption. *Nature* **535**, 556-560, doi:10.1038/nature18929 (2016).
- 147 Haynes, B. F., Kelsoe, G., Harrison, S. C. & Kepler, T. B. B-cell-lineage immunogen design in vaccine development with HIV-1 as a case study. *Nat Biotechnol* **30**, 423-433, doi:10.1038/nbt.2197 (2012).
- 148 Saunders, K. O. *et al.* Targeted selection of HIV-specific antibody mutations by engineering B cell maturation. *Science* **366**, doi:10.1126/science.aay7199 (2019).

- 149 Smith, E. C., Blanc, H., Surdel, M. C., Vignuzzi, M. & Denison, M. R. Coronaviruses lacking exoribonuclease activity are susceptible to lethal mutagenesis: evidence for proofreading and potential therapeutics. *PLoS Pathog* **9**, e1003565, doi:10.1371/journal.ppat.1003565 (2013).
- 150 Liu, Z. *et al.* Identification of SARS-CoV-2 spike mutations that attenuate monoclonal and serum antibody neutralization. *Cell Host Microbe* **29**, 477-488 e474, doi:10.1016/j.chom.2021.01.014 (2021).
- 151 Jangra, S. *et al.* The E484K mutation in the SARS-CoV-2 spike protein reduces but does not abolish neutralizing activity of human convalescent and post-vaccination sera. *medRxiv*, doi:10.1101/2021.01.26.21250543 (2021).
- 152 Wang, P. *et al.* Antibody Resistance of SARS-CoV-2 Variants B.1.351 and B.1.1.7. *bioRxiv*, doi:10.1101/2021.01.25.428137 (2021).
- 153 Goel, R. R. *et al.* mRNA vaccines induce durable immune memory to SARS-CoV-2 and variants of concern. *Science* **374**, abm0829, doi:10.1126/science.abm0829 (2021).
- 154 Appay, V., Douek, D. C. & Price, D. A. CD8+ T cell efficacy in vaccination and disease. *Nat Med* **14**, 623-628, doi:10.1038/nm.f.1774 (2008).
- 155 McMahan, K. *et al.* Correlates of protection against SARS-CoV-2 in rhesus macaques. *Nature* **590**, 630-634, doi:10.1038/s41586-020-03041-6 (2021).
- 156 Chandrashekar, A. *et al.* Vaccine protection against the SARS-CoV-2 Omicron variant in macaques. *Cell* **185**, 1549-1555 e1511, doi:10.1016/j.cell.2022.03.024 (2022).
- 157 Pardieck, I. N. *et al.* A third vaccination with a single T cell epitope confers protection in a murine model of SARS-CoV-2 infection. *Nat Commun* **13**, 3966, doi:10.1038/s41467-022-31721-6 (2022).
- 158 Ishii, H. *et al.* Neutralizing-antibody-independent SARS-CoV-2 control correlated with intranasal-vaccine-induced CD8(+) T cell responses. *Cell Rep Med* **3**, 100520, doi:10.1016/j.xcrm.2022.100520 (2022).
- 159 Fumagalli, V. *et al.* Antibody-independent protection against heterologous SARS-CoV-2 challenge conferred by prior infection or vaccination. *Nat Immunol*, doi:10.1038/s41590-024-01787-z (2024).
- 160 Collier, A. Y. *et al.* Differential Kinetics of Immune Responses Elicited by Covid-19 Vaccines. *N Engl J Med* **385**, 2010-2012, doi:10.1056/NEJMc2115596 (2021).
- 161 Uddback, I. *et al.* Prevention of respiratory virus transmission by resident memory CD8(+) T cells. *Nature* **626**, 392-400, doi:10.1038/s41586-023-06937-1 (2024).
- 162 Liu, L. *et al.* Striking antibody evasion manifested by the Omicron variant of SARS-CoV-2. *Nature* **602**, 676-681, doi:10.1038/s41586-021-04388-0 (2022).
- 163 Alter, G. *et al.* Immunogenicity of Ad26.COVS vaccine against SARS-CoV-2 variants in humans. *Nature* **596**, 268-272, doi:10.1038/s41586-021-03681-2 (2021).
- 164 Liu, J. *et al.* Vaccines elicit highly conserved cellular immunity to SARS-CoV-2 Omicron. *Nature* **603**, 493-496, doi:10.1038/s41586-022-04465-y (2022).

- 165 Bolinger, B. *et al.* Adenoviral Vector Vaccination Induces a Conserved Program of CD8(+) T Cell Memory Differentiation in Mouse and Man. *Cell Rep* **13**, 1578-1588, doi:10.1016/j.celrep.2015.10.034 (2015).
- 166 Huttner, A. *et al.* The effect of dose on the safety and immunogenicity of the VSV Ebola candidate vaccine: a randomised double-blind, placebo-controlled phase 1/2 trial. *Lancet Infect Dis* **15**, 1156-1166, doi:10.1016/S1473-3099(15)00154-1 (2015).
- 167 Hangartner, L., Zinkernagel, R. M. & Hengartner, H. Antiviral antibody responses: the two extremes of a wide spectrum. *Nat Rev Immunol* **6**, 231-243, doi:10.1038/nri1783 (2006).
- 168 Plesa, G., McKenna, P. M., Schnell, M. J. & Eisenlohr, L. C. Immunogenicity of cytopathic and noncytopathic viral vectors. *J Virol* **80**, 6259-6266, doi:10.1128/JVI.00084-06 (2006).
- 169 Frenz, T. *et al.* Concomitant type I IFN receptor-triggering of T cells and of DC is required to promote maximal modified vaccinia virus Ankara-induced T-cell expansion. *Eur J Immunol* **40**, 2769-2777, doi:10.1002/eji.201040453 (2010).
- 170 Palacio, N. *et al.* Early type I IFN blockade improves the efficacy of viral vaccines. *J Exp Med* **217**, doi:10.1084/jem.20191220 (2020).
- 171 Zhong, C. *et al.* Type I Interferon Promotes Humoral Immunity in Viral Vector Vaccination. *J Virol* **95**, e0092521, doi:10.1128/JVI.00925-21 (2021).
- 172 Evrard, M. *et al.* Sphingosine 1-phosphate receptor 5 (S1PR5) regulates the peripheral retention of tissue-resident lymphocytes. *J Exp Med* **219**, doi:10.1084/jem.20210116 (2022).
- 173 Omilusik, K. D. *et al.* Transcriptional repressor ZEB2 promotes terminal differentiation of CD8+ effector and memory T cell populations during infection. *J Exp Med* **212**, 2027-2039, doi:10.1084/jem.20150194 (2015).
- 174 Forbes, E. K. *et al.* Combining liver- and blood-stage malaria viral-vectored vaccines: investigating mechanisms of CD8+ T cell interference. *J Immunol* **187**, 3738-3750, doi:10.4049/jimmunol.1003783 (2011).
- 175 Stojdl, D. F. *et al.* VSV strains with defects in their ability to shutdown innate immunity are potent systemic anti-cancer agents. *Cancer Cell* **4**, 263-275, doi:10.1016/s1535-6108(03)00241-1 (2003).
- 176 Crouse, J. *et al.* Type I interferons protect T cells against NK cell attack mediated by the activating receptor NCR1. *Immunity* **40**, 961-973, doi:10.1016/j.immuni.2014.05.003 (2014).
- 177 van Boxel-Dezaire, A. H., Rani, M. R. & Stark, G. R. Complex modulation of cell type-specific signaling in response to type I interferons. *Immunity* **25**, 361-372, doi:10.1016/j.immuni.2006.08.014 (2006).
- 178 Coughlan, L. Factors Which Contribute to the Immunogenicity of Non-replicating Adenoviral Vectored Vaccines. *Front Immunol* **11**, 909, doi:10.3389/fimmu.2020.00909 (2020).
- 179 Kolumam, G. A., Thomas, S., Thompson, L. J., Sprent, J. & Murali-Krishna, K. Type I interferons act directly on CD8 T cells to allow clonal expansion and memory formation in response to viral infection. *J Exp Med* **202**, 637-650, doi:10.1084/jem.20050821 (2005).

- 180 Starbeck-Miller, G. R., Xue, H. H. & Harty, J. T. IL-12 and type I interferon prolong the division of activated CD8 T cells by maintaining high-affinity IL-2 signaling in vivo. *J Exp Med* **211**, 105-120, doi:10.1084/jem.20130901 (2014).
- 181 Thompson, L. J., Kolumam, G. A., Thomas, S. & Murali-Krishna, K. Innate inflammatory signals induced by various pathogens differentially dictate the IFN-I dependence of CD8 T cells for clonal expansion and memory formation. *J Immunol* **177**, 1746-1754, doi:10.4049/jimmunol.177.3.1746 (2006).
- 182 Grob, P. *et al.* Role of the individual interferon systems and specific immunity in mice in controlling systemic dissemination of attenuated pseudorabies virus infection. *J Virol* **73**, 4748-4754, doi:10.1128/JVI.73.6.4748-4754.1999 (1999).
- 183 Muller, U. *et al.* Functional role of type I and type II interferons in antiviral defense. *Science* **264**, 1918-1921, doi:10.1126/science.8009221 (1994).
- 184 Hogquist, K. A. *et al.* T cell receptor antagonist peptides induce positive selection. *Cell* **76**, 17-27, doi:10.1016/0092-8674(94)90169-4 (1994).
- 185 Battagay, M. *et al.* Quantification of lymphocytic choriomeningitis virus with an immunological focus assay in 24- or 96-well plates. *J Virol Methods* **33**, 191-198, doi:10.1016/0166-0934(91)90018-u (1991).
- 186 Charan, S. & Zinkernagel, R. M. Antibody mediated suppression of secondary IgM response in nude mice against vesicular stomatitis virus. *J Immunol* **136**, 3057-3061 (1986).
- 187 Pope, C. *et al.* Organ-specific regulation of the CD8 T cell response to *Listeria monocytogenes* infection. *J Immunol* **166**, 3402-3409, doi:10.4049/jimmunol.166.5.3402 (2001).
- 188 Marx, A. F. *et al.* The alarmin interleukin-33 promotes the expansion and preserves the stemness of Tcf-1(+) CD8(+) T cells in chronic viral infection. *Immunity* **56**, 813-828 e810, doi:10.1016/j.immuni.2023.01.029 (2023).
- 189 Dhenni, R. & Phan, T. G. The geography of memory B cell reactivation in vaccine-induced immunity and in autoimmune disease relapses. *Immunol Rev* **296**, 62-86, doi:10.1111/imr.12862 (2020).
- 190 Kurosaki, T., Kometani, K. & Ise, W. Memory B cells. *Nat Rev Immunol* **15**, 149-159, doi:10.1038/nri3802 (2015).
- 191 Weisel, F. & Shlomchik, M. Memory B Cells of Mice and Humans. *Annu Rev Immunol* **35**, 255-284, doi:10.1146/annurev-immunol-041015-055531 (2017).
- 192 Dan, J. M. *et al.* Immunological memory to SARS-CoV-2 assessed for up to 8 months after infection. *Science* **371**, doi:10.1126/science.abf4063 (2021).
- 193 Laidlaw, B. J. & Cyster, J. G. Transcriptional regulation of memory B cell differentiation. *Nat Rev Immunol* **21**, 209-220, doi:10.1038/s41577-020-00446-2 (2021).
- 194 Garcia-Beltran, W. F. *et al.* Multiple SARS-CoV-2 variants escape neutralization by vaccine-induced humoral immunity. *Cell* **184**, 2523, doi:10.1016/j.cell.2021.04.006 (2021).

- 195 Mathieu, E. *et al.* A global database of COVID-19 vaccinations. *Nat Hum Behav* **5**, 947-953, doi:10.1038/s41562-021-01122-8 (2021).
- 196 Khoury, D. S. *et al.* Neutralizing antibody levels are highly predictive of immune protection from symptomatic SARS-CoV-2 infection. *Nat Med* **27**, 1205-1211, doi:10.1038/s41591-021-01377-8 (2021).
- 197 Kim, W. *et al.* Germinal centre-driven maturation of B cell response to SARS-CoV-2 vaccination. *bioRxiv*, doi:10.1101/2021.10.31.466651 (2021).
- 198 Foster, W. S. *et al.* Tfh cells and the germinal center are required for memory B cell formation & humoral immunity after ChAdOx1 nCoV-19 vaccination. *Cell Rep Med* **3**, 100845, doi:10.1016/j.xcrm.2022.100845 (2022).
- 199 Klok, F. A., Pai, M., Huisman, M. V. & Makris, M. Vaccine-induced immune thrombotic thrombocytopenia. *Lancet Haematol* **9**, e73-e80, doi:10.1016/S2352-3026(21)00306-9 (2022).
- 200 Zhang, Y. *et al.* Vaccine-Induced Immune Thrombotic Thrombocytopenia: Clinicopathologic Features and New Perspectives on Anti-PF4 Antibody-Mediated Disorders. *J Clin Med* **13**, doi:10.3390/jcm13041012 (2024).
- 201 Wang, Z. *et al.* Humoral immunity to SARS-CoV-2 elicited by combination COVID-19 vaccination regimens. *J Exp Med* **219**, doi:10.1084/jem.20220826 (2022).
- 202 Ramasamy, M. N. *et al.* Safety and immunogenicity of ChAdOx1 nCoV-19 vaccine administered in a prime-boost regimen in young and old adults (COV002): a single-blind, randomised, controlled, phase 2/3 trial. *Lancet* **396**, 1979-1993, doi:10.1016/S0140-6736(20)32466-1 (2021).
- 203 Turner, J. S. *et al.* SARS-CoV-2 mRNA vaccines induce persistent human germinal centre responses. *Nature* **596**, 109-113, doi:10.1038/s41586-021-03738-2 (2021).
- 204 Banki, Z. *et al.* Heterologous ChAdOx1/BNT162b2 vaccination induces stronger immune response than homologous ChAdOx1 vaccination: The pragmatic, multi-center, three-arm, partially randomized HEVACC trial. *EBioMedicine* **80**, 104073, doi:10.1016/j.ebiom.2022.104073 (2022).
- 205 Kuraoka, M. *et al.* Recall of B cell memory depends on relative locations of prime and boost immunization. *Sci Immunol* **7**, eabn5311, doi:10.1126/sciimmunol.abn5311 (2022).
- 206 Mesin, L. *et al.* Restricted Clonality and Limited Germinal Center Reentry Characterize Memory B Cell Reactivation by Boosting. *Cell* **180**, 92-106 e111, doi:10.1016/j.cell.2019.11.032 (2020).
- 207 Dogan, I. *et al.* Multiple layers of B cell memory with different effector functions. *Nat Immunol* **10**, 1292-1299, doi:ni.1814 [pii] 10.1038/ni.1814 (2009).
- 208 Voysey, M. *et al.* Single-dose administration and the influence of the timing of the booster dose on immunogenicity and efficacy of ChAdOx1 nCoV-19 (AZD1222) vaccine: a pooled

- analysis of four randomised trials. *Lancet* **397**, 881-891, doi:10.1016/S0140-6736(21)00432-3 (2021).
- 209 Laidlaw, B. J. & Ellebedy, A. H. The germinal centre B cell response to SARS-CoV-2. *Nat Rev Immunol* **22**, 7-18, doi:10.1038/s41577-021-00657-1 (2022).
- 210 Wang, R. *et al.* SARS-CoV-2 Omicron Variants Reduce Antibody Neutralization and Acquire Usage of Mouse ACE2. *Front Immunol* **13**, 854952, doi:10.3389/fimmu.2022.854952 (2022).
- 211 Barros-Martins, J. *et al.* Immune responses against SARS-CoV-2 variants after heterologous and homologous ChAdOx1 nCoV-19/BNT162b2 vaccination. *Nat Med* **27**, 1525-1529, doi:10.1038/s41591-021-01449-9 (2021).
- 212 Barouch, D. H. *et al.* Immunogenicity of recombinant adenovirus serotype 35 vaccine in the presence of pre-existing anti-Ad5 immunity. *J Immunol* **172**, 6290-6297, doi:10.4049/jimmunol.172.10.6290 (2004).
- 213 Roltgen, K. *et al.* Immune imprinting, breadth of variant recognition, and germinal center response in human SARS-CoV-2 infection and vaccination. *Cell* **185**, 1025-1040 e1014, doi:10.1016/j.cell.2022.01.018 (2022).
- 214 Goel, R. R. *et al.* Efficient recall of Omicron-reactive B cell memory after a third dose of SARS-CoV-2 mRNA vaccine. *Cell* **185**, 1875-1887 e1878, doi:10.1016/j.cell.2022.04.009 (2022).
- 215 Kasturi, S. P. *et al.* Programming the magnitude and persistence of antibody responses with innate immunity. *Nature* **470**, 543-547, doi:10.1038/nature09737 (2011).
- 216 Le Gallou, S., Nojima, T., Kitamura, D., Weill, J. C. & Reynaud, C. A. The AID-Cre-ERT2 Model: A Tool for Monitoring B Cell Immune Responses and Generating Selective Hybridomas. *Methods Mol Biol* **1623**, 243-251, doi:10.1007/978-1-4939-7095-7\_19 (2017).
- 217 Baden, L. R. *et al.* Efficacy and Safety of the mRNA-1273 SARS-CoV-2 Vaccine. *N Engl J Med* **384**, 403-416, doi:10.1056/NEJMoa2035389 (2021).
- 218 Guo, S. *et al.* Dosing interval regimen shapes potency and breadth of antibody repertoire after vaccination of SARS-CoV-2 RBD protein subunit vaccine. *Cell Discov* **9**, 79, doi:10.1038/s41421-023-00585-5 (2023).
- 219 Tortorici, M. A. & Vesler, D. Structural insights into coronavirus entry. *Adv Virus Res* **105**, 93-116, doi:10.1016/bs.aivir.2019.08.002 (2019).
- 220 Grau, S. *et al.* COVID-19 mRNA Vaccines Preserve Immunogenicity after Re-Freezing. *Vaccines (Basel)* **10**, doi:10.3390/vaccines10040594 (2022).
- 221 Pinto, D. *et al.* Cross-neutralization of SARS-CoV-2 by a human monoclonal SARS-CoV antibody. *Nature* **583**, 290-295, doi:10.1038/s41586-020-2349-y (2020).
- 222 Gallardo, J., Perez-Illana, M., Martin-Gonzalez, N. & San Martin, C. Adenovirus Structure: What Is New? *Int J Mol Sci* **22**, doi:10.3390/ijms22105240 (2021).
- 223 Davison, A. J., Benko, M. & Harrach, B. Genetic content and evolution of adenoviruses. *J Gen Virol* **84**, 2895-2908, doi:10.1099/vir.0.19497-0 (2003).
- 224 Human Adenovirus Working Group, <<http://hadvwg.gmu.edu/>> (2023).

- 225 McPherson, R. A., Rosenthal, L. J. & Rose, J. A. Human cytomegalovirus completely helps adeno-associated virus replication. *Virology* **147**, 217-222, doi:10.1016/0042-6822(85)90243-0 (1985).
- 226 Zhao, Z., Anselmo, A. C. & Mitragotri, S. Viral vector-based gene therapies in the clinic. *Bioeng Transl Med* **7**, e10258, doi:10.1002/btm2.10258 (2022).
- 227 M., H. M. Head, What happened to the AstraZeneca vaccine? Now rare in rich countries, it's still saving lives around the world. *The Conversation* (2022).
- 228 Mendonca, S. A., Lorincz, R., Boucher, P. & Curiel, D. T. Adenoviral vector vaccine platforms in the SARS-CoV-2 pandemic. *NPJ Vaccines* **6**, 97, doi:10.1038/s41541-021-00356-x (2021).
- 229 Sadarangani, M., Marchant, A. & Kollmann, T. R. Immunological mechanisms of vaccine-induced protection against COVID-19 in humans. *Nat Rev Immunol* **21**, 475-484, doi:10.1038/s41577-021-00578-z (2021).
- 230 Tian, J. *et al.* Binding of adenovirus species C hexon to prothrombin and the influence of hexon on vector properties in vitro and in vivo. *PLoS Pathog* **18**, e1010859, doi:10.1371/journal.ppat.1010859 (2022).
- 231 Waddington, S. N. *et al.* Adenovirus serotype 5 hexon mediates liver gene transfer. *Cell* **132**, 397-409, doi:10.1016/j.cell.2008.01.016 (2008).
- 232 Alba, R. *et al.* Identification of coagulation factor (F)X binding sites on the adenovirus serotype 5 hexon: effect of mutagenesis on FX interactions and gene transfer. *Blood* **114**, 965-971, doi:10.1182/blood-2009-03-208835 (2009).
- 233 Greinacher, A. *et al.* Insights in ChAdOx1 nCoV-19 vaccine-induced immune thrombotic thrombocytopenia. *Blood* **138**, 2256-2268, doi:10.1182/blood.2021013231 (2021).
- 234 Pavord, S. *et al.* Vaccine induced immune thrombocytopenia and thrombosis: summary of NICE guidance. *BMJ* **375**, n2195, doi:10.1136/bmj.n2195 (2021).
- 235 Cines, D. B. & Bussel, J. B. SARS-CoV-2 Vaccine-Induced Immune Thrombotic Thrombocytopenia. *N Engl J Med* **384**, 2254-2256, doi:10.1056/NEJMe2106315 (2021).
- 236 Krauel, K. *et al.* Platelet factor 4 binds to bacteria, [corrected] inducing antibodies cross-reacting with the major antigen in heparin-induced thrombocytopenia. *Blood* **117**, 1370-1378, doi:10.1182/blood-2010-08-301424 (2011).
- 237 Brandt, E., Ludwig, A., Petersen, F. & Flad, H. D. Platelet-derived CXC chemokines: old players in new games. *Immunol Rev* **177**, 204-216, doi:10.1034/j.1600-065x.2000.17705.x (2000).
- 238 Mussbacher, M. *et al.* Optimized plasma preparation is essential to monitor platelet-stored molecules in humans. *PLoS One* **12**, e0188921, doi:10.1371/journal.pone.0188921 (2017).
- 239 Kotulska, K., Fattal-Valevski, A. & Haberlova, J. Recombinant Adeno-Associated Virus Serotype 9 Gene Therapy in Spinal Muscular Atrophy. *Front Neurol* **12**, 726468, doi:10.3389/fneur.2021.726468 (2021).

- 240 Chan, Y. K. & Flotte, T. R. Analyzing clinical observations to better understand and manage immune responses to AAV gene therapies. *Mol Ther* **31**, 913-914, doi:10.1016/j.ymthe.2023.02.020 (2023).
- 241 Zhang, W. *et al.* An Engineered Virus Library as a Resource for the Spectrum-wide Exploration of Virus and Vector Diversity. *Cell Rep* **19**, 1698-1709, doi:10.1016/j.celrep.2017.05.008 (2017).
- 242 Denard, J. *et al.* AAV-8 and AAV-9 Vectors Cooperate with Serum Proteins Differently Than AAV-1 and AAV-6. *Mol Ther Methods Clin Dev* **10**, 291-302, doi:10.1016/j.omtm.2018.08.001 (2018).
- 243 Sumida, S. M. *et al.* Neutralizing antibodies to adenovirus serotype 5 vaccine vectors are directed primarily against the adenovirus hexon protein. *J Immunol* **174**, 7179-7185, doi:10.4049/jimmunol.174.11.7179 (2005).
- 244 Carlisle, R. C. *et al.* Human erythrocytes bind and inactivate type 5 adenovirus by presenting Coxsackie virus-adenovirus receptor and complement receptor 1. *Blood* **113**, 1909-1918, doi:10.1182/blood-2008-09-178459 (2009).
- 245 Wang, X. *et al.* Analysis of the Prevalence of Binding and Neutralizing Antibodies against 39 Human Adenovirus Types in Student Cohorts Reveals Low-Prevalence Types and a Decline in Binding Antibody Levels during the SARS-CoV-2 Pandemic. *J Virol* **96**, e0113322, doi:10.1128/jvi.01133-22 (2022).
- 246 Field, D. J. *et al.* Platelet factor 4 increases bone marrow B cell development and differentiation. *Immunol Res* **65**, 1089-1094, doi:10.1007/s12026-017-8951-x (2017).
- 247 Lyons, M. *et al.* Adenovirus type 5 interactions with human blood cells may compromise systemic delivery. *Mol Ther* **14**, 118-128, doi:10.1016/j.ymthe.2006.01.003 (2006).
- 248 Eichholz, K. *et al.* Adenovirus-alpha-Defensin Complexes Induce NLRP3-Associated Maturation of Human Phagocytes via Toll-Like Receptor 4 Engagement. *J Virol* **96**, e0185021, doi:10.1128/jvi.01850-21 (2022).
- 249 Persson, B. D. *et al.* Lactoferrin-Hexon Interactions Mediate CAR-Independent Adenovirus Infection of Human Respiratory Cells. *J Virol* **94**, doi:10.1128/JVI.00542-20 (2020).
- 250 Stichling, N. *et al.* Lung macrophage scavenger receptor SR-A6 (MARCO) is an adenovirus type-specific virus entry receptor. *PLoS Pathog* **14**, e1006914, doi:10.1371/journal.ppat.1006914 (2018).
- 251 Lemckert, A. A. *et al.* Immunogenicity of heterologous prime-boost regimens involving recombinant adenovirus serotype 11 (Ad11) and Ad35 vaccine vectors in the presence of anti-ad5 immunity. *J Virol* **79**, 9694-9701, doi:10.1128/JVI.79.15.9694-9701.2005 (2005).
- 252 Zabaleta, N. *et al.* An AAV-based, room-temperature-stable, single-dose COVID-19 vaccine provides durable immunogenicity and protection in non-human primates. *Cell Host Microbe* **29**, 1437-1453 e1438, doi:10.1016/j.chom.2021.08.002 (2021).



- 253 Bliss, C. M. *et al.* Targeting Antigen to the Surface of EVs Improves the In Vivo Immunogenicity of Human and Non-human Adenoviral Vaccines in Mice. *Mol Ther Methods Clin Dev* **16**, 108-125, doi:10.1016/j.omtm.2019.12.003 (2020).
- 254 Wang, X., Hetzel, M., Zhang, W., Ehrhardt, A. & Bayer, W. Comparative analysis of the impact of 40 adenovirus types on dendritic cell activation and CD8(+) T cell proliferation capacity for the identification of favorable immunization vector candidates. *Front Immunol* **14**, 1286622, doi:10.3389/fimmu.2023.1286622 (2023).
- 255 Shiver, J. W. & Emini, E. A. Recent advances in the development of HIV-1 vaccines using replication-incompetent adenovirus vectors. *Annu Rev Med* **55**, 355-372, doi:10.1146/annurev.med.55.091902.104344 (2004).
- 256 Kuhn, I. *et al.* Directed evolution generates a novel oncolytic virus for the treatment of colon cancer. *PLoS One* **3**, e2409, doi:10.1371/journal.pone.0002409 (2008).
- 257 O'Cathail, S. M. *et al.* A Phase 1 Trial of the Safety, Tolerability, and Biological Effects of Intravenous Enadenotucirev (EnAd), a Novel Oncolytic Virus, in Combination with Chemoradiotherapy in Locally Advanced Rectal Cancer (CEDAR). *International Journal of Radiation Oncology\*Biophysics\*Physics* **117**, e329-e330, doi:10.1016/j.ijrobp.2023.06.2379 (2023).
- 258 Fakhri, M. *et al.* Safety and efficacy of the tumor-selective adenovirus enadenotucirev, in combination with nivolumab, in patients with advanced/metastatic epithelial cancer: a phase I clinical trial (SPICE). *J Immunother Cancer* **11**, doi:10.1136/jitc-2022-006561 (2023).
- 259 Atasheva, S. *et al.* Systemic cancer therapy with engineered adenovirus that evades innate immunity. *Sci Transl Med* **12**, doi:10.1126/scitranslmed.abc6659 (2020).
- 260 Nicolai, L. *et al.* Thrombocytopenia and splenic platelet-directed immune responses after IV ChAdOx1 nCov-19 administration. *Blood* **140**, 478-490, doi:10.1182/blood.2021014712 (2022).
- 261 Dabbiru, V. A. S., Muller, L., Schonborn, L. & Greinacher, A. Vaccine-Induced Immune Thrombocytopenia and Thrombosis (VITT)-Insights from Clinical Cases, In Vitro Studies and Murine Models. *J Clin Med* **12**, doi:10.3390/jcm12196126 (2023).
- 262 Greinacher, A. & Warkentin, T. E. Platelet factor 4 triggers thrombo-inflammation by bridging innate and adaptive immunity. *Int J Lab Hematol* **45 Suppl 2**, 11-22, doi:10.1111/ijlh.14075 (2023).
- 263 Warkentin, T. E. & Greinacher, A. Spontaneous HIT syndrome: Knee replacement, infection, and parallels with vaccine-induced immune thrombotic thrombocytopenia. *Thromb Res* **204**, 40-51, doi:10.1016/j.thromres.2021.05.018 (2021).
- 264 Schonborn, L. *et al.* Anti-PF4 immunothrombosis without proximate heparin or adenovirus vector vaccine exposure. *Blood* **142**, 2305-2314, doi:10.1182/blood.2023022136 (2023).
- 265 Ivanov, D. G. *et al.* Reverse Engineering of a Pathogenic Antibody Reveals the Molecular Mechanism of Vaccine-Induced Immune Thrombotic Thrombocytopenia. *J Am Chem Soc* **145**, 25203-25213, doi:10.1021/jacs.3c07846 (2023).

- 266 Parker, Z. F. *et al.* Platelet Factor 4 Inhibits and Enhances HIV-1 Infection in a Concentration-Dependent Manner by Modulating Viral Attachment. *AIDS Res Hum Retroviruses* **32**, 705-717, doi:10.1089/AID.2015.0344 (2016).
- 267 Saif, M. W. & Greenberg, B. HIV and thrombosis: a review. *AIDS Patient Care STDS* **15**, 15-24, doi:10.1089/108729101460065 (2001).
- 268 Goeijenbier, M. *et al.* Review: Viral infections and mechanisms of thrombosis and bleeding. *J Med Virol* **84**, 1680-1696, doi:10.1002/jmv.23354 (2012).
- 269 Kanack, A. J. *et al.* Human papilloma virus vaccine and VITT antibody induction. *Am J Hematol* **97**, E363-E364, doi:10.1002/ajh.26659 (2022).
- 270 Scholz, J. *et al.* An Adenoviral Vector as a Versatile Tool for Delivery and Expression of miRNAs. *Viruses* **14**, doi:10.3390/v14091952 (2022).
- 271 Roelvink, P. W., Mi Lee, G., Einfeld, D. A., Kovesdi, I. & Wickham, T. J. Identification of a conserved receptor-binding site on the fiber proteins of CAR-recognizing adenoviridae. *Science* **286**, 1568-1571, doi:10.1126/science.286.5444.1568 (1999).
- 272 Jager, L. *et al.* A rapid protocol for construction and production of high-capacity adenoviral vectors. *Nat Protoc* **4**, 547-564, doi:10.1038/nprot.2009.4 (2009).
- 273 Weinmann, J. *et al.* Identification of a myotropic AAV by massively parallel in vivo evaluation of barcoded capsid variants. *Nat Commun* **11**, 5432, doi:10.1038/s41467-020-19230-w (2020).
- 274 Heim, A., Ebnet, C., Harste, G. & Pring-Akerblom, P. Rapid and quantitative detection of human adenovirus DNA by real-time PCR. *J Med Virol* **70**, 228-239, doi:10.1002/jmv.10382 (2003).
- 275 Kim, J. *et al.* Simple, low-cost, and well-performing method, the outgrowth technique, for the isolation of cells from nasal polyps. *BMC Mol Cell Biol* **24**, 31, doi:10.1186/s12860-023-00493-2 (2023).
- 276 Aydin, M. *et al.* The mystery behind the nostrils - technical clues for successful nasal epithelial cell cultivation. *Ann Anat* **238**, 151748, doi:10.1016/j.aanat.2021.151748 (2021).
- 277 Chan, C. K., Singharoy, A. & Tajkhorshid, E. Anionic Lipids Confine Cytochrome c(2) to the Surface of Bioenergetic Membranes without Compromising Its Interaction with Redox Partners. *Biochemistry* **61**, 385-397, doi:10.1021/acs.biochem.1c00696 (2022).
- 278 Shekhar, M. *et al.* Revealing a Hidden Intermediate of Rotatory Catalysis with X-ray Crystallography and Molecular Simulations. *ACS Cent Sci* **8**, 915-925, doi:10.1021/acscentsci.1c01599 (2022).
- 279 Singharoy, A. *et al.* Atoms to Phenotypes: Molecular Design Principles of Cellular Energy Metabolism. *Cell* **179**, 1098-1111 e1023, doi:10.1016/j.cell.2019.10.021 (2019).
- 280 Bonilla, W. V. *et al.* Heterologous arenavirus vector prime-boost overrules self-tolerance for efficient tumor-specific CD8 T cell attack. *Cell Rep Med* **2**, 100209, doi:10.1016/j.xcrm.2021.100209 (2021).

- 281 Ng'uni, T., Chasara, C. & Ndhlovu, Z. M. Major Scientific Hurdles in HIV Vaccine Development: Historical Perspective and Future Directions. *Front Immunol* **11**, 590780, doi:10.3389/fimmu.2020.590780 (2020).
- 282 Law, J. L., Logan, M., Landi, A., Tyrrell, D. L. & Houghton, M. Progress toward approval of an HCV vaccine. *Can Liver J* **1**, 130-138, doi:10.3138/canlivj.2018.0010 (2018).
- 283 Khoury, D. S. *et al.* Correlates of Protection, Thresholds of Protection, and Immunobridging among Persons with SARS-CoV-2 Infection. *Emerg Infect Dis* **29**, 381-388, doi:10.3201/eid2902.221422 (2023).
- 284 Goldblatt, D., Alter, G., Crotty, S. & Plotkin, S. A. Correlates of protection against SARS-CoV-2 infection and COVID-19 disease. *Immunol Rev* **310**, 6-26, doi:10.1111/imr.13091 (2022).
- 285 Rhee, E. G. *et al.* Multiple innate immune pathways contribute to the immunogenicity of recombinant adenovirus vaccine vectors. *J Virol* **85**, 315-323, doi:10.1128/JVI.01597-10 (2011).
- 286 Cobleigh, M. A., Bradfield, C., Liu, Y., Mehta, A. & Robek, M. D. The immune response to a vesicular stomatitis virus vaccine vector is independent of particulate antigen secretion and protein turnover rate. *J Virol* **86**, 4253-4261, doi:10.1128/JVI.05991-11 (2012).
- 287 Feikin, D. R. *et al.* Duration of effectiveness of vaccines against SARS-CoV-2 infection and COVID-19 disease: results of a systematic review and meta-regression. *Lancet* **399**, 924-944, doi:10.1016/S0140-6736(22)00152-0 (2022).
- 288 Srivastava, K. *et al.* SARS-CoV-2-infection- and vaccine-induced antibody responses are long lasting with an initial waning phase followed by a stabilization phase. *Immunity* **57**, 587-599 e584, doi:10.1016/j.immuni.2024.01.017 (2024).
- 289 Tatsis, N. *et al.* Adenoviral vectors persist in vivo and maintain activated CD8+ T cells: implications for their use as vaccines. *Blood* **110**, 1916-1923, doi:10.1182/blood-2007-02-062117 (2007).
- 290 Racanelli, V., Behrens, S. E., Aliberti, J. & Rehmann, B. Dendritic cells transfected with cytopathic self-replicating RNA induce crosspriming of CD8+ T cells and antiviral immunity. *Immunity* **20**, 47-58, doi:10.1016/s1074-7613(03)00353-4 (2004).
- 291 Mack, C. A. *et al.* Circumvention of anti-adenovirus neutralizing immunity by administration of an adenoviral vector of an alternate serotype. *Hum Gene Ther* **8**, 99-109, doi:10.1089/hum.1997.8.1-99 (1997).
- 292 Nunez, N. G. *et al.* High-dimensional analysis of 16 SARS-CoV-2 vaccine combinations reveals lymphocyte signatures correlating with immunogenicity. *Nat Immunol* **24**, 941-954, doi:10.1038/s41590-023-01499-w (2023).
- 293 Logunov, D. Y. *et al.* Safety and immunogenicity of an rAd26 and rAd5 vector-based heterologous prime-boost COVID-19 vaccine in two formulations: two open, non-randomised phase 1/2 studies from Russia. *Lancet* **396**, 887-897, doi:10.1016/S0140-6736(20)31866-3 (2020).

- 294 Hashimoto, T. *et al.* High anaphylaxis rates following vaccination with the Pfizer BNT162b2 mRNA vaccine against COVID-19 in Japanese healthcare workers: a secondary analysis of initial post-approval safety data. *J Travel Med* **28**, doi:10.1093/jtm/taab090 (2021).
- 295 Moghimi, S. M. Allergic Reactions and Anaphylaxis to LNP-Based COVID-19 Vaccines. *Mol Ther* **29**, 898-900, doi:10.1016/j.ymthe.2021.01.030 (2021).
- 296 Kozma, G. T. *et al.* Role of anti-polyethylene glycol (PEG) antibodies in the allergic reactions to PEG-containing Covid-19 vaccines: Evidence for immunogenicity of PEG. *Vaccine* **41**, 4561-4570, doi:10.1016/j.vaccine.2023.06.009 (2023).
- 297 Mevorach, D. *et al.* Myocarditis after BNT162b2 mRNA Vaccine against Covid-19 in Israel. *N Engl J Med* **385**, 2140-2149, doi:10.1056/NEJMoa2109730 (2021).
- 298 Kato, S., Horita, N. & Utsunomiya, D. Incidence of Myocarditis after Messenger RNA Vaccine for COVID-19 in Young Male Recipients. *Am J Cardiol* **172**, 159-161, doi:10.1016/j.amjcard.2022.02.010 (2022).
- 299 El Hasbani, G. & Uthman, I. ANCA-Associated Vasculitis following the First Dose of Pfizer-BioNTech COVID-19 Vaccine. *Nephron* **147**, 103-107, doi:10.1159/000525562 (2023).
- 300 Andrews, N. *et al.* Duration of Protection against Mild and Severe Disease by Covid-19 Vaccines. *N Engl J Med* **386**, 340-350, doi:10.1056/NEJMoa2115481 (2022).

# Curriculum vitae

## Matias Ciancaglini

Date of birth: 09/03/1991 Nationality: Argentinian, Italian Phone number: (+41) 788015153 (Mobile).  
Email address: matias.cianca@gmail.com Address: Klybeckstrasse 142, 4057, Basel, Switzerland

### Education

---

#### **PhD in Biomedicine**

University of Basel (Basel Switzerland)

31/08/2019 – 28.06.2024

Field of study: Virology / Immunology

Thesis: Mechanisms of vectored vaccination for durable effector T cell immunity and sustained germinal center reactions

Final grade: Summa cum laude

#### **Master of Science in Infection Biology**

Hannover Medical School

07/2017 – 07/2019 (Hannover Germany)

Field of study: Infection Biology / Immunology

Final grade: 1.3

Thesis: Diversity of the hepatic lipid droplet population and interplay with hepatitis C virus assembly

#### **Bachelor in Biotechnology**

National University of Quilmes

2008 – 2014 (Bernal, Argentina)

Field of study: Biochemistry / Biology

Final grade: 8.7/10

Thesis: Development of an antigenic platform display for Rotavirus based on *Lactococcus lactis*

### Work experience

---

#### **Professional research assistant**

National Institute of Infectious Diseases - Branch: National Reference Laboratory of Hantavirus

11/2014 – 04/2017 (Buenos Aires, Argentina)

### Skills and training

---

#### **Languages**

Spanish (native), English (fluent), German (basic)

#### **Courses certifications**

Vaccinology (07/02/2022 – 04/03/2022). Institut Pasteur (Paris, France)

Introductory Course in Laboratory Animal Science for experimenters (21/10/2019 – 21/10/2019). University of Zurich, Institute of Laboratory Animal Science, ETH, Swiss Federal Institute of Technology Zurich (Zurich, Switzerland).

Lower Saxony International Summer Academy (LISA). “Inflammation, Regeneration and Immunity – Basic Aspects, Novel Approaches and Experimental Models” (12/08/2017 – 26/08/2017). Hannover Medical School (Hannover, Germany).

Validation and Verification for Molecular Diagnostic Assays (08/11/2015 – 12/11/2015). INEI - ANLIS “Dr. C. G. Malbrán” (Buenos Aires, Argentina).

Biosafety and Biosecurity in health facilities (31/08/2015 – 29/09/2015). INEI - ANLIS “Dr. C. G. Malbrán”, Operative Unit Biological Containment Center (UOCCB) (Buenos Aires, Argentina).

## Scientific publications

---

Jonathan Cramer, Adem Lakkaichi, Butrint Aliu, Roman P. Jakob, Sebastian Klein, Ivan Cattaneo, Xiaohua Jiang, Said Rabbani, Oliver Schwardt, Gert Zimmer, Matias Ciancaglini, Tiago Abreu Mota, Timm Maier, and Beat Ernst. Sweet Drugs for Bad Bugs: A Glycomimetic Strategy against the DC-SIGN-Mediated Dissemination of SARS-CoV-2. 2021. Journal of the American Chemical Society, 143, 17465-17478, 10.1021/jacs.1c06778

Peter Reuther, Katrin Martin, Mario Kreuzfeldt, Matias Ciancaglini, Florian Geier, Diego Calabrese, Doron Merkler, Daniel D. Pinschewer. Persistent RNA virus infection is short-lived at the single-cell level but leaves transcriptomic footprints. 2021. Journal of Experimental Medicine, 218, 10, 10.1084/jem.20210408

Kimia T. Maleki, Marina García, Ayelén Iglesias, Daniel Alonso, Matías Ciancaglini, Ulf Hammar, Hans-Gustaf Ljunggren, Pablo Schierloh, Valeria P. Martínez, and Jonas Klingström. Serum Markers Associated with Severity and Outcome of Hantavirus Pulmonary Syndrome. 2019. Journal of Infectious Diseases, 219, 10.1093/infdis/jiz005

Matías Ciancaglini, Carla M. Bellomo, Clara L. Torrez Cabrerros, Daniel Alonso, Sabrina C. Bassi, Ayelen A. Iglesias and Valeria P. Martínez. Hantavirus pulmonary syndrome in Tucumán province associated to an unexpected viral genotype. 2017. Medicina (Buenos Aires). ISSN 1669-9106.

## Acknowledgements

I would like to express my deepest gratitude to my main supervisor, Daniel, whose guidance, insight, and relentless support were crucial in the completion of this thesis. Thank you, Daniel, for sharing your expertise and provide thoughtful and constructive feedback that challenged me to refine my ideas. Thank you also for the patience and encouragement, the countless hours dedicated to analyzing data and giving advice. Your positive attitude always helped me to find motivation and confidence. More importantly, I am profoundly grateful for the space to talk openly about personal circumstances. Lastly, thank you for give us freedom in our research and plenty of resources to test our ideas, we really appreciate it even if sometimes we spend too much money. This thesis would not have been possible without your mentorship and commitment.

In second place I want to thank my secondary supervisor, Prof. Dirk Bumann, who accepted to be part of my PhD committee and provided critical insights and valuable feedback during my PaC meetings. I extend my gratitude to to Prof. Ulrich Kalinke for accepting to be my external expert, whose research experience represents an excellent match to my thesis projects. Thanks also to Ingo Drexler, who was my initial external advisor and gave me advice during the PaC meetings.

Then I want to thank Katrin, for taking me under your wing when I was just starting in the lab and guided me through the initial phase of my PhD.

A wholeheartedly Thank You: to the whole Experimental Virology group current members. Anna, Mirela, Katrin, Min, Sonia, Weldy, Tiago, Lena, Karen, Cemre, Davide, Jonas and Karsten. Thank you for every working day shared. The good and the bad ones. Thank you for the laughs, the coffee breaks, the discussion, the debates. I always felt fortunate to have a chilled atmosphere in the lab. This is something cannot be taken for granted and I really appreciate it. Also thank you for all the support provided: from personal advice to a cup of coffee, and of course for all the funny moments in and outside the lab.

Many thanks to the former lab members of EV: Yusuf, Marianna, Peter and Kerstin. It was always a lot of fun with you in the lab. Special thanks to Mehmet, for being my closest friend, for the amazing times spent together in and outside the lab. For the crazy trips.

Thank you, Karsten, for keeping our mice always on check. Thank you for all your patience with my mice handling and mostly with my German!

Por último, quiero agradecer a mi familia y amigos argentinos por estar siempre presente a pesar de las distancias. Gracias por la confianza y el aliento que siempre me brindaron en mis búsquedas personales. A mis padres por la libertad incondicional y siempre empujarme para adelante. Gracias Matthieu, por ser mi mayor apoyo emocional estos últimos años y estar a mi lado en momentos adversos.